



**HAL**  
open science

# Modeling the rheology of wet granular materials

Thanh Trung Vo

► **To cite this version:**

Thanh Trung Vo. Modeling the rheology of wet granular materials. Materials. Université Montpellier, 2019. English. NNT: 2019MONTTS103 . tel-03003108

**HAL Id: tel-03003108**

**<https://theses.hal.science/tel-03003108>**

Submitted on 13 Nov 2020

**HAL** is a multi-disciplinary open access archive for the deposit and dissemination of scientific research documents, whether they are published or not. The documents may come from teaching and research institutions in France or abroad, or from public or private research centers.

L'archive ouverte pluridisciplinaire **HAL**, est destinée au dépôt et à la diffusion de documents scientifiques de niveau recherche, publiés ou non, émanant des établissements d'enseignement et de recherche français ou étrangers, des laboratoires publics ou privés.

**THÈSE POUR OBTENIR LE GRADE DE DOCTEUR  
DE L'UNIVERSITÉ DE MONTPELLIER**

**Mécanique et Génie Civil**

École Doctorale: **Information, Structures et Systèmes**

**Laboratoire de Mécanique et Génie Civil**

**MODÉLISATION DE LA RHÉOLOGIE DES  
MATÉRIAUX GRANULAIRES HUMIDES**

**MODELING THE RHEOLOGY OF WET  
GRANULAR MATERIALS**

Presented by **Thanh Trung VO**

Defense date - 12<sup>th</sup> November 2019

**Raporters**

Gaël COMBE      Professor      Grenoble Alpes University  
Maxime NICOLAS      Professor      Aix-Marseille University

**Before the jury composed of**

Gaël COMBE	Professor	Grenoble Alpes University	Reporter
Maxime NICOLAS	Professor	Aix-Marseille University	Reporter
Anne MANGENEY	Professor	University Paris Diderot	Examiner
Lydie STARON	Researcher	CNRS-Sorbonne University	Examiner
Edouard IZARD	Researcher	ArcelorMittal Maizières Research	Examiner
Farhang RADJAI	Director of research	CNRS-University of Montpellier	Supervisor
Jean-Yves DELENNE	Director of research	INRA	Co-Supervisor
Saeid NEZAMABADI	Ass. Professor	University of Montpellier	Co-Supervisor



**UNIVERSITÉ  
DE MONTPELLIER**







# Resumé

Dans cette thèse, nous avons étudié par simulations numériques la rhéologie et le processus d'agglomération de matériaux granulaires humides impliquant des interactions cohésives et visqueuses venant s'ajouter à celles de contact-frottant. Des écoulements en cisaillement, simulés par une approche de type éléments discrets 3D, nous ont permis de montrer que les variables caractérisant le comportement (coefficient de frottement effectif et compacité) ainsi que celles décrivant la texture (nombre de coordination et anisotropie) peuvent être décrites comme fonction d'un unique nombre sans dimension ; incorporant les forces inertielles, cohésives et visqueuses. Nous nous sommes également intéressés à l'évolution d'un agglomérat à l'intérieur d'un écoulement de particules sèches cisillées ainsi que dans un tambour rotatif contenant des particules humides. Il a été montré que l'évolution de l'agglomérat dépend de la dynamique d'accrétion et d'érosion et que celle-ci est régie par les interactions cohésives. Des diagrammes de phase en termes de croissance, de déformation, d'endommagement et d'érosion sont présentés en fonction de l'indice de cohésion et du nombre inertiel. Enfin, la résistance à la compression des agglomérats a été également étudiée sous compression diamétrale. On montre qu'elle est proportionnelle à la force d'adhésion entre particules avec un pré-facteur qui dépend de la connectivité des particules primaires.



# Summary

By means of extensive particle dynamics simulations in three dimensions, we investigate the rheology and agglomeration process of granular materials such as wet powders, which involve cohesive and viscous interactions in addition to frictional contact forces. In shear flow simulations, we show that the flow variables such as effective friction coefficient and packing fraction and texture variables such as coordination number and anisotropy can be described as a function of a single dimensionless number that incorporates the inertial, cohesive and viscous forces. We also study the evolution of an agglomerate inside a granular shear flow of dry particles and in a rotating drum containing wet particles. The evolution of the agglomerate depends on the accretion and erosion dynamics, which are governed by cohesive interactions. We determine the phase-space diagrams in terms of the agglomerate growth, deformation, damage and erosion as a function of the cohesion index and inertial number. The compressive strength of the agglomerates is also investigated under diametral compression and shown to be proportional to the adhesion force between the particles with a pre-factor that depends on the connectivity of the primary particles.



# Contents

<b>Resumé</b>	<b>v</b>
<b>Summary</b>	<b>vii</b>
<b>General Introduction</b>	<b>1</b>
<b>1 Literature review</b>	<b>5</b>
1.1 Dry granular materials . . . . .	7
1.2 Wet granular materials . . . . .	9
1.2.1 Liquid states . . . . .	9
1.2.2 Effects of cohesive stress . . . . .	11
1.2.3 Effects of viscous stress . . . . .	13
1.3 Agglomeration of granular materials . . . . .	15
1.3.1 Granulation process . . . . .	15
1.3.2 Froude number and flow regimes . . . . .	17
1.3.3 Relation between agglomeration and flow properties . . . . .	18
1.4 Numerical method . . . . .	20
1.4.1 Discrete Element Method . . . . .	20
1.4.2 Contact force laws . . . . .	21
1.4.3 Capillary cohesion and viscous forces . . . . .	22
1.5 Conclusion . . . . .	25
<b>2 Additive rheology of inertial flows of cohesive particles</b>	<b>27</b>
Introduction . . . . .	29
Results . . . . .	31
Discussion . . . . .	37
Method . . . . .	38
Supplemental Material . . . . .	39
<b>3 Agglomeration of wet particles in dense granular flows</b>	<b>47</b>
3.1 Introduction . . . . .	51
3.2 Model description and numerical method . . . . .	53
3.2.1 Physical assumptions . . . . .	53

3.2.2	Drum flow . . . . .	54
3.3	Growth, accretion and erosion . . . . .	58
3.4	Effects of material parameters . . . . .	62
3.5	Phase diagram . . . . .	65
3.6	Conclusions . . . . .	66
<b>4</b>	<b>Mechanical strength of wet particle agglomerates</b>	<b>67</b>
4.1	Introduction . . . . .	71
4.2	Numerical procedures . . . . .	72
4.2.1	Physical assumptions . . . . .	72
4.2.2	Ideal granules . . . . .	73
4.3	Granule strength . . . . .	76
4.4	Analytical model . . . . .	78
4.5	Conclusions . . . . .	82
<b>5</b>	<b>Evolution of a wet agglomerate in inertial shear flow of dry granular materials</b>	<b>83</b>
5.1	Introduction . . . . .	85
5.2	Model descriptions and parameters . . . . .	86
5.3	Time evolution of agglomerates . . . . .	88
5.4	Scaling behavior . . . . .	94
5.5	Conclusion . . . . .	97
	<b>General Conclusions and outlook</b>	<b>99</b>
	General Conclusions . . . . .	101
	Outlook . . . . .	104
	<b>Summary in French</b>	<b>107</b>
	<b>Bibliography</b>	<b>112</b>

# List of Figures

1.1	<i>Hourglass represents the behavior of granular materials in three different phases (Copyright Walls Cover: <a href="https://www.stickpng.com/img/objects/hourglasses/hourglass-grey-sand">https://www.stickpng.com/img/objects/hourglasses/hourglass-grey-sand</a>).</i>	7
1.2	<i>Snapshot of six different configurations: (a) simple shear plane, (b) annular shear, (c) vertical-chute flow, (d) inclined plane, (e) heap flow, and (f) rotating drum. [1]</i>	8
1.3	<i>Schematic drawing of different liquid regimes in a granular packing: (a) pendular, (b) funicular, (c) capillary, and (d) slurry. [2]</i>	10
1.4	<i>Evolution of normalized cohesion (a), normalized packing fraction (b), coordination number (c), and the contact anisotropy (d) for different values of the cohesion index.[3]</i>	12
1.5	<i>(a) Schematic representation the simulated system of grains immersed in a viscous fluid subjected to the Couette shear flow, (b) Snapshots of fluid pressure field and contact force chains, (c) Snapshots of fluid and particle velocity fields.[4]</i>	14
1.6	<i>(a) Effective friction coefficient <math>\mu</math> and (b) packing fraction <math>\Phi</math> as a function of the visco-inertial number <math>I_m</math> (similar to <math>I_\vartheta</math> in this thesis) for different values of liquid viscosity <math>\eta_f</math>, shear rate <math>\dot{\gamma}</math>, normal stress <math>\sigma_s</math>, and particle density <math>\rho_s</math>.[4]</i>	15
1.7	<i>Experimental drum demonstrating the agglomeration of single wet agglomerate in dense granular flows of dry particles (a), the geometrical granule after 50 rotations of drum (b). Experiments by R. Contreras in CRM Group, Liège.</i>	16
1.8	<i>Six flow regimes of granular materials in a rotating drum by increasing the Froude number <math>Fr</math> or drum size.</i>	18
1.9	<i>Schematic representation contact force laws in the DEM.</i>	21
1.10	<i>Schematic drawing of two different cases of capillary bridges: particle <math>i</math> in contact with particle <math>j</math> and without contact with particle <math>k</math>.</i>	22
1.11	<i>Capillary cohesion force <math>f_c</math> decreases in absolute value as a function of the gap <math>\delta_n</math> between two particles in the capillary bridge contact for different values of the liquid volume <math>V_b</math> of capillary bond. The capillary force exists up to the rupture distance <math>d_{rupt}</math>.</i>	23

1.12	<i>Viscous force <math>f_{vis}</math> declines as a function of the gap <math>\delta_n</math> between two particles in the capillary contact for different values of the size ratio <math>\alpha</math> which is the ratio between the largest and smallest particle diameter. The viscous force exists up to the rupture distance <math>d_{rupt}</math>. This force is plotted for systematic parameters in Chapter 3 and keeping a fixed relative normal velocity <math>\dot{\delta}_n = 5 \cdot 10^{-3}</math>.</i>	25
2.1	<i>(a) Simulated system of wet spherical particles under a constant confining stress <math>\sigma_p</math> and sheared by a constant horizontal velocity <math>v</math> of the top rough wall. The particle colors are proportional to particle diameters. (b, c) Snapshot of compressive (grey) and tensile (blue) force chains. Line thickness is proportional to normal force. (d) Snapshot of contact forces (violet) and non-contact capillary forces (green). (e) Snapshot of the particle velocity field in steady flow.</i>	30
2.2	<i>Apparent friction coefficient <math>\mu</math> (a) and packing fraction <math>\Phi</math> (b) as a function of the inertial number <math>I</math>. The data are averaged over the steady state. The error bars represent the standard deviation of the data in each simulation. For each set of simulations, the symbols and their colors correspond to the parameters that are varied with their ranges, all other parameters being kept constant.</i>	31
2.3	<i>(a) Normalized effective friction coefficient <math>\mu/\mu_c</math> and (b) normalized packing fraction <math>\phi/\phi_c</math> as a function of the modified inertial number <math>I_m</math> defined by equation (2.1) with <math>\alpha \simeq 0.062</math> and <math>\beta \simeq 0.075</math>. The error bars represent the standard deviation over the steady state. The black-solid lines are analytical expressions (2.6) and (2.7). The insets show the evolution of the quasistatic functions <math>\mu_c</math> and <math>\Phi_c</math> with the cohesion index <math>\xi</math>, with linear fits (blue-solid lines).</i>	32
2.4	<i>(a) Normalized bulk viscosity <math>c_n</math> and (b) shear viscosity <math>c_t</math> as a function of the normalized packing fraction <math>\Phi/\Phi_c</math>. The error-bar symbols and their colors are the same as those in Fig. 2.2. The solid lines are the functional forms (2.27) and (2.26), respectively.</i>	36
2.5	<i>Number density <math>Z</math> of capillary bonds (a) and bond anisotropy <math>A</math> (b) as a function of the modified inertial number <math>I_m</math> for different parameter values. The error-bar symbols and their colors are the as in Fig. 2.2.</i>	37
2.6	<i>Velocity profiles in the steady state for different values of the inertial number, with cohesion index <math>\xi = 0.5</math> and liquid viscosity <math>\eta_f = 1</math> mPa.s. The velocities are average values on in the steady flow state and they are normalized by the shear velocity applied on the top wall.</i>	42
2.7	<i>Velocity profiles in the steady state for different values of the inertial number <math>I</math> and liquid viscosity <math>\eta_f</math> (in mPa.s) in cohesionless samples. The velocities are average values on in the steady flow state and they are normalized by the shear velocity applied on the top wall.</i>	43

---

LIST OF FIGURES

2.8	Number density of capillary bonds (a) and bond anisotropy (b) in the quasi-static state as a function of the cohesion index $\xi$ . The symbols and their colors correspond to different values of the control parameters as in Fig. 2 of the paper. . . . .	44
3.1	<i>Snapshots of the initial state (a) and stable flow (b) in the drum for <math>\alpha = 5</math>. The colors show the magnitudes of particle velocities varying from red (fast particles at the free surface) to blue (slowest particles in the middle of the drum).</i> . . . . .	55
3.2	<i>(a) Snapshot of the granular bed showing the distribution of dry particles (in white) and wet particles (in black) both those inside the initially defined granule in the center of the bed and those randomly distributed throughout the bed; (b) Force chains during agglomeration: line thickness is proportional to normal force between neighboring particles with compressive forces in blue and tensile forces in red.</i> . . . . .	56
3.3	<i>The mean velocity <math>v</math> of drum flow for dry particles and in the presence of wet particles with <math>Fr = 0.5</math> as a function of the number of rotations of the drum. The inset shows the evolution of the free surface inclination angle <math>\beta</math> as a function of the number of rotations.</i> . . . . .	57
3.4	<i>Evolution of the granule size <math>N_g</math> (in number of particles) for different values of size ratio <math>\alpha</math> and <math>d_{min} = 10 \mu m</math>. The solid lines are exponential fits given by equation (3.6).</i> . . . . .	58
3.5	<i>Variation <math>\Delta V</math> of the volume of particles inside the granule as a function of their number <math>N_g</math> for different values of size ratio <math>\alpha</math> and <math>d_{min} = 10 \mu m</math>.</i> . . . . .	59
3.6	<i>Cumulative accretion (a) and cumulative erosion (b) of particles for different values of the size ratio <math>\alpha</math>. The lines are fitting forms given by equations (3.7) and (3.8), respectively.</i> . . . . .	60
3.7	<i>Fitted values of accretion rate <math>k^+</math> and erosion rate <math>k^-</math> as a function of polydispersity parameter <math>\alpha</math>.</i> . . . . .	61
3.8	<i>Evolution of the cumulative number of wet particles for accretion (solid lines) and erosion (dashed lines) for four different values of the mean particle diameter <math>\langle d \rangle</math> and size ratio <math>\alpha = 5</math>, as a function of the number of drum rotations.</i> . . . . .	62
3.9	<i>Cumulative accretion (solid lines) and erosion (dashed lines) of wet particles for five different values of the friction coefficient <math>\mu</math>, size ratio <math>\alpha = 5</math> and <math>d_{min} = 10 \mu m</math>, as a function of the number of drum rotations. The lines are fitting forms given by equations (3.7) and (3.8).</i> . . . . .	63
3.10	<i>Fitted values of erosion rate <math>k^-</math> and accretion rate <math>k^+</math> as a function of friction coefficient <math>\mu</math> for size ratio <math>\alpha = 5</math>.</i> . . . . .	63
3.11	<i>Cumulative accretion (solid lines) and erosion (dashed lines) for four different values of the liquid viscosity <math>\eta</math> for size ratio <math>\alpha = 5</math> and <math>d_{min} = 10 \mu m</math> as a function of the number of drum rotations. The solid and dashed lines are exponential and linear fits to the data points, respectively.</i> . . . . .	64

---

**LIST OF FIGURES**

3.12	<i>Erosion rate <math>k^-</math> and accretion rate <math>k^+</math> as a function of liquid viscosity <math>\eta</math> for size ratio <math>\alpha = 5</math> and <math>d_{min} = 10 \mu m</math>. . . . .</i>	64
3.13	<i>Phase diagram of granule growth in the parametric space of <math>\langle d \rangle</math> vs. <math>\alpha</math> for <math>\eta = 1 mPa.s</math> and <math>\mu = 0.5</math>. The granule grows only in the light blue region and disappears otherwise. . . . .</i>	65
4.1	<i>Schematic representation of diametrical compression test (a), and snapshots of granules composed from 5000 primary spherical particles before diametrical compression for (b) <math>\alpha = 1</math>; (c) <math>\alpha = 2</math>, and (d) <math>\alpha = 5</math>. . . . .</i>	75
4.2	Snapshot of a granule under diametrical compression for $\alpha = 1$ . The lines are force chains joining the particle centers. . . . .	76
4.3	<i>Vertical strength <math>\sigma_{zz}</math> normalized by the reference stress <math>\sigma_c</math> for different values of friction coefficient <math>\mu</math>, size ratio <math>\alpha</math> and the debonding distance <math>d_{rupt}</math>, as a function of cumulative vertical strain <math>\varepsilon</math>. . . . .</i>	77
4.4	<i>Normalized plastic strength of the granule for several values of the debonding distance as a function of the size ratio <math>\alpha</math>. The inset shows the non-normalized value of the strength as a function of <math>\alpha</math>. . . . .</i>	77
4.5	<i>Normalized plastic strength <math>\sigma_p/\sigma_c</math> of the granules for different values of the size ratio as a function of debonding distance <math>d_{rupt}</math>. . . . .</i>	78
4.6	<i>The initial wet coordination number <math>Z_0</math> of the granules for different values of debonding distance as a function of the size ratio <math>\alpha</math>. . . . .</i>	79
4.7	<i>The prefactor <math>\eta</math> in equation (4.15) as a function of the debonding distance <math>d_{rupt}</math> for different values of <math>\alpha</math>. . . . .</i>	80
4.8	<i>The <math>Z\Phi</math>s in equation (4.15) as a function of the debonding distance <math>d_{rupt}</math> for different values of <math>\alpha</math>. . . . .</i>	81
5.1	Velocity profiles in steady shear state for different values of the cohesion index $\xi$ (a) with $I \simeq 10^{-3}$ , and for different values of the inertial number $I$ with $\xi = 5.0$ (b). . . . .	88
5.2	(a) Simulated model of a wet agglomerate in a granular bed of dry particles subjected to a homogeneous shear flow; (b) elongation and erosion of the agglomerate; (c) elongation, erosion, and breakage modes; (d) spontaneous dispersion of wet particles. . . . .	89
5.3	Evolution of cumulative elongation $M_g$ (a) and breakage $M_b$ (b) of a wet agglomerate inside a homogeneous shear flow of dry particles as a function of cumulative shear strain $\varepsilon$ for different values of the cohesion index $\xi$ and for $I \simeq 10^{-3}$ . . . . .	90
5.4	Evolution of cumulative erosion as a function of shear strain $\varepsilon$ for different values of the cohesion index $\xi$ and for $I \simeq 0.1$ . . . . .	91
5.5	Elongation rate $K_g$ (a), erosion rate $K_e$ (b), and breakage rate $K_b$ (c) of the wet agglomerate as a function of the inertial number $I$ for different values of the cohesion index $\xi$ . . . . .	92

5.6	Average normal force (a) and tangential force (b) at the contacts between the dry particles of the flow and the wet particles of the agglomerate as a function of the inertial number for different values the cohesion index. The forces are normalized by the confining force $\sigma_p \langle d \rangle^2$ . . . . .	93
5.7	Normalized elongation rate $K_g t_i$ as a function of the scaling parameter $I_g = \xi I^{\alpha_g}$ with $\alpha_g = 1$ for all our simulations. The symbols and their colors represent the same values of cohesion index $\xi$ as in Fig. 5.3. The solid line is a power-law fitting form (Eq. 5.10). . . . .	95
5.8	Normalized breakage rate $K_b t_i$ as a function of the scaling parameter $I_b = \xi I^{\alpha_b}$ with $\alpha_b = 1$ for all our simulations. The symbols and their colors represent the same values of cohesion index $\xi$ as in Fig. 5.3. The solid line is a power-law fitting form (Eq. 5.11). . . . .	95
5.9	Normalized erosion rate $K_e t_i$ as a function of the scaling parameter $I_e \simeq I^{\alpha_e} \xi^{\beta_e}$ with $\alpha_e = 0.25$ and $\beta_e = -1$ for all our simulations. The symbols and their colors represent the same values of cohesion index $\xi$ as in Fig. 5.3. The solid line is a truncated power-law fitting form Eq. (5.13). . . . .	96
5.10	Diagram of erosion states in the phase space $(I, \xi)$ . The filled and empty symbols represent the states of erosion and vanishing erosion, respectively, for all the simulated values of $I$ and $\xi$ with a power-law frontier $\xi = I^{1/4}/I_0$ between them. The half-filled symbols correspond to the simulations where the agglomerate breaks up spontaneously, i.e. over one time step. . . . .	97

# General Introduction

## Introduction

Granular materials play fundamental and important roles in natural and industrial processes. A granular material is a collection or assembly of discrete solid macroscopic particles, such as sand in an hourglass, cereal grains in a silo and ballast grains on the railway. Depending on the kinetic energy involved and confining pressure, they are found in three different states: solid-like such as a sandpile, liquid-like such as an avalanche of grains and gas-like such as a intensively vibrated powder. In the natural events and industrial manufacturing, granular materials can be found in their different parts in each of these states.

The most basic types of granular materials are composed of dry grains interacting via frictional contacts. But more complex granular materials involve also cohesive interactions or viscous forces. They affect the strength and packing-flow properties of the material both in a solid-like static state under external loading and during their shear flow. A typical example is wet granular materials such as wet soil or powders at high humidity. The binding liquid induces both a capillary cohesive force and a viscous force during granular flow. Another example is dense suspensions of colloidal particles in a fluid where both lubricating and colloidal forces come into play. The cohesive materials have been investigated by experiments and particle dynamics simulations and applied to the agglomeration process. In the same way, the effects of viscous forces on the rheology of dense granular media have been investigated in suspensions and for assemblies of particles interacting through lubrication forces. However, the joint effects of viscous and cohesive forces remain an open question.

## Goals and questions

The aim of this thesis is to model and investigate complex granular flows involving cohesive and viscous interactions in addition to frictional contacts between particles. We use particle dynamics simulations based the Molecular Dynamics or Discrete-Element method with spherical particles and consider several different case studies, including inertial granular

---

flows with the visco-capillary interparticle forces and agglomeration of wet particles. This work was initiated within a collaborative project on “Multi-scale approach to the agglomeration process” from 2015 to 2017, funded by ArcelorMittal (Maizières Research laboratory, France) with Massachusetts Institute of Technology (Joint CNRS-MIT lab) and Ingénierie des Agropolymères et Technologies Emergentes (IATE, INRA, Montpellier).

Some of the general and specific research questions that we will address in this work are as follows:

1. Is rheology of wet granular materials an extension of dry rheology or are they completely different?
2. How much do the cohesion and viscous forces affect the particle interactions including contact and friction?
3. How do such interactions affect the shear strength, compressive strength, microstructure, and flows of wet granular materials?
4. Is it possible to define a single dimensionless scaling parameter that controls the rheology as the inertial number in dry granular flows?
5. How are local cohesive and viscous forces and the macroscopic strength and texture variables connected?
6. How the mechanical strength of cohesive agglomerates is related to the capillary forces?
7. How do agglomerates of wet particles grow in a rotating drum?

These questions will be addressed with different configurations, including the simple shear model of wet granular materials by using pressure-controlled conditions, diametrical compression test of wet aggregates, and evolution of wet granules inside dense granular flows and homogeneous shear flows of a granular bed of dry particles. Each simulated system will be subjected to detailed parametric investigation by varying the material and control parameters. In each case, we try to elaborate on the numerical data to obtain the most general model for the system behavior.

## Thesis overview

This thesis is organized in several chapters. After literature review in Chapter 1, we present our investigation of wet granular flows in Chapter 2. Chapter 3 is devoted to the investigation of the growth of a single wet granule within a dense granular flow as a result of accretion and erosion phenomena during the agglomeration. Then, we introduce a diametrical compression test in order to investigate the mechanical strength and microstructure of wet particle agglomerates which created in the agglomeration in Chapter 4. In order to

---

characterize the interactions between a wet agglomerate and a granular flow, we present the in Chapter 5 a detailed study of the evolution of a single wet agglomerate in a homogeneous flow of dry particles. Finally, we conclude with a summary of the most salient results of this thesis and possible further research directions.

The literature review of granular materials as well as the numerical approach are presented in Chapter 1. We will present a number of concepts and results that will be useful in the next chapters.

In Chapter 2, we investigate the effects of cohesion and viscous forces between wet particles on the rheology and scaling behavior of unsaturated granular flows in the steady inertial state by using the stress-controlled and boundary conditions subjected to a plane shear flow in the framework of Discrete Element Method. The DEM with the capillary cohesion law enhanced by the cohesive and viscous forces due to the presence of the interstitial liquid is used for this work. The granular flows will be characterized in terms of two macroscopic variables: effective friction coefficient  $\mu(I, \xi, St)$  and packing fraction  $\phi(I, \xi, St)$  as a function of three dimensionless control parameters: the inertial number  $I$ , the cohesion index  $\xi$ , and the Stokes number  $St$ . We show that the data points for both variables collapse on a master curve for a broad range of input parameters such as confining stress, shear rate, cohesion number, and Stokes number with a dimensionless modified inertial number (*visco-cohesive* inertial number). We also show that the bond orientation anisotropy and coordination number, as descriptors of granular texture are scaled by the same modified inertial number.

Chapter 3 considers the growth of a granule composed of wet particles in dense granular flows in a rotating drum. The liquid is assumed to be transported by wet particles. The granular bed consists of a single wet agglomerate in the center of the bed and free wet particles randomly distributed within the granular bed. Wet particles interact via the capillary and viscous force laws. The granule growth is a function of the number of drum rotations for different values of material parameters such as the particle size distribution  $\alpha$ , the mean particle size  $\langle d \rangle$ , friction coefficient  $\mu$ , and the liquid viscosity  $\eta$  as a result of the capture and detachment of wet particles. The accretion and erosion rates are also investigated in more detail. A phase diagram of agglomeration is proposed for size polydispersity and mean particle size.

In Chapter 4, the diametrical compression of cohesive agglomerates (granules) is investigated by numerical simulations. We are interested in the mechanical strength and microstructure of the agglomerate. The compressive strength of the granule depends on its internal structure and cohesion forces acting between particles due to the presence of capillary bonds. Due to the rearrangements of primary particles and irreversible loss of capillary contacts, the compressive stress undergoes increases towards a plastic plateau. We compare the measured plastic strength with the available experimental data.

Chapter 5 numerically investigates the behavior of a single wet agglomerate embedded in a homogeneous shear flow. The agglomerate elongates, breaks, and is eroded due to the interactions with surrounding dry particles flow. These dispersion modes are controlled by both inertial effects of the flow and cohesion of the agglomerate, characterized respectively by two dimensionless numbers: inertial number and cohesion index. We show that the

---

rates of elongation, breakage, and erosion can be expressed as functions of dimensionless numbers combining the cohesion index and inertial number. We also determine their functional dependence. We show that in the phase space defined by the cohesion index and inertial number there is a well-defined borderline between states of erosion and states of vanishing erosion.

Finally, we present major results and outlooks of this thesis and future directions of research.

*“Everything should be made as simple  
as possible but not simpler”*

---

Albert Einstein (1879-1955)

## Chapter 1

# Literature review

**I**n this chapter, we present a brief review of the physical and mechanical properties of granular flows and the agglomeration process of solid particles. The granular flow behaves differently depending on different loading and boundary conditions such as simple shear, annular shear, inclined plane, vertical-chute, heap and drum flows. The rheology of dry granular materials has been a subject of extensive research work, but the behavior of wet granular flows remains poorly understood. Indeed, in the wet granular system, the interactions between particles are enhanced by the cohesive and viscous forces induced by the binding liquid. This liquid may be distributed between particles in different states such as pendular, funicular, capillary, and slurry. The agglomeration process of solid particles in a rotating drum is an example where cohesive and viscous interactions are important. The particle dynamics simulations can be used as a powerful tool to investigate the rheology down to the particle scale.

## Contents

---

<b>1.1</b>	<b>Dry granular materials</b>	<b>7</b>
<b>1.2</b>	<b>Wet granular materials</b>	<b>9</b>
1.2.1	Liquid states	9
1.2.2	Effects of cohesive stress	11
1.2.3	Effects of viscous stress	13
<b>1.3</b>	<b>Agglomeration of granular materials</b>	<b>15</b>
1.3.1	Granulation process	15
1.3.2	Froude number and flow regimes	17
1.3.3	Relation between agglomeration and flow properties	18
<b>1.4</b>	<b>Numerical method</b>	<b>20</b>
1.4.1	Discrete Element Method	20
1.4.2	Contact force laws	21
1.4.3	Capillary cohesion and viscous forces	22

**1.5 Conclusion . . . . . 25**

---

## 1.1 Dry granular materials

Divided or granular media constitute a common form of solid matter in nature and in many industrial sectors. Dry granular materials interact only via frictional contacts. The absence of cohesive forces gives them intermediate mechanical properties between solid and liquid. If it is a solid, it is an amorphous solid like glasses and if it is a liquid, it is a non-Brownian liquid. The granular materials can flow under low stress gradients or under its inertia. As a simple example, one can consider the sand flow inside an hourglass shown in Fig. 1.1. On the top of the hourglass, the particles are stationary and behave like solids. Moving down close to the bottom of the top section, near the nozzle of the hourglass, the grains are flowing like a liquid. The grains form a conical heap due to their own weight in the bottom section of the top compartment, unlike a standard liquid. This example shows complex behaviors of granular materials. Since many consumer products are in a granular form, or have been in a divided form in one of the stages of their manufacturing process, any progress in understanding the behavior of granular media can have significant consequences for the industry.

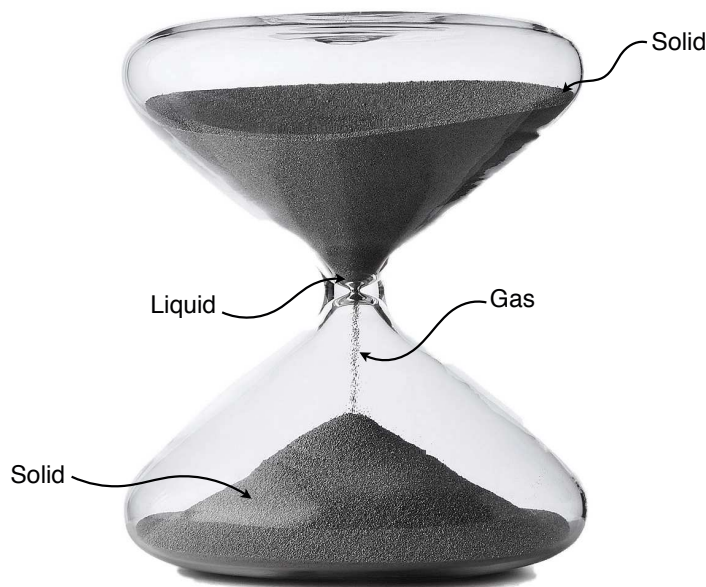


Figure 1.1 – Hourglass represents the behavior of granular materials in three different phases (Copyright Walls Cover: <https://www.stickpng.com/img/objects/hourglasses/hourglass-grey-sand>).

In dry granular materials, most of studies has focused on the granular packing and

constitutive behavior of dense flows of granular materials in terms of internal friction laws [1, 5, 6, 7]. Numerical simulations, considering the simple model of spherical particles with frictional contacts, were carried out for all complex behaviors of granular materials. The effect of different parameters such as particle shape, particle size distribution, and inter-particle friction for both space-filling and shear characteristics of granular materials, was investigated. Meanwhile, the effects of particle size distribution and particle shape govern the space-filling and microstructure of the system, and the shear properties mainly affect the shear strength and rheology of granular flows [7]. Here, the rheology is only governed by momentum transfer and energy dissipation (friction and inelastic collisions) occurring in the contacts [8].

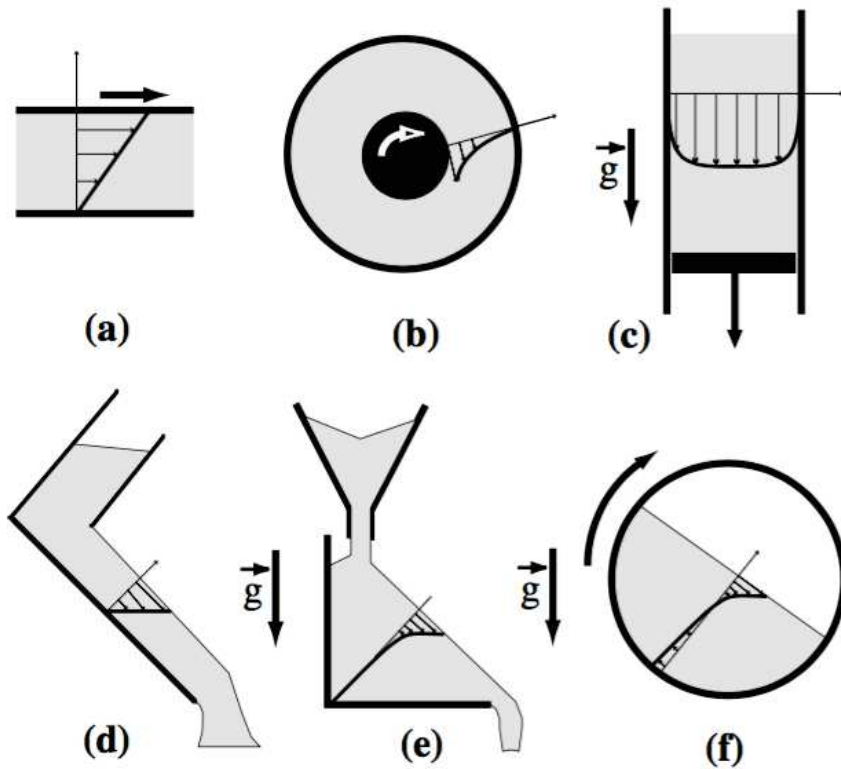


Figure 1.2 – Snapshot of six different configurations: (a) simple shear plane, (b) annular shear, (c) vertical-chute flow, (d) inclined plane, (e) heap flow, and (f) rotating drum. [1]

The dry granular flows are mostly investigated by accounting six different configurations shown in Fig. 1.2 [1, 6, 9]. They allow achieving a simple shear flow for measuring appropriately rheological properties such as velocity profiles, packing fraction, shear strength, effective friction coefficient... These configurations are classified in two categories: confined and free surface flows. The confined flow occurs when materials imprison between walls and the walls move, as shown in Fig. 1.2(a), (b), and (c). The free surface flows are the granular flows on a rough inclined plane (Fig. 1.2(d)), at the surface of a pile (Fig. 1.2(e)), and in a rotating drum (Fig. 1.2(f)). Here, the driving force is the gravity.

In order to describe the granular flow properties, the inertial number  $I$ , as a dimensionless number, is defined by considering the simple shear flow configuration [1, 10]:

$$I = \dot{\gamma} \langle d \rangle \sqrt{\frac{\rho_s}{\sigma_p}}, \quad (1.1)$$

where  $\rho_s$  and  $\langle d \rangle$  are the density and mean diameter of grains, and  $\dot{\gamma}$  and  $\sigma_p$  denote the applied shear rate and confining pressure. Indeed, the inertial number  $I$  is the ratio between the inertial time  $(\sigma_p/\rho_s)^{1/2}/\langle d \rangle$  and the shear time  $1/\dot{\gamma}$ .

To generate the simple shear flow, two methods can be considered. In the first method, the granular system is sheared by applying a constant velocity, meanwhile it is subjected to a constant confining pressure. In this case, the effective friction coefficient  $\mu$  increases as a function of the inertial number  $I$  whereas the packing fraction  $\phi$  (ratio between the volume of particles and the volume of granular system) decreases [11]. The second method consists in fixing the volume of granular system (i.e. packing fraction). Here, the confining stress  $\sigma_p$  and the shear rate  $\dot{\gamma}$  are variables and  $\sigma_p$  increases with the applied shear rate  $\dot{\gamma}$ . The results obtained from these two methods are equivalent [10]. The rheology of these two simple granular flows could be extended and applied for other flow geometries [1]. The velocity fields and stresses predicted by the rheology of the simple shear flow are generally in good agreement with experimental and numerical observations [12, 13, 14]. Nevertheless, it is worth noting that flows even for simple geometries are not necessarily homogeneous and deformation gradients depending on the flow thickness and wall roughness, can be observed. These phenomena are considered as non-local effects related to high correlations of particle velocities, and theoretical models have been proposed to describe them.

The rheology and texture of granular flows can be characterized by the effective friction coefficient  $\mu$ , the packing fraction  $\Phi$ , the coordination number  $Z$ , and contact anisotropy  $a_c$ , and these parameters are totally controlled by the inertial number  $I$  [11, 10]. Indeed, the flow of granular materials presents different regimes depending on the value of the inertial number  $I$ . When  $I$  is small, typically less than  $10^{-3}$ , the flow corresponds to the "quasi-static" regime, in which, the macroscopic deformation is very small compared to the microscopic rearrangement of particles. For very large values of  $I$ , the flow is in a "collisional" regime, in which, the interactions between particles are mainly binary collisions and the material may be described as a granular gas. For the values of  $I$  between those two regimes, the material is in a dense flow regime or "granular liquid". In other words, the flows of granular materials change from quasi-static regime to inertial regime.

## 1.2 Wet granular materials

### 1.2.1 Liquid states

Granular materials evolve most of the time in humid environments in industrial processes such as iron-making industry, powder metallurgy, or pharmaceutical manufacturing as well as in geology and civil engineering, or in natural phenomena such as landslides and

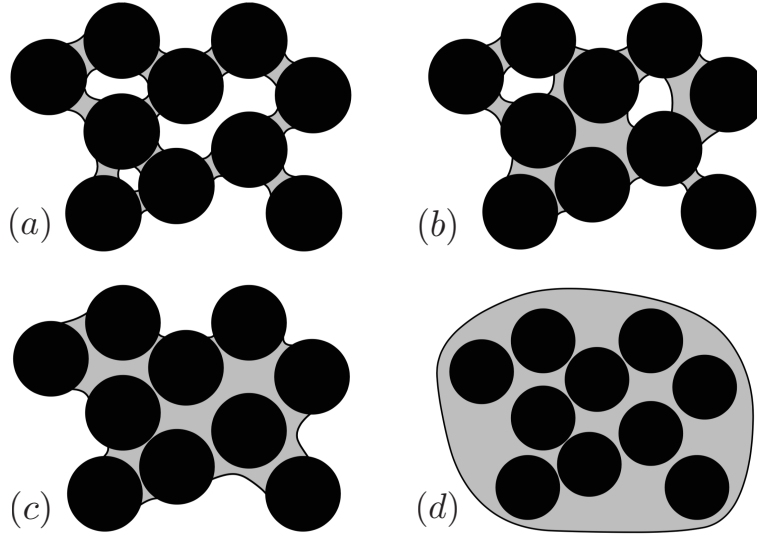


Figure 1.3 – Schematic drawing of different liquid regimes in a granular packing: (a) pendular, (b) funicular, (c) capillary, and (d) slurry. [2]

avalanches [15, 16, 17, 18, 19]. The characteristics of wet granular materials do not only depend on the properties of raw materials such as particle size distribution, particle shape, particle roughness, and process parameters such as the shear rate but also drastically depend on the liquid properties such as liquid surface tension and liquid viscosity due to the presence of the interstitial liquid in the systems. The complex behaviors of wet granular materials are induced by the collisional-frictional/capillary-viscous interactions of wet grains after forming the liquid bridge at the contact points [20, 21]. Thus, the amount of liquid is an important parameter, which directly affects the compressive strength, shear strength, and texture of wet granular flows [3, 8, 22, 23].

Depending on the amount of the liquid, four basic regimes of wet granular materials are observed: pendular, funicular, capillary, and slurry [2, 8, 20]. In the *Pendular* regime (Fig. 1.3(a)), liquid bridges are formed at the contact points between particles. In the *funicular* regime (1.3(b)), in addition to the formed capillary bridges, some pores between particles are filled with liquid. In the *capillary* regime (Fig. 1.3(c)), all pores are fully saturated with liquid and the surface liquid is drawn back into the pores under the capillary action. In the *slurry* regime (Fig. 1.3(d)), all particles are fully immersed in liquid, the surface liquid is convex, i.e. no capillary action exists anymore. All these states can be easily described by the amount of liquid content.

Wet granular materials, in the presence of small amount of liquid in the *pendular* state, are characterized by a network of capillary bonds, which give rise to capillary cohesion force and viscous force between particles [24]. In addition to the repulsive contact forces, these forces determine the equilibrium state of granular materials. The capillary cohesion force between two particles comes from the surface tension at the contact line between particles and the liquid. This suction pressure depends on the curvature of the liquid bridge. The

*pendular* state not only represents the simplest topology of the liquid phase, but also gives the highest values of the capillary cohesion force. This force is a function of the distance between particles, particle size and liquid volume. The viscous force (lubrication force) depends on the liquid viscosity and relative normal velocity between two moving particle [25].

Contrary to dry granular materials, the behavior of wet granular media cannot be described only by the inertial number  $I$ . In order to characterize the flow of solid particles in the presence of the interstitial liquid, some dimensionless parameters such as the cohesion number  $\xi$  (or the reduced pressure  $P^*$ ), the Stokes number  $St$  and the capillary number  $Ca$  can be considered. The cohesion number  $\xi$  is the ratio between cohesion stress  $\sigma_c$  and the confining stress  $\sigma_p$  [3] (similarly, the "reduced pressure"  $P^* = 1/\xi$ , was defined in [8, 22]). To account the effect of viscous forces, the Stokes number  $St$  is defined as the ratio between the inertial stress  $\sigma_i \sim \rho_s \langle d \rangle \dot{\gamma}^2$  and the viscous stress  $\sigma_v \sim \eta \dot{\gamma}$  for the case of dry grains immersed in a viscous fluid or  $\sigma_v \sim \eta \dot{\gamma} \langle d \rangle / \delta_0$  for unsaturated dry granular materials [4]. The Capillary number  $Ca$  also presents the ratio between the viscous stress  $\sigma_v$  and the cohesion stress  $\sigma_c$  [20]:  $Ca = \sigma_v / \sigma_c \sim \eta \dot{\gamma} \langle d \rangle / \gamma_s$ .

During last decades, researchers have separately studied the cohesive and viscous effects of the binding liquid on the physical and mechanical behaviors of wet granular materials because of the complex interactions between particles due to these forces. Meanwhile, the cohesive forces are investigated in the context of agglomeration [26, 27, 28, 29, 30, 31], granular flows in different simple configurations [32, 33, 34, 35, 36, 37, 38, 39, 40], granular packing [29, 24], and mechanical strength and failure of granular materials [41, 42, 43, 44]. The viscous effects are mainly considered when dry particles are immersed in a viscous fluid [4, 45, 46, 47]. However, it is necessary to combine the effects of cohesive and viscous stresses in order to account for the influence of the liquid on the static and dynamic states of wet granular materials [48]. Pitois et al. (2000) [49] experimentally studied the effect of these forces on the capillary contact between two moving spheres in different regimes: *capillary* regime, *viscous* regime and *intermediate* regime. The cohesive and viscous forces act within a rupture distance between two moving particles. In the following, we present a brief review of the works in which the effects of the cohesive and viscous forces have investigated separately.

### 1.2.2 Effects of cohesive stress

As mentioned before, the cohesion affects strongly the mechanical and rheological properties of wet granular materials [2, 33, 50]. The action of the cohesion forces such as capillary and van der Waals forces can be split into an internal angle of friction, like in the case of cohesionless granular materials, and a macroscopic cohesion which comes from the aptitude of granular materials to develop tensile stresses [51, 52]. The cohesion stress in combination with granular disorder has important effects on the equilibrium states. The packing fraction varies in a broader range and often long force chains build up despite locally loose structures [53, 54].

The compaction and flowability properties are essential for the manufacture of homo-

geneous and resistant compacts in powder technology [55]. The effects of cohesive stress on granular materials have been investigated by experiments and numerical simulations for a better understanding of the scale-up of interactions between particles. Loose packings characterized by low connectivity and force chain structures have been evidenced in assemblies of grains governed by the cohesion forces [54]. Moreover, the effects of cohesive stresses on the mechanical properties of wet granular materials are mainly governed by the compressive and tensile strengths of wet agglomerates or tablets. The compressive strength of cohesive powder mixtures is an increasing function of the cohesive stress [56]. The diametrical compression test is a simple experiment for measuring the tensile strength of powder compacts.

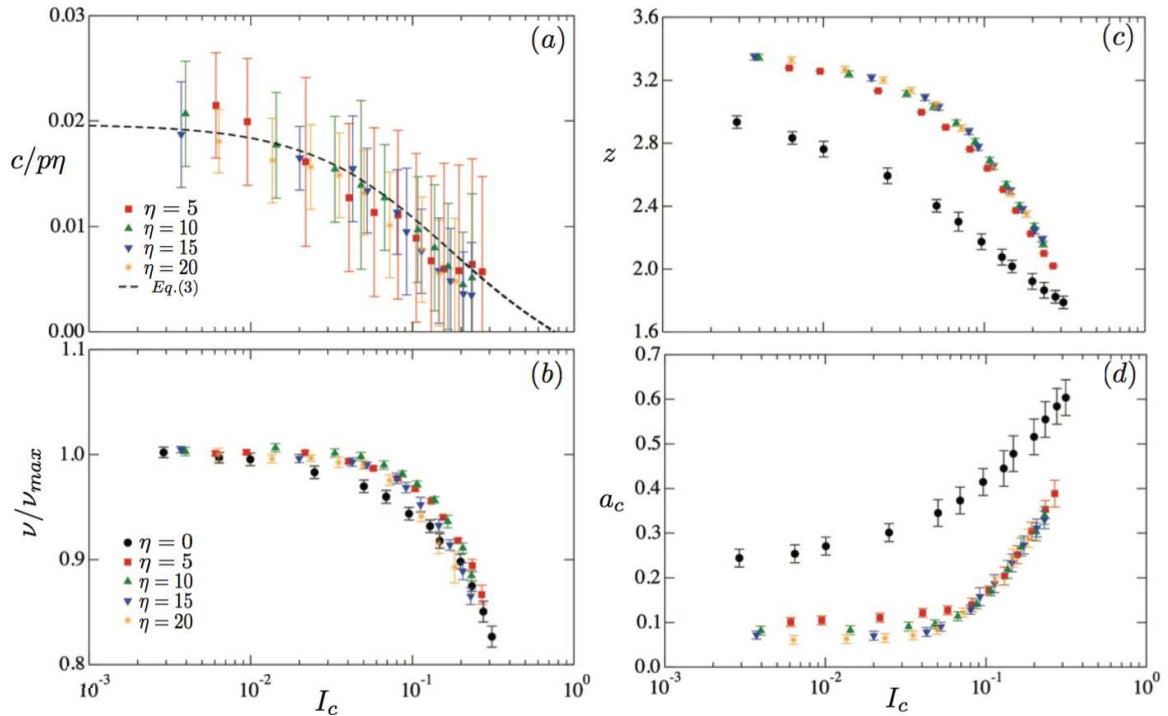


Figure 1.4 – Evolution of normalized cohesion (a), normalized packing fraction (b), coordination number (c), and the contact anisotropy (d) for different values of the cohesion index.[3]

When a cohesive granular material flows, its characteristic cohesive stress  $\sigma_c \simeq f_c/\langle d \rangle^2$  has the same effects as the confining stress  $\sigma_p$ . It tends to prevent the particle from expansion between, enhance the contact forces, and reduce the relaxation of the particles time. Hence, in a cohesive granular flow, two principal macroscopic parameters, the apparent friction coefficient  $\mu$  and packing fraction  $\Phi$  depend also on the cohesion. Note that in cohesionless granular flows, these parameters are defined as a function of the inertial number  $I$ , which only depends on the confining stress  $\sigma_p$ . But, to account for the cohesive stress  $\sigma_c$ , one can replace the confining stress  $\sigma_p$  in the definition of the inertial number  $I$  by

$\sigma_p + \alpha\sigma_c$ , where  $\alpha$  is a weight parameter, which depends on other material parameters of the flow. Consequently, to describe the "cohesive-inertial regimes", a well-defined inertial number  $I_c$  was introduced to quantify the influence of cohesion force [3]:

$$I_c = \dot{\gamma}\langle d \rangle \left( \frac{\rho_s}{\sigma_p + \alpha f_c / \langle d \rangle^2} \right)^{1/2} = \frac{I}{(1 + \alpha\xi)^{1/2}} \quad (1.2)$$

This modified inertial number  $I_c$  is equivalent to the inertial number  $I$  if the cohesion number  $\xi = f_c / \sigma_p \langle d \rangle^2 \rightarrow 0$  (cohesionless flow). By this meaningful variable, Berger et al. (2014) [3] found that the effects of cohesion forces is quite similar to that of particle inertia. This was shown through the scaling of the cohesive strength and granular texture in 2D cohesive granular flows. Not only the cohesive strength and packing fraction but also the granular texture are well described in terms of the modified inertial number  $I_c$  with  $\alpha = 0.08$ ; see Fig. 1.4.

### 1.2.3 Effects of viscous stress

The granular media immersed in a viscous fluid (suspensions) can be found in many natural phenomena such as avalanches, landslides, dune dynamics [57, 58, 59, 60], as well as in various industrial processes and materials (cement, concrete, fluidized bed, granulation, and mixing) [61]. The understanding of the laws governing these mixtures is difficult due to their two-phase nature, involving both a fluid (continuous) and particle (discrete) phase, where particle-particle interactions and fluid-particle interactions contribute to the behavior of the mixture.

For modeling these mixtures, two different points of view can be considered. From the granular point of view, the behavior of a dense granular materials is influenced by the fluid (lubrication force). In the point of view of the fluid mechanics, the rheology of the suspension is modified according to the concentration of the particles [62]. The effective viscosity of the mixtures increases with the density of the particles. The models developed in these fields are problematic when the concentration approaches the critical packing fraction. In this limit, there is also a problem with the principle of constant volume rheometry due to Reynolds dilatancy [45, 63]. Theoretical and experimental models are essentially developed in the two limits respectively dominated by the hydrodynamic forces and by the contact forces.

In the same way as in cohesive granular materials described above, Amarsid *et al.* (2017) [4] numerically simulated granular materials immersed in a viscous liquid by using coupling DEM-Lattice Boltzmann Method in the steady state flow. The granular materials are sheared by the viscous fluid, as shown in Fig. 1.5(a). In this case, the inertial stress of immersed granular flow  $\sigma_i$  is replaced by a linear combination with the viscous stress  $\sigma_\vartheta$ . However, since  $\sigma_\vartheta$  represents only an order of magnitude of the viscous stress, it should be weighted by a coefficient  $\beta$ . Thus, the inertial stress  $\sigma_i$  is replaced by  $\sigma_i + \beta\sigma_\vartheta$ , leading to

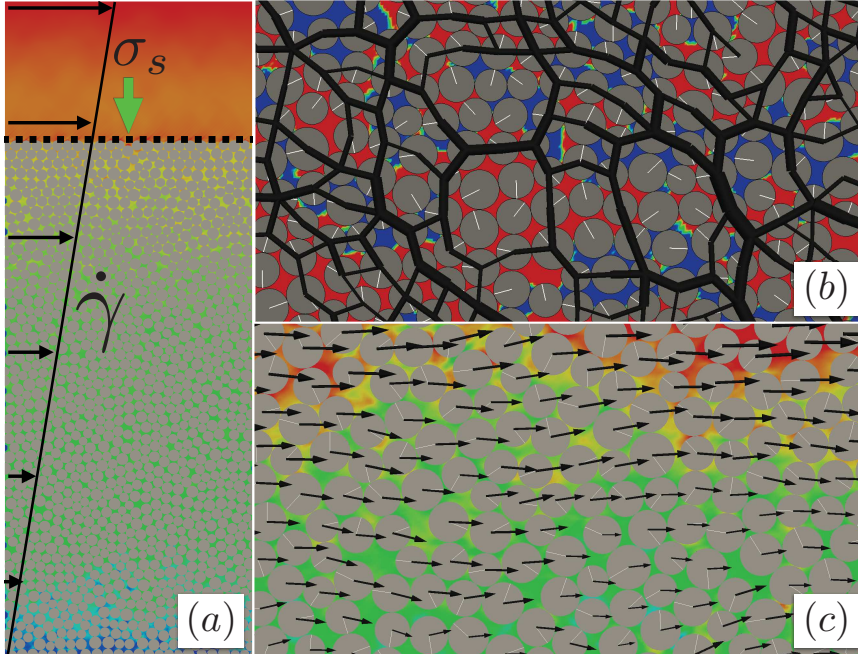


Figure 1.5 – (a) Schematic representation the simulated system of grains immersed in a viscous fluid subjected to the Couette shear flow, (b) Snapshots of fluid pressure field and contact force chains, (c) Snapshots of fluid and particle velocity fields.[4]

the definition of a “visco-inertial” number  $I_m$  (similar to  $I_\vartheta$  in this thesis) by

$$I_\vartheta = I \left( 1 + \frac{\beta}{St} \right)^{1/2}, \quad (1.3)$$

where  $St \equiv \sigma_i/\sigma_\vartheta$  is the Stokes number,  $\beta = 2.0$ . This visco-inertial number scales both the effective friction coefficient  $\mu$  and packing fraction  $\Phi$  for a broad range of values of different control parameters and material parameters of the flow; see Fig. 1.6. The robustness of the visco-inertial regime was also shown for the viscous description of the flow and for granular texture variables.

Amarsid and coworkers extended the scope of a framework introduced by Boyer *et al.* (2011) [45] and Trulsson *et al.* (2012) [46]. Indeed, the analysis proposed by [45] showed that the viscous number  $I_v$  provides a good agreement between the rheology of immersed flows and dry inertial flows. But inertial effects also exist in immersed flows and it is necessary to introduce two additional dimensionless numbers. The flow regimes described by Courrech *et al.* (2003) [64] distinguish these different regimes, but do not allow describing the rheology in a single framework. Trulsson *et al.* (2012) [46] carried out the particle flow simulations using a simple approach that applies the viscous drag force directly to the particles. The effective friction coefficient and packing fraction are nicely fit by replacing  $I$  by  $\sqrt{K}$ , where  $K = J + 0.063I^2$  ( $J \equiv I_v$ ).

These studies on the effects of cohesive and viscous forces on the rheology and texture

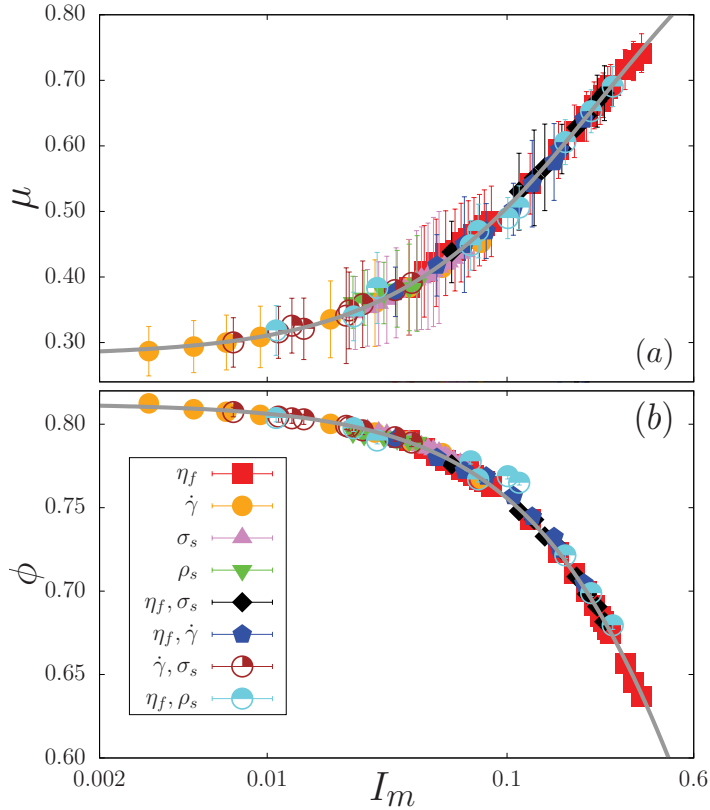


Figure 1.6 – (a) Effective friction coefficient  $\mu$  and (b) packing fraction  $\Phi$  as a function of the visco-inertial number  $I_m$  (similar to  $I_\vartheta$  in this thesis) for different values of liquid viscosity  $\eta_f$ , shear rate  $\dot{\gamma}$ , normal stress  $\sigma_s$ , and particle density  $\rho_s$ . [4]

of wet granular flows, lead to the conjecture that wet granular flows may be fundamentally described by introducing a new dimensionless control parameter based on the addition of cohesive and viscous stresses into the particle inertia which combines all complex interactions including frictional/collisional and viscous/capillary contacts. With this new dimensionless number, the rheology and granular texture of wet granular materials could be scaled on single curves. This issue will be addressed in this thesis.

## 1.3 Agglomeration of granular materials

### 1.3.1 Granulation process

The granulation or agglomeration process of solid particles is a fundamental process in many phenomena occurring in nature and industrial processes, such as pharmaceuticals [65], fertilizers, powder metallurgy [66] and iron-making industry [67, 68, 69]. The enlargement of the size of agglomerates [15] is achieved by collisions of moist particles in a bed

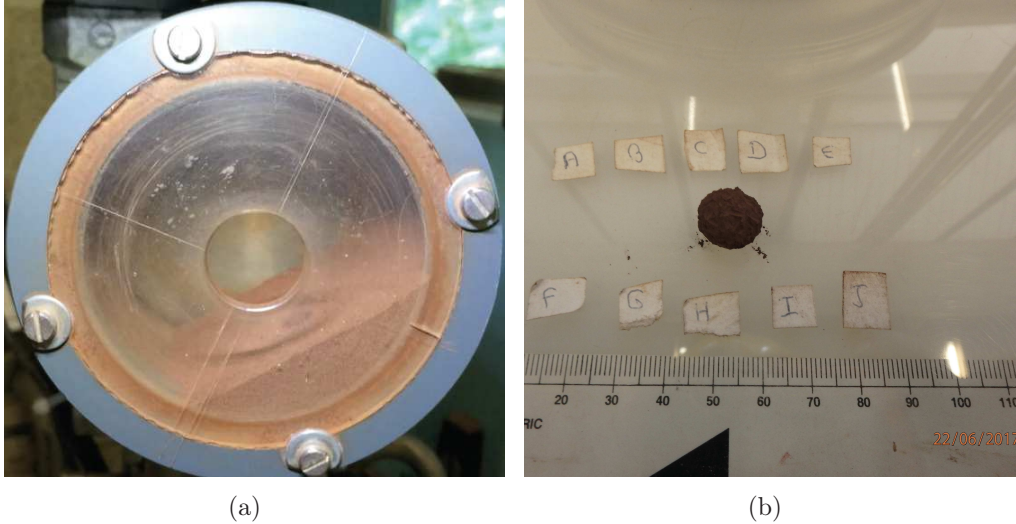


Figure 1.7 – *Experimental drum demonstrating the agglomeration of single wet agglomerate in dense granular flows of dry particles (a), the geometrical granule after 50 rotations of drum (b). Experiments by R. Contreras in CRM Group, Liège.*

undergoing rolling motion [69]. The presence of granules could improve the flow properties, reduce the segregation of different types of particles such as shape, size, mass of primary particles or enhance the permeability for the interstitial gas between grains [20, 70, 71, 72]. The wet particles can be created inside or outside the granulator by mixing raw particles with binding materials which is generally a liquid [72, 73, 74, 75, 76, 77, 78, 79, 80]. Hence, the size and the growth rate of agglomerates in rotating drum are governed by the agglomeration of small primary particles with the activation of the capillary cohesion forces and viscous forces due to the presence of liquid bonds [73, 81, 82, 83, 84, 85].

The agglomeration should produce granules with high packing fraction and homogeneous distribution of primary raw particles in order to get large size and high strength [86, 87, 88, 89, 90]. The size, granule growth, strength, and texture of agglomerates depend on different types of control parameters. They can be divided into two different classes: process and material parameters. The process parameters mainly come from the method of mixing solid particles with the binding liquid, the amount of liquid volume [69, 91, 92], the granulator size such as the size ratio between drum and primary particles diameter, the rotation speed of granulator, the horizontal or inclined drum [93, 94, 95], the filling degree [96], and the drum with or without scraper bar (flights) [97, 98]. The material parameters such as the binding liquid and raw material properties include liquid viscosity, size distribution, mean particle size and friction coefficient of raw particles [78, 92, 99]. It is necessary to investigate the effects of these parameters on the agglomeration process although the growth of agglomerates in a rotating drum is not simple as it involves the transport of the binding liquid inside the partially wet granule and inside the flowing particles, and collisions between wet and dry particles [73, 100, 101, 102, 103, 104]. Hence,

the assumption of binary collisions between wet particles is a simplified but efficient way of modeling the granulation in a fluidized bed in a horizontal rotating drum [79, 80, 105].

We also note that there are three stages in the agglomeration process [106, 87, 107]: wetting and nucleation, coalescence and consolidation, and attrition and breakage. In the wetting and nucleation stage, the binding liquid is sprayed or poured or dripped into the powder mix of dry granular materials in order to form sticky surface and nuclei granules. During the drum rotations, the coalescence and consolidation or growth of agglomerates could occur due to the collisions between granules or granules and feed powder. Due to the interactions between dry particles or granulator equipment and wet granules, the attrition and breakage of granules could appear, wet agglomerates may break into smaller granules. These phenomena depend on the material properties as well as the dynamic nature of granular materials. In order to design and control the agglomeration process of wet granular materials, a better understanding of the dynamic flow of granular materials in a rotating drum is necessary.

### 1.3.2 Froude number and flow regimes

The rheology of dense granular flow has been investigated in rotating drums by means of careful experiments [25, 67, 108, 109, 110], simulations [91, 111, 112, 113]. The granular flow in a rotating drum is often described by a flowing active free surface layer taking place on a dense packing driven by drum rotation. The particles placed at the top of the free surface tend to reach a highest velocity when activating the rotation of drum. This velocity in the surface flowing layer decreases essentially linearly with the depth of the granular bed and tends to reach zero at the plane which divides the granular bed into two flow regions: active and passive flows.

The dynamic properties of wet granular flows in a rotating drum depend on the filling rate, rotation speed  $\omega$  of the granulator and its radius  $R$ . The effect of centrifugal forces is quantified by its ratio to the gravity, which defined the Froude number

$$Fr = \omega^2 \frac{R}{g}. \quad (1.4)$$

Depending on the  $Fr$  or  $R$ , the flow can occur in different regimes described as slumping, surging, rolling, cascading, cataracting and centrifuging regimes [110, 114, 115], see Fig. 1.8.

The flow regimes of dry granular materials in a rotating drum depend on the Froude number  $Fr$ , but also filling rate and friction conditions between particles drum walls. With small values of Froude number and smooth cylinder walls, the *Slipping* regime can occur, as shown in Fig. 1.8(a). The granular bed reaches a constant sliding state on the wall. When the wall friction is increased, the *slipping* regime turns to *surging* regime, where the granular bed adheres to the rotating wall up to a high angle and subsequently slides back to the lowest position of the drum, see Fig. 1.8(b). The mixing of particles can not take place in the slipping and surging regimes. With the increase of the drum wall friction, filling rate and rotation speed, the *rolling* regime is observed. In this regime, the granular bed

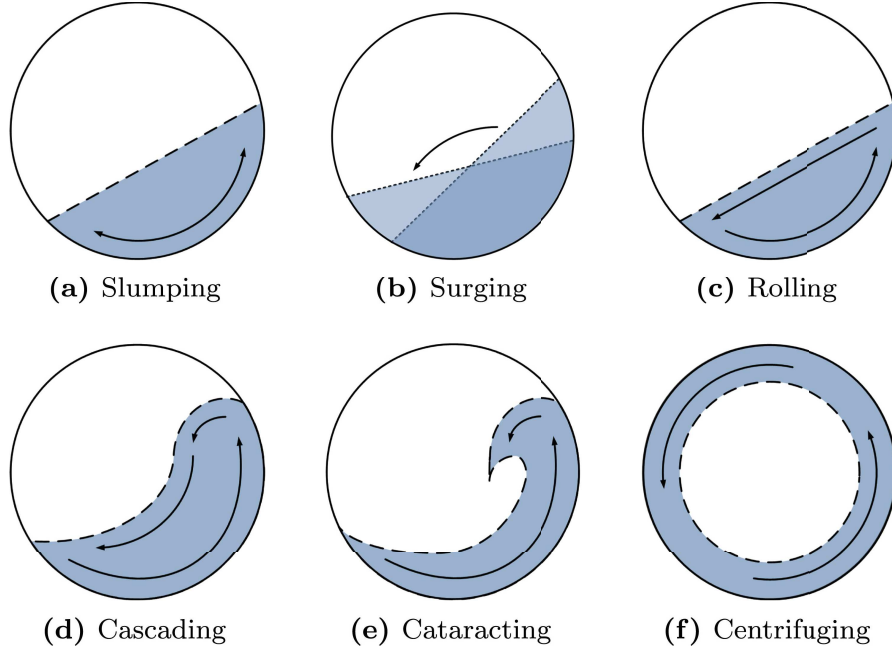


Figure 1.8 – Six flow regimes of granular materials in a rotating drum by increasing the Froude number  $Fr$  or drum size.

is always divided into two parts: active and passive regions. The particles flow downward in the active region, whereas the particles are transported upwards by solid body rotation with the rotation of drum in the passive regime. The thickness of the active flow always is nearly one third of that of the passive layer [116]. The *cascading* regime is observed for larger values of the Froude number. The free surface of granular flow has a curved shape due to centrifugal forces and inertial flow at the free surface. For further increase of  $Fr$ , the flow enters the *cataracting* regime, where the particles detach from the bed of the granular flow and follow a ballistic motion towards the free surface downstream; see Fig. 1.8(e). For even larger values of  $Fr$ , the particles begin to adhere to the drum wall and the *centrifuging* regime is observed, as shown in Fig. 1.8(f). In the granulation process, the particles should be well-mixed and undergo fluctuating motions. Thus, granular flows in the intermediate state between rolling and cascading regimes are appropriate geometries for the granulation of wet particles.

### 1.3.3 Relation between agglomeration and flow properties

The growth of wet agglomerates could modify the rheological properties of granular materials and may improve the flow properties, reduce the segregation of different types of granular materials or enhance the permeability for the interstitial gas between grains [72, 71, 117, 106]. Fine powders often exhibit flow problems in a hopper, bin or silo such as flow arrest, erratic flow, and limited discharge rates. Reduced flow speed or flow arrest

is due to the presence of attraction forces such as capillary cohesion force or van der Waals force between particles within the granular flow. If the cohesive strength is large enough, the flow becomes stable as flow channel empties, the flow arrest may occur. In the rotating drum, wet granular materials are often less sensitive than dry materials. Wet agglomerates may prevent the free rolling and moving of dry granular materials. This phenomenon creates the higher value of the dynamic angle of repose compared to the dry case. This means that the materials need higher potential energy for the avalanches to occur. Our numerical results will confirm the modifications of rheological properties of granular materials via a modified inertial number  $I_m$  incorporating the cohesive and viscous forces with the particle inertia. The increase of the dynamic angle of repose or the liquid volume cause also the reduction of the axial and radial segregations of particles [72].

On the other hand, the flow properties of granular materials directly affect the behavior, microstructure, and mechanical strength of the granules. Besides the effects of material parameters such as the particle size distribution, the mean particle diameter, and the properties of the binding liquid, the granule growth and properties depend on the nature of flow in the rotating drum. The interactions between the granule and the flow may lead to the consolidation of the granule provided the local stresses arising from inertial effects or capillary forces are not too strong to damage the granule or erode it [26, 73, 88]. These interactions lead to the accretion, coalescence and consolidation of granules. The consolidation requires the decrease of porosity inside wet agglomerates since the granule properties such as strength and hardness are directly related to the internal porosity. If the inertial forces too high, the erosion or attrition and breakage phenomena will reduce the size of the granules.

The issue is that the flow properties of granular materials in a rotating drum are complicated due to different flow properties in different parts of the drum (active, passive, and non-flow regions). Thus, the rates of accretion, erosion, and breakage of wet agglomerates depend on the positions of the granule. The coalescence and consolidation may take place mostly in the passive region of granular flow in a rotating drum where the inertial number  $I$  is small enough to allow for a long-time interaction between agglomerates and diffusion of the binding liquid whereas the erosion and breakage may more easily occur in the active region and close to the free surface where the flow is rapid and impacts are strong enough to detach the primary wet particles from the agglomerate surface or break it into smaller agglomerates.

In order to deal with such difficulties, simplified systems and configurations have been used to study wet agglomeration. Lefebvre *et al.* [25] experimentally investigated the erosion dynamics of a fixed granule at the center of drum and impacted by dry granular flows in a half-filled rotating drum. The dry particles flow around the fixed obstacle during the drum rotation. They found that the granule diameter decreases linearly with time for different values of the liquid properties such as surface tension and viscosity, and the erosion is governed by very strong force chains and may occur even for strongly bonded granules. Lefebvre and coworkers also studied the erosion of a wet granular pile by a dry dense granular flow [118]. The instability of the wet granular pile strongly depends on the flow properties of dry granular materials characterized by the flowing angle of the confined

flow on a dry heap. The accretion dynamics of dry particles on wet agglomerate was experimentally studied by Saingier and coworkers [39]. The granule was fully saturated and the growth dynamics of wet agglomerate is controlled by the liquid fraction on the granule surface.

Besides the accretion and erosion dynamics of wet agglomerates inside granular flows, the deformation and breakage behaviors of granules have also been considered in simple shear flows [119, 120, 121, 122, 123, 124, 125, 126, 127, 128]. The single wet agglomerate made of sticky primary wet particles is embedded in a granular bed of dry granular materials. The wet granule can be deformed or broken into small aggregates due to the effects of interface energy between the primary particles, which depends on the size ratio between the granule and surrounding particles [126, 127, 128, 129, 123]. However, all those previous investigations did not consider the viscous effects of the binding liquid.

## 1.4 Numerical method

### 1.4.1 Discrete Element Method

The Discrete Element Method (DEM) has been extensively used for the simulation of granular materials [130, 131, 132, 133]. It is based on the step-wise integration of the equations of motion for all particles by taking into account the particle interactions. In advanced applications of the DEM, it is now possible to implement also the presence of an interstitial fluid or a solid binding matrix [81, 134]. However, such applications require substantially more computation power and memory in order to discretize the degrees of freedom associated with the interstitial phase. For this reason, in DEM simulations of wet granular materials, it is necessary to set up a modeling strategy by making appropriate choices that allow for a balance between computational efficiency (large number of particles) and physical realism. In the case of unsaturated wet granular materials, it is found that the fluid phase can be correctly represented by its cohesive and viscous effect in the particle-particle interactions [135]. Hence, we rely on this approach to model the binding liquid in different examples of wet granular materials.

The Molecular Dynamics (MD) method is simple and flexible, and provides a versatile tool for the simulation of model granular materials [133]. This method applies Newton's second law together with contact interactions to determine the contact forces between particles at each time step. The flexibility of the MD numerical scheme is mainly based the possibility of choosing different types of contact force laws. These could include elastic repulsion, friction, cohesion and external forces. The method is also really general because it could be used in order to model a wide range of granular phenomena such as dry and wet granular flows, agglomeration processes, compression tests for different models of granular materials, or coupling with Lattice Boltzmann Method (LBM) [136, 84, 4] or Computational Fluid Dynamics (CFD) techniques [137, 138, 139] in order to simulate the fluid-grain interactions in various cases in nature and industry. In the following, we present the numerical approach used in this thesis.

### 1.4.2 Contact force laws

In the DEM, the particles interact via visco-elastic forces as a function of the local contact strain defined from the relative displacements of the particles. Since the particles are assumed to be rigid, a large repulsive stiffness and thus a high time resolution is required for the calculation of the interactions between particles. The motion of each rigid spherical particle  $i$  of radius  $R_i$  is governed by Newton's second law under the action of normal contact forces  $f_n$ , tangential contact forces  $f_t$ , capillary forces  $f_c$ , viscous forces  $f_{vis}$  and particle weight  $m_i \mathbf{g}$ :

$$\begin{aligned} m_i \frac{d^2 \mathbf{r}_i}{dt^2} &= \sum_j [(f_n^{ij} + f_c^{ij} + f_{vis}^{ij}) \mathbf{n}^{ij} + f_t^{ij} \mathbf{t}^{ij}] + m_i \mathbf{g} \\ \mathbf{I}_i \frac{d\boldsymbol{\omega}_i}{dt} &= \sum_j f_t^{ij} \mathbf{c}^{ij} \times \mathbf{t}^{ij} \end{aligned} \quad (1.5)$$

where  $\boldsymbol{\omega}_i$  is the rotation vector of particle  $i$ , and  $m_i$ ,  $\mathbf{I}_i$ ,  $\mathbf{r}_i$  and  $\mathbf{g}$  are the mass, inertia matrix, position and gravity acceleration vector of particle  $i$ , respectively.  $\mathbf{n}^{ij}$  denotes the unit vector perpendicular to the contact plane with particle  $j$  and pointing from  $j$  to  $i$ ,  $\mathbf{t}^{ij}$  is the unit vector belonging to the contact plane  $ij$  and pointing in the direction opposite to the relative displacement of the two particles and  $\mathbf{c}^{ij}$  is the vector pointing from the center of particle  $i$  to the contact point with particle  $j$ . The tangential viscous dissipation, as compared to the normal lubrication force, is neglected [25]. The equations of motion are integrated according to a velocity-Verlet time-stepping scheme [133, 140].

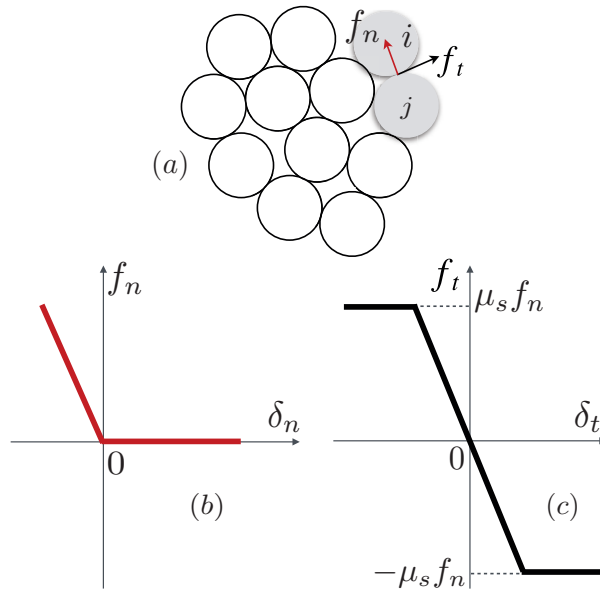


Figure 1.9 – Schematic representation contact force laws in the DEM.

The normal contact force  $f_n$  involves two components [36, 44, 141]:

$$f_n = f_n^e + f_n^d . \quad (1.6)$$

The normal elastic force  $f_n^e = k_n \delta_n$  is a linear function of the normal elastic deflection  $\delta_n$ , with  $k_n$  as the normal stiffness constant, and the normal damping force  $f_n^d = \gamma_n \dot{\delta}_n$  is proportional to the relative normal velocity  $\dot{\delta}_n$ , with  $\gamma_n$  as the normal viscous damping parameter. These both forces appear only when there is an overlap, i.e. for  $\delta_n < 0$ .

The tangential contact force  $f_t$  is the sum of an elastic force  $f_t^e = k_t \delta_t$  and a damping force  $f_t^d = \gamma_t \dot{\delta}_t$ , where  $k_t$  is the tangential stiffness,  $\gamma_t$  denotes the tangential viscous damping parameter and  $\delta_t$  and  $\dot{\delta}_t$  are the tangential displacement and velocity in contact, respectively. According to the Coulomb friction law, the tangential force is bounded by a force threshold  $\mu f_n$ , where  $\mu$  is the friction coefficient [38, 142, 143, 144]. Both the normal and tangential contact forces are shown in Fig. 1.9:

$$f_t = -\min \left\{ (k_t \delta_t + \gamma_t \dot{\delta}_t), \mu f_n \right\} . \quad (1.7)$$

### 1.4.3 Capillary cohesion and viscous forces

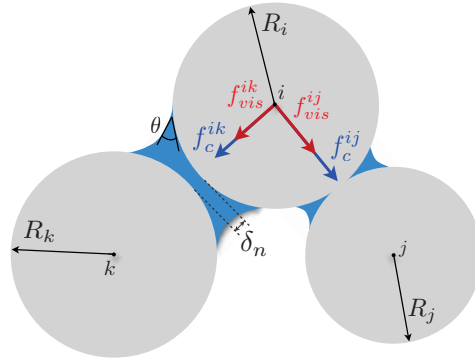


Figure 1.10 – Schematic drawing of two different cases of capillary bridges: particle  $i$  in contact with particle  $j$  and without contact with particle  $k$ .

Recent experiments and numerical simulations show that the liquid clusters condensed from a vapor or introduced by mixing the liquid with particles can be characterized by their connectivity with the particles [82, 84]. The number of liquid clusters connected to two particles prevails for low amounts of the liquid. In this thesis, we simulate wet granular materials in the ‘pendular’ regime in which, the liquid is in the form of binary bridges. As the amount of liquid increases, the clusters involve more and more particles until a single cluster spans the whole packing. The cohesive effect of the liquid in thermodynamic equilibrium is controlled by the total wetted surface and the Laplace pressure. The cohesion rapidly increases as the amount of liquid is increased in the pendular state, and then, it

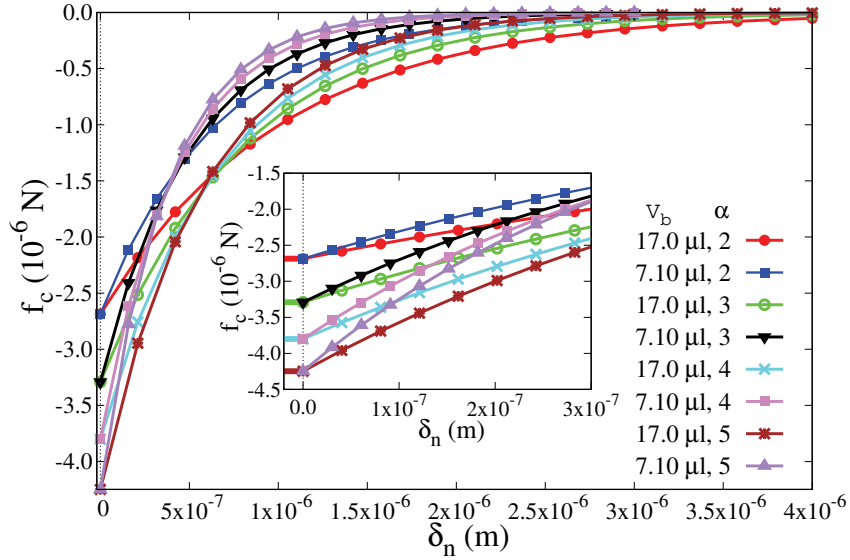


Figure 1.11 – Capillary cohesion force  $f_c$  decreases in absolute value as a function of the gap  $\delta_n$  between two particles in the capillary bridge contact for different values of the liquid volume  $V_b$  of capillary bond. The capillary force exists up to the rupture distance  $d_{rupt}$ .

keeps a nearly constant value (or slightly increases) with increasing amount of the liquid before declining for large amounts of the liquid [82, 84].

This description assumes, however, that the particles are in quasi-static equilibrium and the liquid is in thermodynamic equilibrium. The negative Laplace pressure within the liquid phase is not uniformly distributed if the system is out of equilibrium. Furthermore, if the granular material flows, the liquid clusters undergo large distortions, and the liquid is continuously re-distributed as a result of coalescence and separation of liquid clusters [145, 146]. In practice, a small amount of the added liquid is adsorbed into the particle rough surfaces and is not directly involved in capillary bonding between particles.

These features suggest that in wet granular materials, for a broad range of the amounts of liquid, the cohesive capillary stress is nearly independent of the amount of liquid, and therefore the effect of liquid volume can be accounted for by the number of wet particles. In the same way, the viscous effects of the binding liquid also need to be considered to reflect exactly the fluid-grains interactions in wet granular materials. Due to the domination of normal cohesive and viscous effects compared to tangential cohesive and viscous forces, we considered only first-order theoretical expressions (normal components) of the capillary force  $f_c$  and viscous force  $f_v$  acting between two particles; see Fig. 1.10.

The capillary attraction force  $f_c$  between two particles of radii  $R_i$  and  $R_j$  acts along the axis joining the particle centers. This cohesion force is a function of the liquid volume  $V_b$  of the capillary bond, liquid-vapor surface tension  $\gamma_s$  and particle-liquid-gas contact angle  $\theta$  [36, 81, 135]; see Fig. 1.10. The capillary force is obtained by integrating the Laplace-Young equation [81, 105, 147]. In the pendular state, an approximate solution is given by

the following expression [38, 44, 148, 149], which is in good agreement with experiments [21, 105]:

$$f_c = \begin{cases} -\kappa R, & \text{for } \delta_n < 0, \\ -\kappa R e^{-\delta_n/\lambda}, & \text{for } 0 \leq \delta_n \leq d_{rupt}, \\ 0, & \text{for } \delta_n > d_{rupt}, \end{cases} \quad (1.8)$$

where  $R = \sqrt{R_i R_j}$  is the geometrical mean radius of two particles of radii  $R_i$  and  $R_j$  and the capillary force pre-factor  $\kappa$  is [38]:

$$\kappa = 2\pi\gamma_s \cos \theta. \quad (1.9)$$

This force exists up to a debonding distance  $d_{rupt}$  given by [81]

$$d_{rupt} = \left(1 + \frac{\theta}{2}\right) V_b^{1/3}. \quad (1.10)$$

The characteristic length  $\lambda$  in equation (1.8) is given by

$$\lambda = c h(r) \left(\frac{V_b}{R'}\right)^{1/2}, \quad (1.11)$$

where  $R' = 2R_i R_j / (R_i + R_j)$  and  $r = \max\{R_i/R_j; R_j/R_i\}$  are the harmonic mean radius and the size ratio between two particles.

The expression (1.8) nicely fits the capillary force as obtained from direct integration of the Laplace-Young equation by setting  $h(r) = r^{-1/2}$  and  $c \simeq 0.9$  [24, 36, 38]; see Fig. 1.11. It is also very close to the expression used in [22].

The normal viscous force  $f_{vis}$  is due to the lubrication effect of liquid bridges between particles. Its classical expression for two smooth spherical particles is [25, 150]:

$$f_{vis} = \frac{3}{2}\pi R^2 \eta \frac{v_n}{\delta_n}, \quad (1.12)$$

where  $\eta$  is the liquid viscosity and  $v_n$  is the relative normal velocity assumed to be positive when the gap  $\delta_n$  is decreasing. This expression implies that the viscous force diverges when the gap  $\delta_n$  tends to zero. With this singularity, two rigid particles can not collide in finite time. However, for slightly rough particles, the surfaces are no longer parallel and the characteristic size of the asperities allows for collision in finite time. Hence, we introduce a characteristic length  $\delta_{n0}$  representing the size of asperities and assume that the lubrication force is given by:

$$f_{vis} = \frac{3}{2}\pi R^2 \eta \frac{v_n}{\delta_n + \delta_{n0}} \quad \text{for } \delta_n > 0, \quad (1.13)$$

as long as  $\delta_n > 0$ , i.e. for a positive gap. This expression ensures that the singularity will not occur as long as there is no contact. When a contact occurs, i.e. for  $\delta_n < 0$ , we assume that the lubrication force remains equal to its largest value given by

$$f_{vis} = \frac{3}{2}\pi R^2 \eta \frac{v_n}{\delta_{n0}} \quad \text{for } \delta_n \leq 0. \quad (1.14)$$

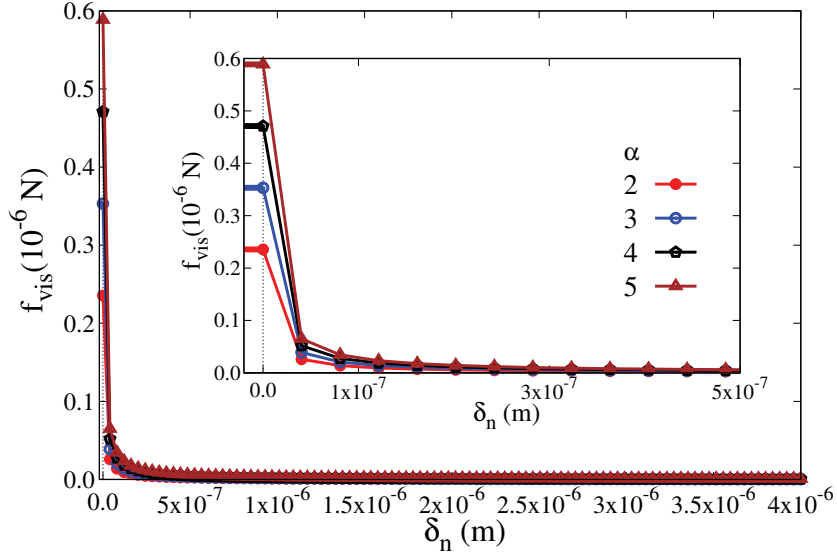


Figure 1.12 – Viscous force  $f_{vis}$  declines as a function of the gap  $\delta_n$  between two particles in the capillary contact for different values of the size ratio  $\alpha$  which is the ratio between the largest and smallest particle diameter. The viscous force exists up to the rupture distance  $d_{rupt}$ . This force is plotted for systematic parameters in Chapter 3 and keeping a fixed relative normal velocity  $\dot{\delta}_n = 5.10^{-3}$ .

In this thesis, the value of  $\delta_{n0}$  is chosen depending on the smallest particles size  $d_{min}$  in each simulated model. This value is small enough to allow lubrication forces to be effective without leading to its divergence at contact. Depending on different studies, the capillary cohesion and viscous forces can be activated together or separately and this will be clearly mentioned for each study presented in this thesis.

## 1.5 Conclusion

In this chapter, we presented a general description of the scientific context regarding wet granular flows and the agglomeration process of solid particles in a rotating drum. We first introduced different studies on the granular flows for both dry and wet granular materials. The rheology of non-cohesive and cohesive granular flows can be controlled by the well-defined of inertial number and modified inertial number, respectively. Obviously, most of granular materials in nature and industrial processes contain the humidity. The interstitial liquid is characterized by the cohesive and viscous effects, which may strongly affect the rheology and microstructure of granular materials. We mentioned several previous studies on the agglomeration processes of wet particles in different configurations.

Through several examples and descriptions of previous investigations, we have illustrated some open issues that are both fundamental and applicative. We also highlighted

the potential contribution of numerical simulations in this field and introduced the numerical approach that will have been used in this thesis. This approach is based on the DEM or, equivalently, Molecular Dynamics method with the capillary cohesion law and lubrication force law in the pendular regime.

*“A new idea comes suddenly in a rather intuitive way but intuition is nothing but the outcome of earlier intellectual experience”*

---

Albert Einstein (1879-1955)

## Chapter 2

# Additive rheology of inertial flows of cohesive particles

This chapter is a reproduction of a submitted paper.

 Granular flows are omnipresent in nature and industrial processes, but their rheological properties such as apparent friction and packing density are still elusive when inertial, cohesive and viscous interactions occur between particles in addition to frictional and elastic forces. Relying on extensive particle dynamics simulations of a model granular system, we show that such complex flows of perfectly rigid particles are governed by a single dimensionless number that, by virtue of stress additivity, accounts for all interactions. We also find that the same dimensionless parameter describes the texture variables such as the contact network connectivity and anisotropy. Encompassing various sources of internal stresses, this unified framework considerably simplifies and extends the modeling scope for granular dynamics, with potential applications in powder technology and risk assessment in natural flows.

## Contents

---

<b>Introduction</b> . . . . .	<b>29</b>
<b>Results</b> . . . . .	<b>31</b>
<b>Discussion</b> . . . . .	<b>37</b>
<b>Method</b> . . . . .	<b>38</b>
<b>Supplemental Material</b> . . . . .	<b>39</b>

---



## Introduction

The crucial role of granular flows in nature (landslides, debris avalanches, slope failure) [151, 152, 153, 154, 155, 156, 157, 158] and industrial processes (handling powders and granulates, additive manufacturing) [105, 88, 70, 33, 117] has been at the focus cross-disciplinary research for more than thirty years [159, 160]. Recent progress in theoretical understanding of granular flows has been mainly inspired by collective effects such as force chains and jamming [161, 162, 163, 164, 165, 24, 166, 167, 168, 169], and by searching for relevant dimensionless control parameters [1, 10, 5, 45, 170, 46, 3, 22, 171, 4, 23]. Basic model granular media are composed of rigid particles with frictional contact interactions and, in contrast to interacting particles at the atomic scale or in colloids, rigid frictional particles are devoid of an intrinsic stress or time scale. The relevant scales are therefore set either externally, such as those arising from a confining pressure  $\sigma_p$ , or by the flow itself as a result of collective particle motions. The granular flow generates an inertial pressure (or kinetic pressure)  $\sigma_i \sim \rho_s \langle d \rangle^2 \dot{\gamma}^2$ , where  $\rho_s$  is the particle density,  $\langle d \rangle$  is the mean particle diameter, and  $\dot{\gamma}$  is the shear rate [172, 10]. Therefore, in a NPT statistical ensemble, the normalized shear strength  $\mu = \tau/\sigma_p$  (apparent friction coefficient) and packing fraction  $\Phi$  are expected to be uniquely dependent on the ratio  $I^2 \equiv \sigma_i/\sigma_p$ , which represents the competing effects of particle inertia and confinement. The dimensionless number  $I$  is the *inertial number*, defined as the ratio of two time scales (relaxation time  $\langle d \rangle (\rho_s/\sigma_p)^{1/2}$  under load vs. shear time  $\dot{\gamma}^{-1}$ ), and it was found to unify experimental and numerical data in different flow geometries [1].

Most of time, however, the particle interactions are not purely frictional and involve characteristic forces inducing additional internal stresses. A well-known example is the cohesive contact force  $f_c$  in fine powders. When a powder flows, the average action of the resulting cohesive stress  $\sigma_c \sim f_c/d^2$  is similar to a confining stress, tending to prevent from dilation during flow, to enhance the contact forces and to reduce the relaxation time under load [36, 32, 3]. As the stresses are additive, one may thus take the cohesive stress into account on the same footing as the confining pressure by replacing  $\sigma_p$  by a linear combination  $\sigma_n = \sigma_p + \alpha\sigma_c$  of confining and cohesive stresses, and therefore replacing  $I^2$  by  $I_c^2 \equiv \sigma_i/\sigma_n = I^2/(1 + \alpha\xi)$ , where  $\xi = \sigma_c/\sigma_p$  is the cohesion index [3]. In the same way, in immersed granular flows, where the viscous drag force  $\sigma_v$  is present,  $\sigma_i$  may be replaced by a linear combination  $\sigma_i + \beta\sigma_v$ , leading to a visco-inertial number  $I_v^2 \equiv (\sigma_i + \beta\sigma_v)/\sigma_p = I^2(1 + \beta/\text{St})$ , where  $\text{St} \equiv \sigma_i/\sigma_v$  is the Stokes number. In dense suspensions,  $I_v$  is found to be the control parameter for both  $\mu$  and  $\Phi$  [46, 4].

The above examples lead to the conjecture that granular flows are fundamentally governed by a single dimensionless parameter combining arbitrary particle interactions by virtue of stress additivity. In this chapter, we address this interesting issue by simulat-

ing wet granular flows such as unsaturated soils and powders at high relative humidity. The liquid bridges between particles induce both capillary and viscous (lubrication) forces whose effects on the flow behavior, together with the confining and inertial stresses, will be quantified for an extensive range of parameter values, which are generally difficult to access by means of experiments. Our results convincingly demonstrate the above conjecture and set the foundation for a unified description of complex granular flows.

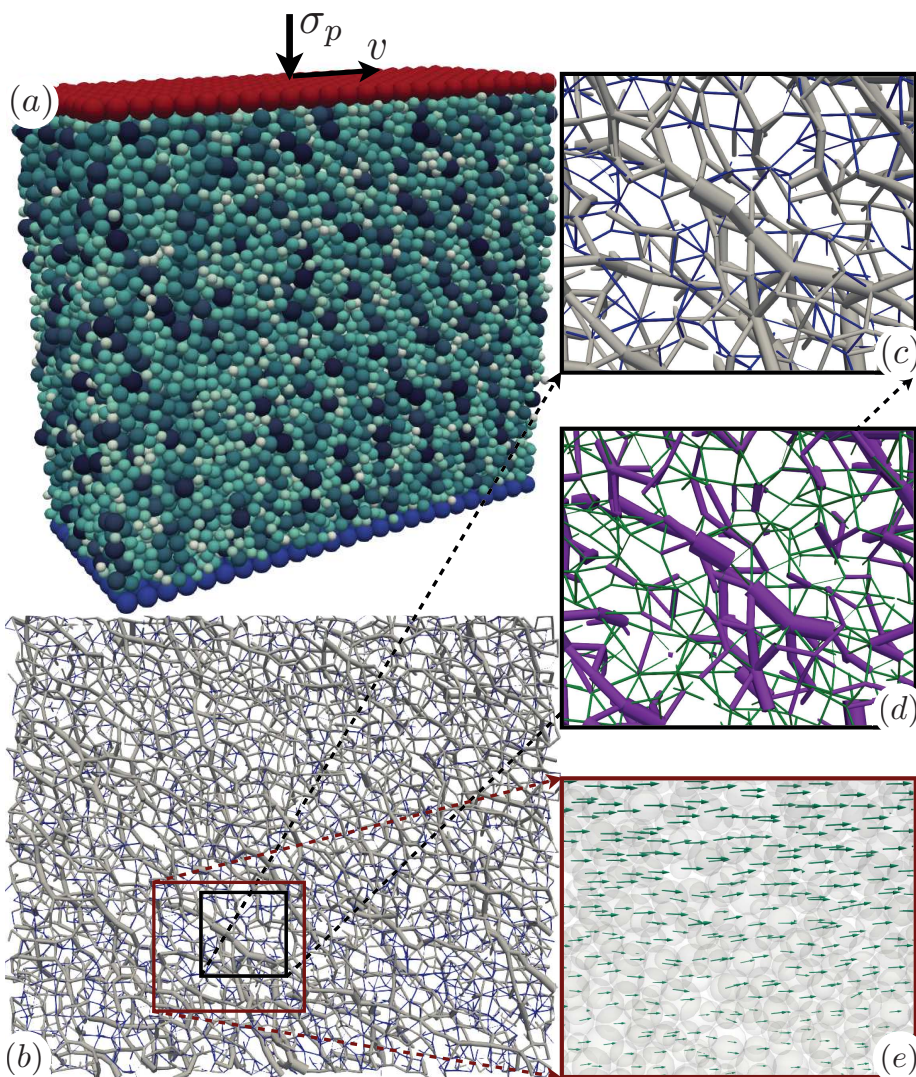


Figure 2.1 – (a) Simulated system of wet spherical particles under a constant confining stress  $\sigma_p$  and sheared by a constant horizontal velocity  $v$  of the top rough wall. The particle colors are proportional to particle diameters. (b, c) Snapshot of compressive (grey) and tensile (blue) force chains. Line thickness is proportional to normal force. (d) Snapshot of contact forces (violet) and non-contact capillary forces (green). (e) Snapshot of the particle velocity field in steady flow.

## Results

We performed extensive 3D long-shear simulations of granular samples composed of nearly 20,000 spherical particles by means of a particle dynamics method and with a broad range of the values of liquid viscosity  $\eta$ , surface tension  $\gamma_s$ , confining stress  $\sigma_p$  and shear rate  $\dot{\gamma}$ . Our results are based on the average values of the stress tensor, velocity fields, packing fraction and granular texture in steady flow of the particles in the simulation cell between top and bottom walls with periodic boundary conditions in the other directions. Besides repulsive elastic force and friction force, the particle interactions include the first-order theoretical expressions of capillary force  $f_c$  and viscous force  $f_v$  acting between neighboring particles (see Methods section). The snapshots of Fig. 2.1 show the boundary conditions, compressive and tensile force chains, contact and non-contact forces (due to capillary bridges) and particle velocities in steady flow.

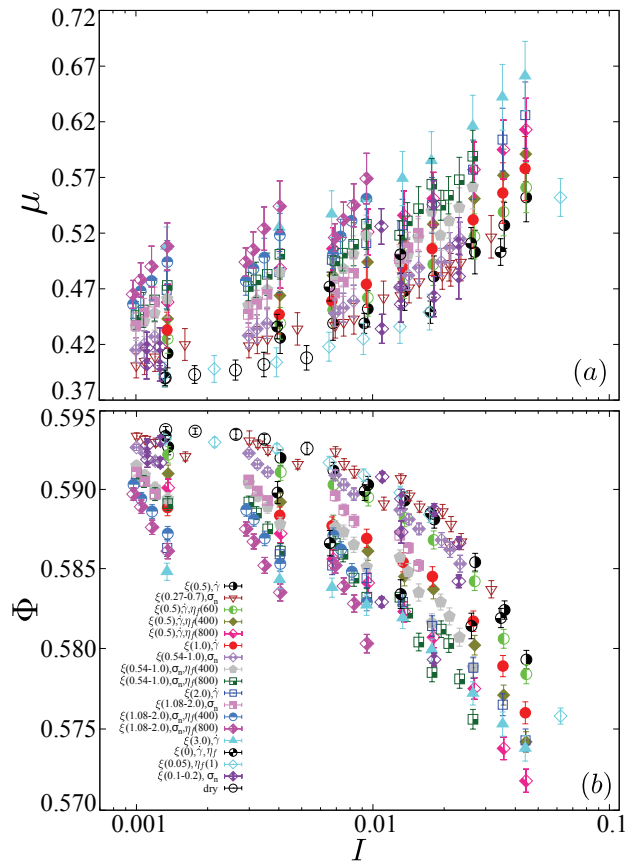


Figure 2.2 – Apparent friction coefficient  $\mu$  (a) and packing fraction  $\Phi$  (b) as a function of the inertial number  $I$ . The data are averaged over the steady state. The error bars represent the standard deviation of the data in each simulation. For each set of simulations, the symbols and their colors correspond to the parameters that are varied with their ranges, all other parameters being kept constant.

Figure 2.2 displays the apparent friction coefficient  $\mu$  and packing fraction  $\Phi$  as a function of the inertial number  $I$  for all our 281 simulations. The confining pressure  $\sigma_p$  was varied in the range [15, 1000] Pa, the cohesion index  $\xi$  in the range [0, 3.0] (by varying  $\gamma_s$  or  $\sigma_p$ ), the liquid viscosity  $\eta$  in the range  $[\eta_w, 800\eta_w]$  (Since we have dry case we should use a range of  $\eta$  between  $[0 \eta_w, 800 \eta_w]$ ), where  $\eta_w$  is the water viscosity, and the shear rate in the wide range  $[0.31, 10.6] \text{ s}^{-1}$ . As in dry flows [10],  $\mu$  increases and  $\Phi$  declines with increasing  $I$  but with different values and at different rates depending on the viscosity and cohesion index. These differences are observed at both low values (quasi-static flow) and high values (inertial flow) of  $I$ , and the variability of  $\mu$  and  $\Phi$  with the variation of  $I$  is of the same order of magnitude as with viscous and cohesive parameters.

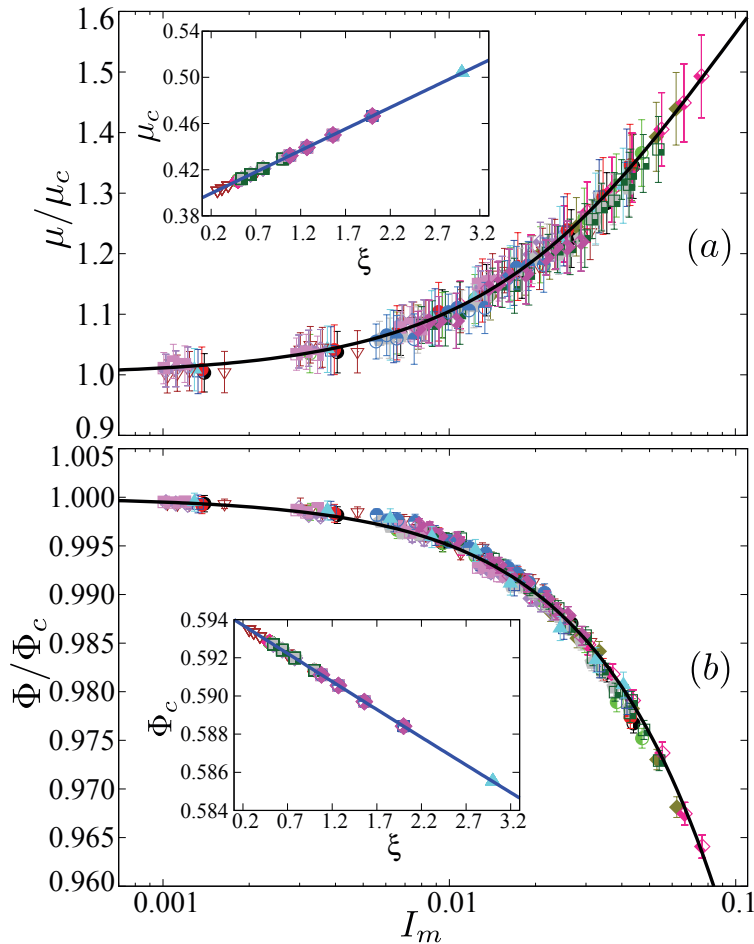


Figure 2.3 – (a) Normalized effective friction coefficient  $\mu/\mu_c$  and (b) normalized packing fraction  $\phi/\phi_c$  as a function of the modified inertial number  $I_m$  defined by equation (2.1) with  $\alpha \simeq 0.062$  and  $\beta \simeq 0.075$ . The error bars represent the standard deviation over the steady state. The black-solid lines are analytical expressions (2.6) and (2.7). The insets show the evolution of the quasistatic functions  $\mu_c$  and  $\Phi_c$  with the cohesion index  $\xi$ , with linear fits (blue-solid lines).

The issue is whether all these different values of apparent friction and packing fraction can be expressed as a collapsed function of a single dimensionless number combining surface tension, liquid viscosity, confining pressure and shear rate. In other words, can  $I$  be replaced by a more general inertial number  $I_m$  that simultaneously accounts for the capillary, viscous and inertial forces? This is indeed what we observe in Fig. 2.3, displaying all the data points of Fig. 2.2 as a function of a modified inertial number defined by

$$I_m = I \left( \frac{1 + \beta/\text{St}}{1 + \alpha\xi} \right)^{1/2}, \quad (2.1)$$

The values of  $\mu$  and  $\Phi$  are normalized by  $\mu_c$  and  $\Phi_c$ , respectively, which design their quasi-static values ( $I_m \rightarrow 0$ ) and vary linearly with  $\xi$ , as shown in the two insets to Fig. 2.3. The parameter values  $\alpha \simeq 0.062$  and  $\beta \simeq 0.075$  were determined from two series of simulations but we see that they lead to data collapse for all other simulations, including those of dry cohesionless flows. This means that  $\alpha$  and  $\beta$  depend only on the material parameters (particle shape and size distribution, friction coefficient between particles) and not on the cohesive and viscous interactions.

The physical argument behind the definition of  $I_m$  is the following. There are four characteristic stresses of different origins governing the flow: confining stress  $\sigma_p$ , inertial stress  $\sigma_i$ , viscous stress  $\sigma_v$ , and capillary stress  $\sigma_c$ . The key variable for inertial flows is the shear rate. We thus distinguish the characteristic stresses that depend on the shear rate, i.e.  $\sigma_i$  and  $\sigma_v$ , from those that are independent of the shear rate, i.e.  $\sigma_p$  and  $\sigma_c$ . In view of stress additivity, the total shear-dependent stress is a linear combination  $\sigma_i + \beta\sigma_v$  of the former, and the total shear-independent stress is a linear combination  $\sigma_p + \alpha\sigma_c$  of the latter. Hence, the flow variables (apparent friction coefficient and packing fraction) are expected to depend on the ratio  $(\sigma_i + \beta\sigma_v)/(\sigma_p + \alpha\sigma_c)$ , which simply represents the relative magnitude of shear-dependent stresses. We define the generalized inertial number  $I_m$  as the square root of this ratio, leading to the expression (2.1) by setting  $I = (\sigma_i/\sigma_p)^{1/2}$ ,  $\xi = \sigma_c/\sigma_p$  and  $\text{St} = \sigma_i/\sigma_v$ .

These primary dimensionless parameters can be evaluated from the system control parameters. The order of magnitude of the viscous stress  $\sigma_v$  is conveniently evaluated by replacing the average relative velocity  $\vartheta \sim \dot{\gamma}\langle d \rangle$  induced by shearing in equation (2.12) and considering the dissipated power per unit volume  $f_v\delta_0/\langle d \rangle^3$ , where  $\delta_0$  is the debonding distance, yielding  $\sigma_v \sim \eta\dot{\gamma}$ . The capillary stress is of the order of the capillary force at contact ( $\delta = 0$ ) in equation (2.15) divided by the cross section  $\langle d \rangle^2$ :  $\sigma_c \sim \gamma_s/\langle d \rangle$ . Hence, the dimensionless parameters are given by  $I = \dot{\gamma}\langle d \rangle(\rho_s/\sigma_p)^{1/2}$ ,  $\xi = \gamma_s/(\sigma_p\langle d \rangle)$ , and  $\text{St} = \rho_s\langle d \rangle^2\dot{\gamma}/\eta$ . Note that all other dimensionless variables can be expressed in terms of these three independent parameters. For example, the capillary number is given by  $\text{Ca} = \sigma_v/\sigma_c = I^2/(\xi\text{St})$ .

According to equation (2.1),  $I_m \rightarrow 0$  only if  $I \rightarrow 0$ . In this quasistatic limit, the flow variables may still depend on  $\xi$ , which is the only dimensionless variable in the absence of inertial and viscous stresses. In this way, the rheology may be described by the following

equations:

$$\mu = \mu_c(\xi) G_\mu(I_m), \quad (2.2)$$

$$\Phi = \Phi_c(\xi) G_\Phi(I_m), \quad (2.3)$$

These equations are based on functional distinction between the quasistatic limit ( $I_m \rightarrow 0$ ) and shear-rate dependent behavior through  $I_m$ . When  $I_m \rightarrow 0$ , we have  $\mu \rightarrow \mu_c$  and  $\Phi \rightarrow \Phi_c$ , so that  $G_\mu \rightarrow 1$  and  $G_\Phi \rightarrow 1$  in this limit. According to the simulation data displayed in Fig. 2.3,  $\mu_c$  and  $\Phi_c$  are linear functions of  $\xi$ :

$$\mu_c \simeq \mu_0(1 + a\xi) \quad (2.4)$$

$$\Phi_c \simeq \Phi_0(1 - b\xi) \quad (2.5)$$

with  $a \simeq 0.095$  and  $b \simeq 0.005$ . The limit values  $\mu_0 \simeq 0.392$  and  $\Phi_0 \simeq 0.594$  are the values of the apparent friction coefficient and packing fraction in the absence of cohesive and viscous forces (dry limit), respectively.

The data points are nicely fitted by the following functional forms:

$$\frac{\mu}{\mu_c} = G_\mu = 1 + \frac{\Delta\mu}{1 + I_\mu/I_m} \quad (2.6)$$

$$\frac{\Phi}{\Phi_c} = G_\Phi = \frac{1}{1 + I_m/I_\Phi} \quad (2.7)$$

with  $\Delta\mu \simeq 1.100$ ,  $I_\mu \simeq 0.095$  and  $I_\Phi \simeq 2.010$ . Interestingly, these functions are strictly the same as those previously used for dry granular flows, with the new *visco-cohesive* inertial parameter  $I_m$  replacing  $I$  [9, 5]. This shows that, up to the values of  $I_\mu$ ,  $I_\Phi$  and  $\Delta\mu$ , our simulation data are consistent with the experimental measurements of Refs. [9] and [5] in the dry case. The values of  $I_\mu$  and  $I_\Phi$  are also very close to those obtained in the simulations of Roy et al. [171] in a ring shear cell once re-expressed in terms of our definitions of the parameters. While the functional forms are general [5, 46, 3, 4, 171], the fitting parameters depend on the space dimension and material properties of the granular materials such as particle size distributions, particle shape and friction coefficient between particles. The values of  $\alpha$  and  $\beta$  reflect the relative roles of viscous, inertial and cohesive forces in collective dissipation mechanisms whereas the values of  $I_\mu$ ,  $I_\Phi$  and  $\Delta\mu$  account for the effects of material parameters. Note also that, given the investigated range of values of  $I_m$ , equation (2.7) can be linearized with an error  $\sim 10^{-3}$ , in agreement with Refs. [11, 3, 171].

The fitting forms reveal the double role played by cohesion. Since  $I_m$  is a decreasing function of  $\xi$ ,  $G_\mu$  declines with increasing  $\xi$  (dynamic effect) whereas  $\mu_c$  increases (quasistatic effect). We can easily check from the parameter values that the quasistatic effect prevails although the dynamic effect becomes important at large values of  $\xi$  and  $I_m$ . These roles are reversed for the packing fraction:  $\Phi_c$  declines whereas  $G_\Phi$  increases when  $\xi$  is increased. In other words, the cohesive interactions lead to lower packing fraction (enhanced dilatancy due to cohesive forces) but the inertial effects tend to increase the packing fraction.

The flow behavior can alternatively be described in the NVT ensemble (constant-volume shearing) in terms of effective normal and shear viscosities  $\eta_n$  and  $\eta_t$ , respectively, defined by  $\sigma_n = \eta_n \dot{\gamma}$  and  $\sigma_t = \eta_t \dot{\gamma}$ , where  $\sigma_t = \mu \sigma_n$  is the shear stress [45]. In this ensemble, the packing fraction  $\Phi$  replaces pressure  $\sigma_n$  as control parameter (i.e. the volume is imposed), and the rheology is characterized by the functions  $\eta_n(\Phi)$  and  $\eta_t(\Phi)$  [45]. This is the approach mostly used in experiments on suspensions. Although our simulations were carried out under NPT conditions, we may deduce  $\eta_n(\Phi)$  and  $\eta_t(\Phi)$  from our  $\mu(I_m)$  and  $\Phi(I_m)$ . Since no external stress is imposed in NVT, the normal and shear stresses  $\sigma_n$  and  $\sigma_t$  are dynamic variables that should scale with the internal shear-dependent stress  $\sigma_i + \beta \sigma_v$ . Hence, according to (2.1),  $\sigma_n = c_n(\sigma_i + \beta \sigma_v) \equiv c_n \sigma_n I_m^2 = \eta_n \dot{\gamma}$ , implying  $c_n = 1/I_m^2 = \eta_n/(\beta \eta + \rho_s \langle d \rangle^2 \dot{\gamma})$ , and  $\sigma_t = c_t(\sigma_i + \beta \sigma_v)$  with  $\sigma_t = \mu/I_m^2 = \eta_t/(\beta \eta + \rho_s \langle d \rangle^2 \dot{\gamma})$ . In this way, in a volume-controlled flow,  $c_n$  and  $c_t$  represent dimensionless viscosities with  $\beta \eta + \rho_s \langle d \rangle^2 \dot{\gamma}$  as reference viscosity; see Supplemental Material for more detail.

Figure 2.4 displays the effective dimensionless viscosities as a function of  $\Phi$ . We see that all the data points collapse on a master curve when  $\Phi$  is normalized by the critical packing fraction  $\Phi_c$ . Both viscosities diverge as  $\Phi \rightarrow \Phi_c$  and they are nicely fitted by the analytic expressions

$$c_n = \frac{1}{I_\Phi^2} \left( \frac{\Phi}{\Phi_c - \Phi} \right)^2, \quad (2.8)$$

$$c_t = \mu c_n = \frac{1}{I_\Phi^2} \left( \frac{\Phi}{\Phi_c - \Phi} \right)^2 \left\{ 1 + \frac{\Delta \mu}{1 + \frac{I_\mu}{I_\Phi} \frac{\Phi}{\Phi_c - \Phi}} \right\}, \quad (2.9)$$

readily deduced from the expressions of  $c_n$  and  $c_t$  as a function of  $I_m$  together with equations (2.6) and (2.7). As compared to suspensions,  $1/c_n = I_m^2$  represents a generalized fluidity parameter of granular flows [173].

Although  $I_m$  provides a unified description of the stress state by capturing the rheology in terms of the apparent friction coefficient and packing fraction or alternatively the effective viscosities, it is essential to check its robustness with respect to microstructural variables. Let us consider the shear plane defined by the directions of shearing  $\dot{\gamma}$  and confining stress  $\sigma_p$  (the flow being translationally invariant in the lateral direction). In this plane, the number density  $E(\Theta)$  of bonds (both contacts and non-contact capillary bridges) per particle along a direction  $\Theta$  can be approximated by [174, 24, 160]

$$E(\Theta) = \frac{Z}{2\pi} \{1 + A \cos 2(\Theta - \Theta_b)\}, \quad (2.10)$$

which represents a truncated Fourier transform of  $E(\Theta)$  with a period  $\pi$  since no intrinsic polarity can be attributed to contact orientations. Higher-order terms are generally negligibly small in granular flows. The coordination number  $Z$  and bond orientation anisotropy  $A$  are the lowest-order descriptors of granular texture. The angle  $\Theta_b$  is the privileged bond orientation, and its value is close to  $\pi/4$  with respect to the flow direction.

Figure 2.5 shows  $Z$  and  $A$  normalized by their quasistatic values  $Z_c$  and  $A_c$ , respectively, as a function of  $I_m$ . We see that, despite their larger variability as compared to  $\mu(I_m)$  and

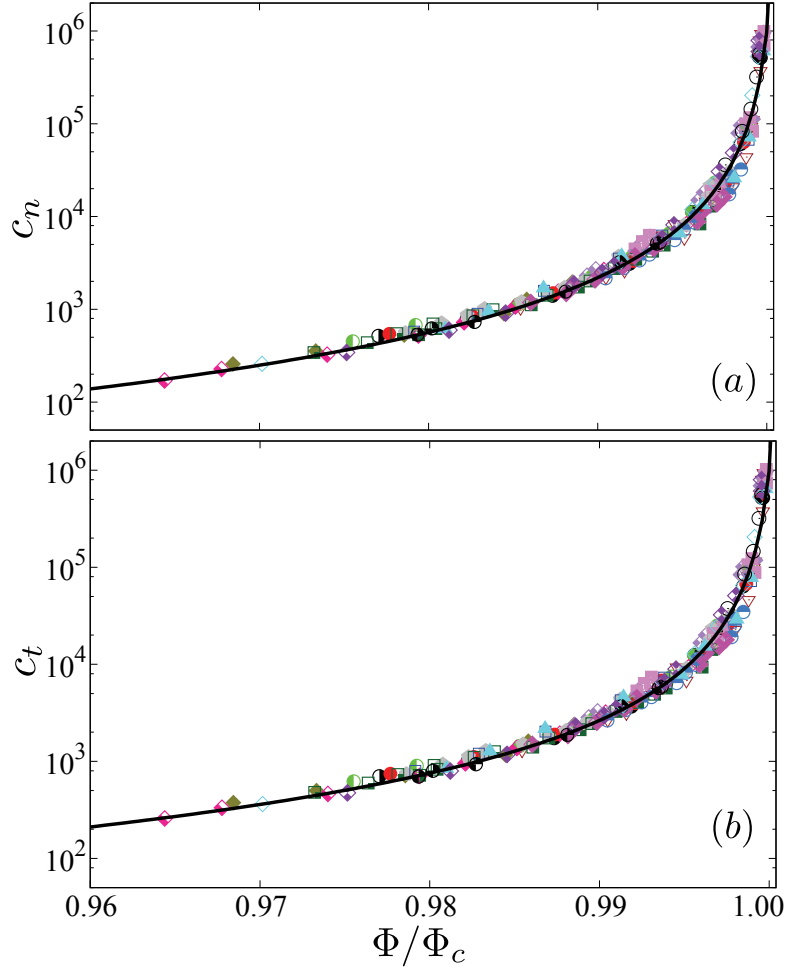


Figure 2.4 – (a) Normalized bulk viscosity  $c_n$  and (b) shear viscosity  $c_t$  as a function of the normalized packing fraction  $\Phi/\Phi_c$ . The error-bar symbols and their colors are the same as those in Fig. 2.2. The solid lines are the functional forms (2.27) and (2.26), respectively.

$\Phi(I_m)$ , the data points collapse on a master curve within our statistical precision as a function of  $I_m$  with the same values  $\alpha \simeq 0.062$  and  $\beta \simeq 0.075$  as in  $\mu(I_m)$  and  $\Phi(I_m)$ . The insets show the extent to which the same data points are dispersed when plotted as a function of  $I$ . We find that  $Z_c$  is a decreasing linear function of  $\xi$  (as  $\Phi_c$ ) and  $A_c$  is an increasing linear function of  $\xi$  (as  $\mu_c$ ). Moreover, the functional forms that fit  $A/A_c$  and  $Z/Z_c$  are the same as in  $G_\mu$  and  $G_\Phi$  as a function of  $I_m$ . This scaling of microstructural variables with  $I_m$  through a functional dependence similar to flow variables clearly indicates that the shear strength is mainly due to the increasing aptitude of the particles to self-organize in an anisotropic network [175, 11].

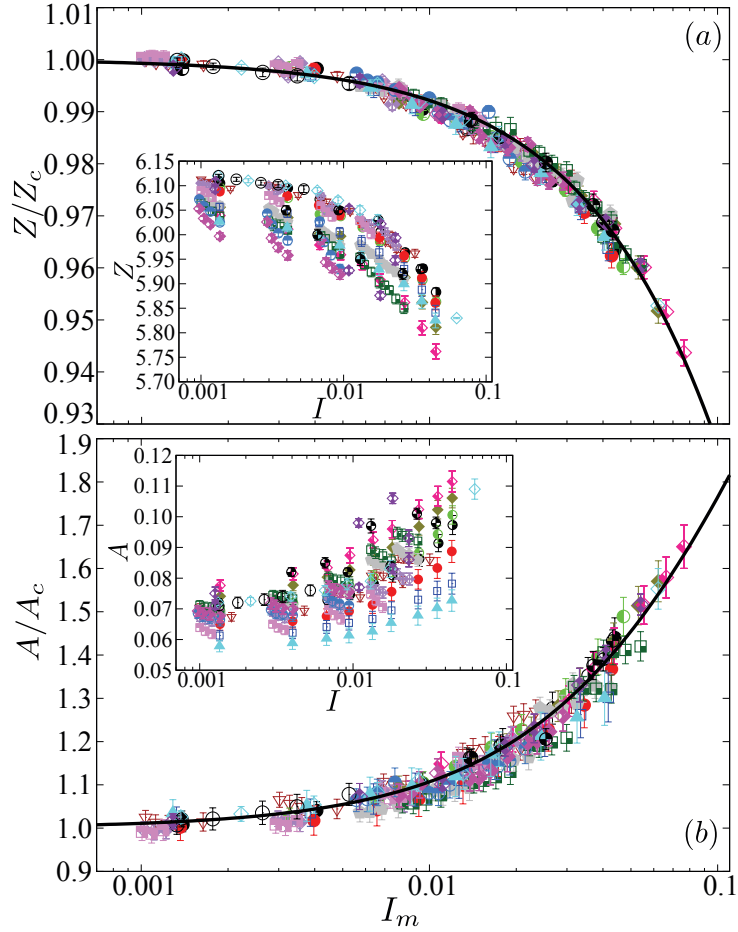


Figure 2.5 – Number density  $Z$  of capillary bonds (a) and bond anisotropy  $A$  (b) as a function of the modified inertial number  $I_m$  for different parameter values. The error-bar symbols and their colors are the as in Fig. 2.2.

## Discussion

The additive rheology of granular materials, as demonstrated in this paper, is by no means self-evident. The expectation that a system involving several dimensionless parameters can ultimately be described by a single parameter combining those parameters is unusual. The deep reason behind such a behavior is the very nature of granular materials in which the particle interactions are concentrated at the contact points and the local dynamics is controlled by the shear rate. Hence, by careful distinction of stresses depending on the shear rate (first group) from those that are independent (second group), a single parameter can be defined by means of the stress additivity property. In this respect, the modified inertial number  $I_m$  is a conceptual extension of the inertial number to arbitrary interactions between particles. Such a scaling works, however, by distinguishing the quasistatic limit and normalizing the packing fraction, apparent friction coefficient, coordination number and

bond orientation anisotropy by their quasistatic limit values that depend on the dimensionless numbers of the second group ( $\xi$  in our case). Encompassing dry and cohesive-viscous flows, quasistatic and dynamic states, flow variables and microstructural parameters, this scaling provides a general framework for complex granular flows.

This framework can be applied to quantify the effects of friction coefficient between particles and particle shape and size distributions as material parameters that can influence the relative roles of internal stresses in the collective flow behavior, and thus the fitting parameters. This is a crucial step forward for application to different types of granular materials and for comparison with experiments. It is also useful to point out that, for given particle size  $d$  and density  $\rho_s$ , each characteristic stress  $\Sigma$  corresponds also to a characteristic time  $T = d(\rho_s/\Sigma)^{1/2}$ . This relation implies that, by virtue of stress additivity, the inverse quadratic times  $1/T^2$  are additive. Hence, using the characteristic times, we arrive at the same expression of  $I_m$  as in equation (2.1) by means of this rule. Another interesting issue concerns an alternative rheology based on a ‘multiplicative’ expression of the flow variables, rather than additive combination of control parameters, as in Ref. [171] applied to a cohesive-frictional granular material. In this approach, the apparent friction coefficient  $\mu$  is expressed as a product of distinct functions of all dimensionless control parameters. This multiplicative partition works quite well for the cohesion index, and a prefactor similar to  $\mu_0(1 + a\xi)$  in equation (2.4) is obtained. For the other functions, it is worth considering in more detail how they relate to the framework developed in this paper.

Let us finally recall that the inertial number was initially introduced in the context of cohesionless granular materials where the gravity or applied confining stress prevail. However, the cohesive stress may largely exceed the confining stress in fine powders, and therefore the inertial and viscous stresses must be advantageously compared to the cohesive stress rather than the confining stress. It is easy to see that, in this limit ( $\sigma_p \rightarrow 0$ ), the modified inertial number is reduced to  $I_m = \{\text{Ca}(\beta + \text{St})/\alpha\}^{1/2}$ . This is a simple expression that is expected to scale cohesive processes such as wet granulation and impact dynamics of cohesive aggregates. We thus propose to use impact experiments as a convenient means to investigate this scaling.

## Method

For the simulations, we used the molecular dynamics (MD) method with frictional contact interactions modeled by linear elastic repulsion along the normal direction and linear spring with a Coulomb threshold along the tangential direction, together with the first-order theoretical expressions of capillary force  $f_c^{ij}$  and viscous force  $f_v^{ij}$  acting between neighboring particles  $i$  and  $j$  [38, 24, 176]:

$$f_c^{ij} \simeq \pi\gamma_s d_g^{ij} \cos\theta e^{-\delta^{ij}/\lambda}, \quad (2.11)$$

$$f_v^{ij} \simeq \frac{3\pi}{8}\eta v_n^{ij} (d_h^{ij})^2 \times \begin{cases} 1/(\delta_0 + \delta^{ij}), & \delta_0 \leq \delta^{ij} \leq \delta_{rup} \\ 1/\delta_0, & \delta^{ij} \leq \delta_0 \end{cases} \quad (2.12)$$

where  $\theta$  is the contact angle of the liquid bridge,  $d_g^{ij}$  and  $d_h^{ij}$  are the geometric and harmonic means of the diameters of particles  $i$  and  $j$ ,  $\delta^{ij}$  is the gap,  $\lambda$  is a characteristic length depending on the liquid bridge parameters,  $\eta$  is liquid viscosity,  $v_n^{ij}$  is the relative normal velocity,  $\delta_0$  is the roughness amplitude and  $\delta_{rup} \simeq (1 + \theta/2)V_b^{1/3}$  is the debonding distance (beyond which a liquid bridge breaks) with  $V_b$  the liquid volume of the bridge [81]. The viscous lubrication force remains constant below a gap equal to  $\delta_0$ , corresponding to the cancellation of an unphysical force divergence by surface roughness. The tangential lubrication force was neglected as it is one order of magnitude below the normal lubrication force. In all simulations, we set  $\theta = 0$  (wetting liquid). For more details, see Supplemental Material.

## Supplemental Material

### Simulation method

The simulations were carried out by means of the Molecular Dynamics (MD) method, in which the particles interact via viscoelastic forces acting at the contact points between rigid particles [144]. The forces are functions of the contact strains defined from the relative displacements of the particles as no degrees of freedom other than rigid-body motions of the particles are considered in the DEM.

The particle displacements are calculated by step-wise resolution of Newton's second law:

$$\begin{aligned} m_i \frac{d^2 \mathbf{r}_i}{dt^2} &= \sum_j [(f_n^{ij} + f_c^{ij} + f_{vis}^{ij}) \mathbf{n}^{ij} + f_t^{ij} \mathbf{t}^{ij}], \\ \mathbf{I}_i \frac{d\boldsymbol{\omega}_i}{dt} &= \sum_j f_t^{ij} \mathbf{c}^{ij} \times \mathbf{t}^{ij}, \end{aligned} \quad (2.13)$$

where particle  $i$  is assumed to interact with its neighbors  $j$  via normal contact forces  $f_n$ , tangential contact forces  $f_t$ , capillary forces  $f_c$ , and viscous forces  $f_{vis}$ .  $\boldsymbol{\omega}_i$  is the rotation vector of particle  $i$ , and  $m_i$ ,  $\mathbf{I}_i$ , and  $\mathbf{r}_i$  are its mass, inertia matrix, and position, respectively.  $\mathbf{n}^{ij}$  denotes the unit vector perpendicular to the contact plane between the particles  $i$  and  $j$  and points from  $j$  to  $i$ .  $\mathbf{t}^{ij}$  is the unit vector in the contact plane pointing in the direction opposite to the relative tangential displacement of the two particles.  $\mathbf{c}^{ij}$  is the vector joining the center of particle  $i$  to the contact point with particle  $j$ .

The normal contact force  $f_n$  is the sum of four contributions:

$$f_n = f_n^e + f_n^d + f_c + f_{vis}. \quad (2.14)$$

The elastic force  $f_n^e = -k_n \delta_n$  is a linear function of the normal elastic deflection  $\delta_n$ , where  $k_n$  is the normal stiffness, and the damping force  $f_n^d = \gamma_n \dot{\delta}_n$  is proportional to the relative normal velocity  $\dot{\delta}_n$ , where  $\gamma_n$  is the normal viscous damping parameter. These forces occur only when two particles are in contact ( $\delta_n < 0$ ).

We assume that the liquid inside the agglomerate is in the ‘pendular’ state with a uniform distribution of capillary bridges between particles [81, 82, 36, 84, 141, 177]. This distribution may be a consequence of mixing the liquid with the particles, drainage of a saturated packing, or capillary condensation from a vapor. For a separation distance above a debonding distance  $d_{rupt}$ , the bridge breaks and its liquid is shared between the two particles proportionally to their sizes [81, 83].

The capillary force  $f_c$  between two particles depends on the liquid volume  $V_b$  of the bond, liquid-vapor surface tension  $\gamma_s$  and particle-liquid-gas contact angle  $\theta$ . We used the following expression [38]:

$$f_c = \begin{cases} -\kappa R, & \text{for } \delta_n < 0, \\ -\kappa R e^{-\delta_n/\lambda}, & \text{for } 0 \leq \delta_n \leq d_{rupt}, \\ 0, & \text{for } \delta_n > d_{rupt}, \end{cases} \quad (2.15)$$

where  $R = \sqrt{R_i R_j}$  is the geometrical mean radius and the pre-factor  $\kappa$  is

$$\kappa = 2\pi\gamma_s \cos \theta. \quad (2.16)$$

The debonding distance  $d_{rupt}$  is given by [81]

$$d_{rupt} = \left(1 + \frac{\theta}{2}\right) V_b^{1/3}. \quad (2.17)$$

The characteristic length  $\lambda$  in equation (2.15) is given by

$$\lambda = c h(r) \left(\frac{V_b}{R'}\right)^{1/2}, \quad (2.18)$$

where  $R' = 2R_i R_j / (R_i + R_j)$  and  $r = \max\{R_i/R_j; R_j/R_i\}$  are the harmonic mean radius and the size ratio between two particles,  $h(r) = r^{-1/2}$ , and  $c \simeq 0.9$ .

The normal lubrication force  $f_{vis}$  due to the effect of liquid bridges between two smooth spherical particles is given by [150, 25]

$$f_{vis} = \frac{3}{2}\pi R^2 \eta \frac{v_n}{\delta_n}, \quad (2.19)$$

where  $\eta$  is the liquid viscosity and  $v_n$  is the relative normal velocity, assumed to be positive when the gap  $\delta_n$  is decreasing. This force diverges when the gap  $\delta_n$  tends to zero. But for slightly rough particles, the characteristic size of the asperities allows for collision in finite time. Hence, we introduce a characteristic length  $\delta_{n0}$  corresponding to the size of asperities so that the lubrication force for  $\delta_n > 0$  is given by

$$f_{vis} = \frac{3}{2}\pi R^2 \eta \frac{v_n}{\delta_n + \delta_{n0}} \quad \text{for } \delta_n > 0 \quad (2.20)$$

For  $\delta_n < 0$  (a contact between two particles), we assume that the lubrication force remains equal to its largest value:

$$f_{vis} = \frac{3}{2}\pi R^2 \eta \frac{v_n}{\delta_{n0}} \quad \text{for } \delta_n \leq 0. \quad (2.21)$$

In our simulations, we set  $\delta_{n0} = 5.10^{-4}d_{min}$ , where  $d_{min}$  is the smallest particle diameter. This value is sufficiently small to allow the lubrication force to be effective without leading to its divergence at contact.

The tangential force  $f_t$  is composed of an elastic force  $f_t^e = -k_t\delta_t$  and a damping force  $f_t^d = \gamma_t\dot{\delta}_t$ , where  $k_t$  is the tangential stiffness,  $\gamma_t$  is the tangential damping parameter, and  $\delta_t$  and  $\dot{\delta}_t$  are the tangential displacement and velocity, respectively. According to the Coulomb friction law, the tangential force is below  $\mu f_n$ , where  $\mu$  is the friction coefficient [142, 143, 144]:

$$f_t = -\min \left\{ | -k_t\delta_t + \gamma_t\dot{\delta}_t |, |\mu f_n| \right\} \text{sgn}(\dot{\delta}_t). \quad (2.22)$$

Note that the simulated system is an idealized model of wet granular materials in the pendular state. Nevertheless, we believe that our results can be extended to higher amounts of liquid since the liquid can easily flow in an unsaturated material to wet larger particle areas with a lower Laplace pressure. This leads to a nearly constant cohesive stress as far as the material is not fully saturated [82, 84]. Hence, the leading effect of increased liquid volume is simply the increase of debonding distance when equation (2.15) is used.

The equations of motion were integrated by a step-wise velocity-Verlet algorithm [178]. The constant physical parameters were set to typical values of fine granular materials composed of hard particles. We used a weak size polydispersity with a uniform distribution of particle volumes and a ratio 2 between the largest and smallest particle diameters. All the constant physical and numerical parameter values are given in Table 3.1. Note that the relative pressure  $p^* = \sigma_p / (\langle d \rangle k_n)$ , representing the ratio of contact deflection to particle diameter, is of the order of  $10^{-5}$ . Our simulations correspond therefore with a high precision to the ideal limit of perfectly rigid particles.

## Velocity fields

The rheology of complex granular flows investigated in this paper is based on careful measurements of the flow variables and microstructural parameters in the steady flowing state. Although shear-banding (strain localization) can occur in granular materials, it is essential to avoid shear banding for the rheological behavior by an appropriate choice of the boundary and driving conditions. We find that the wall roughness, flow thickness and inertial number determine the velocity profiles. Figures 2.6 and 2.7 display examples of velocity profiles in cohesive and cohesionless flows. We see that in all cases the granular material is sheared in its whole volume, but the velocity profiles are not linear and the material may slip at the walls. This implies that, in general, the average shear rates  $\dot{\gamma}$  can not be simply calculated from the wall displacement rate but should account also for wall

Table 2.1 – Constant simulation parameters

Parameter	Symbol	Value	Unit
Number of particles	$N_p$	19,628	
Smallest particle diameter	$d_{min}$	800	$\mu\text{m}$
Particle density	$\rho_s$	2600	$\text{kg}\cdot\text{m}^{-3}$
Friction coefficient	$\mu_s$	0.4	
Normal stiffness	$k_n$	$10^6$	N/m
Tangential stiffness	$k_t$	$8\cdot 10^5$	N/m
Normal damping	$\gamma_n$	0.5	Ns/m
Tangential damping	$\gamma_t$	0.5	Ns/m
Contact angle	$\theta$	0	degree
Time step	$\delta t$	$3\cdot 10^{-7}$	s

slip. This is what we did for the calculation of  $\dot{\gamma}$ . The shear rates used in the paper are average values over the whole sample.

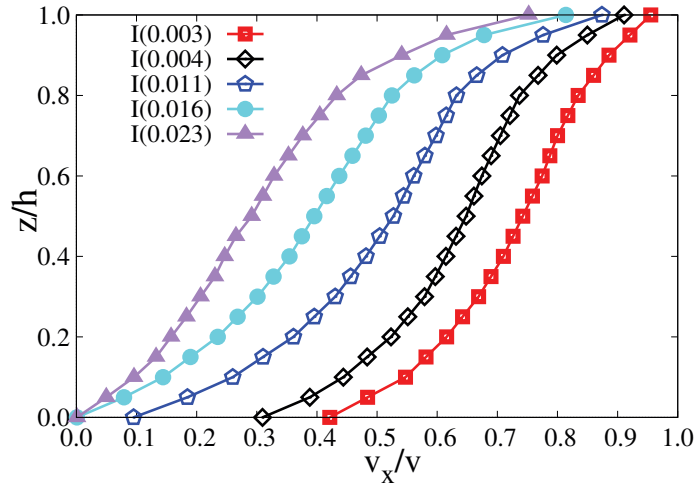


Figure 2.6 – Velocity profiles in the steady state for different values of the inertial number, with cohesion index  $\xi = 0.5$  and liquid viscosity  $\eta_f = 1$  mPa.s. The velocities are average values on in the steady flow state and they are normalized by the shear velocity applied on the top wall.

## Quasi-static microstructure

The microstructure in the quasistatic limit  $I_m \rightarrow 0$  is characterized by the coordination number  $Z_c$  and bond orientation anisotropy  $A_c$ . As the packing fraction  $\Phi$ , both  $Z_c$  and  $A_c$  decline almost linearly with increasing cohesion index  $\xi$ , as shown in Fig. 2.8. The data

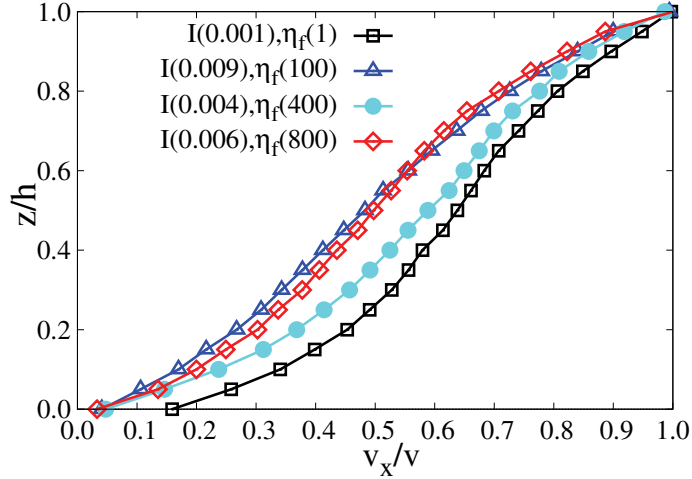


Figure 2.7 – Velocity profiles in the steady state for different values of the inertial number  $I$  and liquid viscosity  $\eta_f$  (in mPa.s) in cohesionless samples. The velocities are average values on in the steady flow state and they are normalized by the shear velocity applied on the top wall.

point for  $\xi = 0$  corresponds to a dry sample with both cohesion and viscous force set to zero. Note that for cohesive contacts, the capillary bonds define a network that includes both the contacts and the pairs of particles separated by a gap below the debonding distance. For the calculation of  $Z_c$  and  $A_c$  in the dry limit, we keep the same network. The value of the coordination number for the contact network is lower whereas the contact network anisotropy is higher.

## Transition from NPT to NVT

We describe here in more detail the derivation of the effective viscosities as a function of the packing fraction  $\Phi$  in the NVT ensemble from the apparent friction coefficient  $\mu$  and  $\Phi$  as a function of the generalized inertial number  $I_m$  in the NPT ensemble. This transition is presented in Ref. [45] for dry granular flows. For wet granular materials, we follow the same argument by accounting for the viscous and cohesive stresses in addition to the confining and inertial stresses.

In the NVT ensemble, the packing fraction  $\Phi$  replaces the normal stress  $\sigma_n$  as control parameter (i.e. the volume is imposed), and the rheology is characterized by the effective normal and shear viscosities,  $\eta_n$  and  $\eta_t$ , as a function of  $\Phi$ . The key point is that at constant volume no external stress  $\sigma_p$  is imposed, and both the normal stress  $\sigma_n$  and shear stress  $\sigma_t$  are induced by the shear rate  $\dot{\gamma}$ . The effective viscosities are defined by

$$\sigma_n = \eta_n \dot{\gamma}, \quad (2.23)$$

$$\sigma_t = \eta_t \dot{\gamma}, \quad (2.24)$$

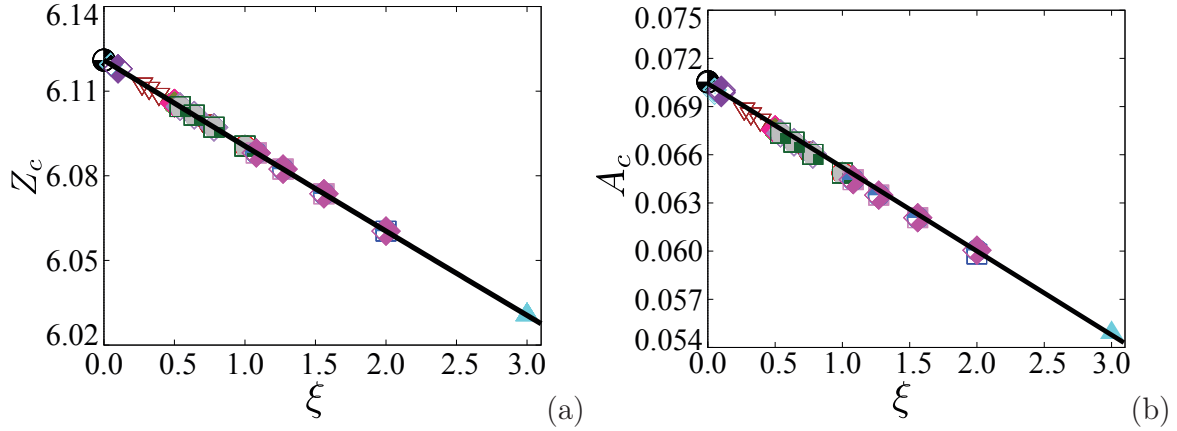


Figure 2.8 – Number density of capillary bonds (a) and bond anisotropy (b) in the quasi-static state as a function of the cohesion index  $\xi$ . The symbols and their colors correspond to different values of the control parameters as in Fig. 2 of the paper.

implying that  $\sigma_n$  and  $\sigma_t$  vanish when  $\dot{\gamma} \rightarrow 0$ .

As in the NPT ensemble, we have

$$\sigma_t = \mu\sigma_n. \quad (2.25)$$

Since no external stress is imposed, the shear stress  $\sigma_t$  should scale with the total shear-dependent internal stress  $\sigma_i + \beta\sigma_v$ , where  $\beta$  is the same factor as in the NPT ensemble. Hence, we set

$$\sigma_t = c_t(\sigma_i + \beta\sigma_v), \quad (2.26)$$

where  $c_t$  is a dimensionless factor. From equations (2.25) and (2.26), we get

$$\sigma_n = c_n(\sigma_i + \beta\sigma_v), \quad (2.27)$$

with

$$c_t = \mu c_n \quad (2.28)$$

Another key point is that the NPT and NVT viewpoints describe the same stress state if the normal stress  $\sigma_n$  in the NVT ensemble is equal to the normal stress imposed in the NPT ensemble. This stress is  $\sigma_p$  enhanced by the presence of the cohesive stress:

$$\sigma_n = \sigma_p + \alpha\sigma_c, \quad (2.29)$$

where  $\alpha$  is the same factor as in the NPT ensemble. Equations (2.23), (2.24), (2.27) and (2.29) together with equation 1 in the paper and the expressions of the inertial number  $I$  and cohesion index  $\xi$ , lead to

$$c_n = \frac{1}{I_m^2} = \frac{\eta_n}{\beta\eta + \rho_s \langle d \rangle^2 \dot{\gamma}}, \quad (2.30)$$

and

$$c_t = \frac{\mu}{I_m^2} = \frac{\eta_t}{\beta\eta + \rho_s \langle d \rangle^2 \dot{\gamma}}. \quad (2.31)$$

These expressions show that  $c_n$  and  $c_t$  are dimensionless viscosities with  $\beta\eta + \rho_s \langle d \rangle^2 \dot{\gamma}$  playing the role of a reference viscosity. The first term is the liquid viscosity and the second term is the shear-induced inertial viscosity. By eliminating  $I_m$  between the analytical expressions of  $\mu(I_m)$  and  $\Phi(I_m)$  and from the above expressions of  $c_n$  and  $c_t$ , one arrives at the expressions of  $c_n(\Phi)$  and  $c_t(\Phi)$  given in the paper.



*“Prediction is very difficult, especially of the future”*

Niels Henrik David Bohr (1885-1962)

Chapter 3

# Agglomeration of wet particles in dense granular flows

This chapter is published as a paper in **European Physical Journal E (EPJ E)**

Eur. Phys. J. E (2019) **42**: 127  
DOI 10.1140/epje/i2019-11892-9

**THE EUROPEAN  
PHYSICAL JOURNAL E**

Regular Article

## Agglomeration of wet particles in dense granular flows

Thanh Trung Vo<sup>1,2</sup>, Saeid Nezamabadi<sup>1,3,a</sup>, Patrick Mutabaruka<sup>1</sup>, Jean-Yves Delenne<sup>3</sup>, Edouard Izard<sup>4</sup>, Roland Pellenq<sup>5</sup>, and Farhang Radjai<sup>1</sup>

<sup>1</sup> LMGC, Université de Montpellier, CNRS, Montpellier, France

<sup>2</sup> Bridge and Road Department, Danang Architecture University, 553000 Da Nang, Vietnam

<sup>3</sup> IATE, UMR1208 INRA - CIRAD - Université de Montpellier - SupAgro, 34060 Montpellier, France

<sup>4</sup> ArcelorMittal R&D Maizières, Voie Romaine, F-57283 Maizières-Lès-Metz, France

<sup>5</sup> (MSE2), UMI 3466 CNRS-MIT, MIT Energy Initiative,  
77 Massachusetts Avenue, Cambridge, MA 02139, USA

Received 3 June 2019 and Received in final form 14 August 2019

Published online: 18 September 2019

© EDP Sciences / Società Italiana di Fisica / Springer-Verlag GmbH Germany, part of Springer Nature, 2019



**S**n order to get insight into the wet agglomeration process, we numerically investigate the growth of a single granule inside a dense flow of an initially homogeneous distribution of dry and wet particles. The simulations are performed by means of the discrete-element method and the binding liquid is assumed to be transported by the wet particles, which interact via capillary and viscous force laws. The granule size is found to be an exponential function of time, reflecting the conservation of the amount of liquid and the decrease of the number of available wet particles inside the flow during agglomeration. We analyze this behavior in terms of the accretion and erosion rates of wet particles for a range of different values of material parameters such as mean particle size, size polydispersity, friction coefficient and liquid viscosity. In particular, we propose a phase diagram of the granule growth as a function of the mean primary particle diameter and particle size span, which separates the parametric domain in which the granule grows from the domain in which the granule does not survive.

## Contents

---

<b>3.1</b>	<b>Introduction</b>	<b>51</b>
<b>3.2</b>	<b>Model description and numerical method</b>	<b>53</b>
3.2.1	Physical assumptions	53
3.2.2	Drum flow	54
<b>3.3</b>	<b>Growth, accretion and erosion</b>	<b>58</b>
<b>3.4</b>	<b>Effects of material parameters</b>	<b>62</b>
<b>3.5</b>	<b>Phase diagram</b>	<b>65</b>
<b>3.6</b>	<b>Conclusions</b>	<b>66</b>

---



### 3.1 Introduction

Wet granulation or agglomeration of fine solid particles into larger particles, called granules or agglomerates, is a widespread technique in industrial processes such as the manufacture of pharmaceuticals [20, 65], fertilizers and food products [179, 117], powder metallurgy [66] and iron-making [67, 68, 69]. The increased size of the granules modifies the rheological properties of the granular material and may improve flow properties, reduce the segregation of different types of primary particles or enhance the permeability for the interstitial gas between grains [117, 180, 106, 70, 71, 72]. The wetting of primary particles is achieved either by mixing them with a binding liquid prior to the process or by dripping or spraying the liquid to the material during the process [72, 73, 74, 75, 76, 77, 78, 79, 80]. The granules nucleate as a result of the collisional-frictional/capillary-viscous interactions of the wet primary particles and then they grow in size by incorporation of the available liquid, accretion of primary finer particles and coalescence with other granules [26]. The existing granules may survive and grow or disappear, depending on the amount of available liquid and the rate of erosion as compared to that of accretion (layering) and coalescence [20, 85].

Given the large number of parameters involved in the agglomeration process, its detailed physical mechanisms and their relative importance for the resulting properties of are complex. One may distinguish two different groups of parameters related to the material and the process [180, 106, 181, 91, 15, 182]. The material parameters are the properties of the binding liquid and raw material such as liquid viscosity, primary particle size distribution, mean particle size and friction coefficient of primary particles [78, 92, 99]. The process parameters are related to the method of mixing solid particles with the binding liquid and the corresponding operating parameters. There are different types of granulators using fluidized beds, high shear or low shear in planetary devices or rotating drums or disks [180]. Major process parameters in all types of granulators are the liquid volume [69, 91, 92], granulator size, rotation speed, inclination angle [93, 94, 95] and filling rate [96]. The agglomeration process often needs to be optimized by playing with all these parameters in order to produce granules of high density, homogeneous distribution of primary particles, a targeted mean size and high strength [86, 87, 88, 89, 90].

The agglomeration process is easier to model and control when particle dynamics is governed by binary collisions, as in granulators based on fluidized bed or high shearing by impellers. Such processes have been extensively investigated in application to the pharmaceutical industry [106]. In contrast, in drum granulators the particles agglomerate in a downward dense granular flow along inclined rotating drum. The drum granulator has the advantage of being a continuous and robust process, but since the rheology of dense granular flows is a matter of current research [1, 183, 4], the agglomeration mechanisms

in this geometry remain quite poorly understood [180, 184]. Granular flows in an inclined rotating drum may show several flow regimes [110, 114, 115] with the common feature of being dense and inhomogeneous, and involving inertial effects [73, 77, 85, 81, 82, 83, 185]. A practical difficulty with drum agglomeration is the in-line monitoring of the kinetics, making it less amenable to theoretical understanding, which is required in order to be able to improve drum granulation plants, often suffering from a significant recycle of undersize and crushed oversize granules [180].

In this chapter, we use the drum geometry to create a steady dense flow of spherical particles in order to investigate the growth of a single pre-nucleated granule composed of wet particles acting as a seed. The granule can grow by capturing free wet particles inside the granular flow, or shrink by losing its wet particles. The particle dynamics is simulated by the Discrete Element Method (DEM) [133], but the binding liquid is accounted for via inter-particle capillary and viscous forces. In other words, it is assumed that the wet particles have a large moisture content either in the form of a liquid layer at the surface of the particles [20, 26] or in the volume of small aggregates of finer particles glued together by the liquid that they transport. Upon contact, such wet particles form a binary liquid bridge whose shape is governed by the Laplace-Young equation. The capillary force law used in this work is an explicit approximative solution of this equation. We also account for the debonding distance as a function of the amount of liquid in a capillary bridge [38].

The DEM allows for direct quantification of particle-scale kinetics and accretion/erosion events. This method has already been applied to investigate agglomeration in granular shear flows. For example, Talu et al. [186] introduced a model of wet granulation in which some of the particles are assumed to be covered by a binder and therefore sticky while the rest are non-cohesive. The binder layer between particles dissipates energy due to viscosity and allows the particles to stick to one another by the action of capillary forces. In other reported DEM simulations of the granulation process, besides capillary and viscous forces, simple empirical rules are used for progressive wetting of the particles [187, 188, 189]. To reduce the high computational cost of DEM simulations, some authors have used the DEM simulation data with a low number of particles to train an artificial neural network or in conjunction with population balance equations for application to the large number of particles [188, 190]. The DEM has, however, only recently been employed for drum granulation using a JKR elastic-adhesive force law with a scale-up procedure based on the cohesion number [184]. In the work presented in this chapter, we consider idealized particles, and drum rotation is used only as a means to sustain a dense continuous flow while we investigate the influence of mean particles size, size ratio, liquid viscosity and friction coefficient on the granule growth.

In the following, in Sect. 3.2, we introduce in detail the numerical approach. Then, we analyze in Sect. 3.3 the growth process in terms of accretion and erosion events, and in Sect. 3.4 we investigate the influence of material parameters on the accretion and erosion rates. In Sect. 3.5, we introduce a phase diagram for granule growth as a function of the mean particle size and size ratio. Finally, we conclude in Sect. 3.6 with a short summary and future research directions.

## 3.2 Model description and numerical method

Our numerical approach for the simulation of the agglomeration process is based on the DEM and a model for the effect of the binding liquid. We first describe below the physical assumptions underlying the model. Then, we briefly present the numerical algorithm with its input parameters and main calculation steps.

### 3.2.1 Physical assumptions

In the DEM, the equations of motion of all particles are integrated according to an explicit time-stepping scheme such as the well-known velocity-Verlet algorithm [133, 191, 192, 193, 194, 132]. A detailed description of the liquid phase and its interaction with solid particles, requires sub-particle discretization of the liquid phase and a numerical model for liquid-gas phase transition [4, 82, 185]. However, such a multi-component model of partially saturated granular materials is not computationally efficient for the simulation of the agglomeration process with a large number of primary particles. An efficient alternative approach consists in accounting for the capillary and lubrication forces between particles as well as a particle-scale model for the distribution and transport of the binding liquid.

Recent experiments and numerical simulations show that the liquid clusters condensed from a vapor or introduced by mixing the liquid with particles can be characterized by their connectivity with the particles [82, 185]. The number of liquid clusters connected to two particles prevails for low amounts of the liquid. In this ‘pendular’ state, the liquid is in the form of binary bridges. As the amount of liquid increases, the clusters involve more and more particles until a single cluster spans the whole packing. The cohesive effect of the liquid in thermodynamic equilibrium is controlled by the total wetted surface and the Laplace pressure. The cohesion rapidly increases as the amount of liquid is increased in the pendular state, and then it keeps a nearly constant value (or slightly increases) with increasing amount of the liquid before declining for large amounts [82, 185]. This description assumes, however, that the particles are in quasi-static equilibrium and the liquid is in thermodynamic equilibrium. The negative Laplace pressure within the liquid phase is not uniformly distributed if the system is out of equilibrium. Furthermore, if the granular material flows, the liquid clusters undergo large distortions, and the liquid is continuously re-distributed as a result of coalescence and separation of liquid clusters [145, 146]. In practice, a small amount of the added liquid is adsorbed into the particle rough surfaces and is not directly involved in capillary bonding between particles.

The above-mentioned features suggest that in a dense granular material, for a broad range of the amount of liquid, the cohesive capillary stress is nearly independent of the amount of liquid, and therefore the effect of liquid volume can be accounted for by the number of wet particles. In a rotating drum, when the liquid is poured onto the granular flow, it has not time to diffuse and the capillary stress leads to the creation of small aggregates of primary particles that are transported by the granular flow. These “micro-aggregates” may deform or break up into smaller aggregates [20]. They may also capture more primary

particles or coalesce into larger aggregates if they have an excess amount of liquid that can be shared with other micro-aggregates as a consequence of their consolidation under the action of contact forces inside the granular flow. The initial size of the micro-aggregates is proportional to that of the droplets but, depending on the wetting method, it can grow rapidly into granules.

This picture of liquid transport by micro-aggregates in their pore volumes or at their surfaces in the form of liquid layer covering the asperities means that the discrete-element model can be based on the micro-aggregates as wet units. In its simplest setting, these basic units can be modeled as particles each transporting a given amount of liquid. Since the number of primary particles embodied in each micro-aggregate is nearly proportional to the droplet size, the size distribution of the basic particles can be regarded as reflecting that of the droplets. When two such wet particles meet, they are subjected to the cohesive action of the spontaneous liquid bridge appearing between them. In this sense, the interactions between wet units are similar to those between particles covered by a liquid layer as in the method introduced by Talu et al. [186] or indirectly through the use of surface tension as in [184]. In the following, we present in more detail our numerical method and all model parameters.

As in this model the liquid is mainly transported by the population of wet particles, the initial distribution and amount of the binding liquid are essentially determined by those of wet particles. It is, however, important to note that we do not consider here the nucleation step in which the processes of wetting and dispersion of the binding liquid are crucial for the early-stage evolution of the system and for which a fluid-resolved method is necessary [20, 185, 195, 196]. Once the granules are nucleated, the subsequent granule growth is mainly controlled by the accretion/erosion mechanisms, and liquid re-distribution takes place by the interactions between the granules and wet or dry particles. In our simulations, we may control the initial state by changing the initial distribution of free wet particles in order to analyze its influence on the growth kinetics of the granules. We will consider below the simple situation of a random distribution of wet particles. Hence, the growth process is mainly governed by the accretion of these free wet particles by a pre-nucleated granule and the erosion of particles from granule by interaction with dry particles without fluctuations arising from an uneven distribution of the binding liquid. Several previous studies of agglomeration suggest that this approximation provides results that are in good agreement with experiments when the material parameters are correctly adjusted [184, 186].

### 3.2.2 Drum flow

The rotating drum is a cylinder of length  $L$  and diameter  $d_c$  constructed geometrically by the juxtaposition of polyhedral rigid elements. Its both ends are closed by two planes and it can rotate around its axis at given angular speed  $\omega$ . In all simulations analyzed below, the drum is horizontal, implying that the gravity is perpendicular to the drum axis.

The drum is filled by allowing 5000 dry particles to fall into it under their own weights until a stabilized granular bed is obtained. The number of particles was limited to 5000 in

order to simulate a large number of drum rotations and many runs with different values of material parameters in a reasonable computation time. In all simulations, the filling level was  $s_f = \frac{2H}{d_c} \simeq 0.56$ , where  $H$  is the filling height of the granular material inside the drum. We considered three different size classes in a range  $[d_{min}, d_{max}]$  with a size ratio  $\alpha = d_{max}/d_{min}$ . All size classes have the same particle volume so that the size distribution is uniform in terms of particle volume fractions. This corresponds to a small number of large particles and a large number of small particles. This distribution generally leads to a large packing fraction since small particles optimally fill the pore space between the large particles [197, 198]. The mean particle diameter  $\langle d \rangle$  can also be defined as a function of  $\alpha$  by

$$\langle d \rangle = d_{min} \frac{2\alpha}{1 + \alpha} = d_{max} \frac{2}{1 + \alpha} \quad (3.1)$$

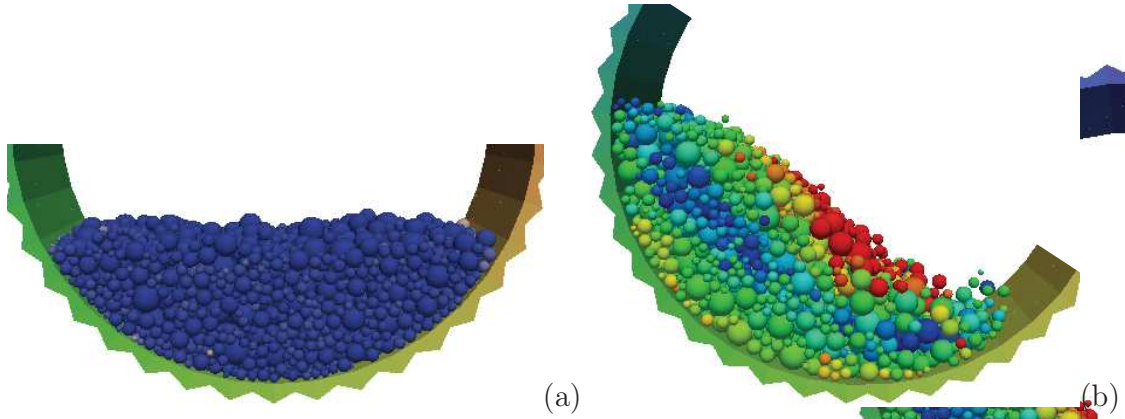


Figure 3.1 – Snapshots of the initial state (a) and stable flow (b) in the drum for  $\alpha = 5$ . The colors show the magnitudes of particle velocities varying from red (fast particles at the free surface) to blue (slowest particles in the middle of the drum).

Figure 3.1(a) shows an example of the initial state in a system with  $\alpha = 5$  and  $\langle d \rangle = 16 \mu\text{m}$ . Fig. 3.1(b) displays the granular flow after 50 rotations. At the beginning, all particles are at rest inside the drum. With drum rotation, a stable flow configuration is reached after nearly four rotations. In particular, in this steady regime the inclination of the free surface remains constant.

A number  $N_w$  of particles distributed randomly inside the drum are wetted by attributing them a given amount of liquid. These wet particles may collide and nucleate into small granules during the steady flow of the particles. However, because of the relatively low number of particles, it is numerically more efficient to start the simulations with a single granule introduced initially in the center of the granular bed. The agglomeration process can then be analyzed by following the particles captured by (accretion) or removed from (erosion) the granule. Obviously, the coalescence of granules can be investigated only by simulations with a much larger number of granules. In this chapter, we focus on the first option with agglomeration around a single wet granule. To define the initial wet granule,

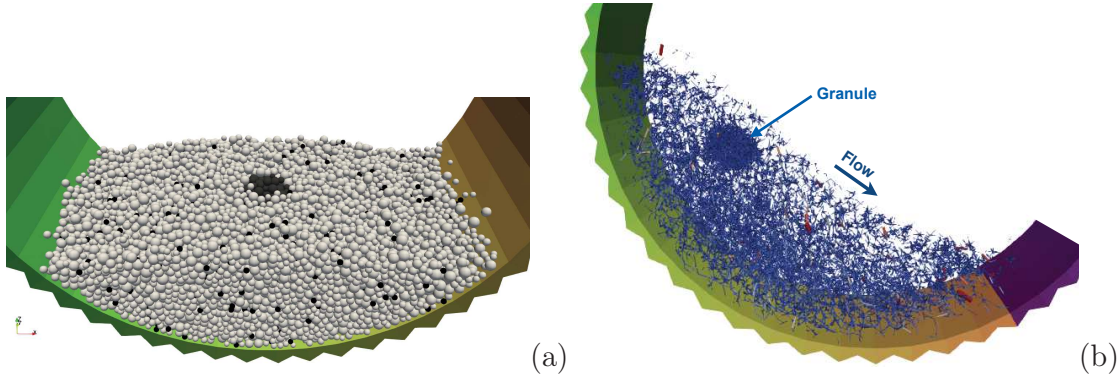


Figure 3.2 – (a) Snapshot of the granular bed showing the distribution of dry particles (in white) and wet particles (in black) both those inside the initially defined granule in the center of the bed and those randomly distributed throughout the bed; (b) Force chains during agglomeration: line thickness is proportional to normal force between neighboring particles with compressive forces in blue and tensile forces in red.

we place a spherical probe in the centre of the granular bed with a radius such that exactly  $N_{g0} = 100$  particles are inside the probe. All these particles are considered to be wet. In addition, we randomly select  $N_w - N_{g0} = 200$  free particles throughout the sample and consider them to be wet. Fig. 3.2 displays the initial state of the granular bed together with the initial granule and free wet particles. The capillary and viscous forces are activated for all wet particles.

The liquid content of wet particles  $w = V_\ell/V_g$ , where  $V_\ell$  is the amount of the liquid and  $V_g$  is the particle volume, is assumed to have the same value for all wet particles. In all our simulations, we set  $w = 0.09$ , which is sufficient to create wet granules in a horizontal rotating drum [68]. When two wet particles meet, the volume of the liquid bridge is  $V_\ell = wV_g$ . We also assume that there is no excess liquid so that a wet particle can not form a liquid bridge with a dry particle.

We performed a large number of simulations with different values of  $d_{min}$  and  $d_{max}$  in the range  $[10, 1500]$   $\mu\text{m}$ , different values of friction coefficient  $\mu$  in the range  $[0.1, 0.9]$  and four values of liquid viscosity  $\eta$ . For each set of values, several independent granular beds were generated. All values of the material parameters used in our simulations are listed in Table 3.1. The choice of most parameter values is guided either by numerical efficiency or by reference to the agglomeration process of iron ores in a rotating drum, e.g. for the density of particles, contact angle and filling level. The contact stiffness is chosen such that the elastic deflection at contact points under the weight of the particles in the center of the drum is below 0.01. This ensures the approximation of nearly rigid particles. The damping parameter is chosen for a restitution coefficient of 0.1. However, for data analysis we rely on dimensionless parameters. For rotating drum, a relevant dimensionless parameter is the Froude number  $Fr$  [114, 115, 31]:

$$Fr = \frac{\omega^2 d_c}{2g}. \quad (3.2)$$

Table 3.1 – Simulation parameters

Parameter	Symbol	Value and Unit
Particle diameters	$d$	[10,1500] $\mu\text{m}$
Density of particles	$\rho$	3500 $\text{kg}\cdot\text{m}^{-3}$
Size ratios	$\alpha$	[1,5]
Number of particles	$N_p$	5000
Filling level	$s_f$	0.56
Friction coefficient	$\mu$	[0.1,0.9]
Normal stiffness	$k_n$	100 N/m
Tangential stiffness	$k_t$	80 N/m
Normal damping	$\gamma_n$	$5\cdot 10^{-5}$ Ns/m
Tangential damping	$\gamma_t$	$5\cdot 10^{-5}$ Ns/m
Surface tension	$\gamma_s$	0.021 N/m
Contact angle	$\theta$	4.0 degree
Liquid viscosity	$\eta$	[10;20;40;60] mPa.s
Time step	$\delta t$	$10^{-7}$ s

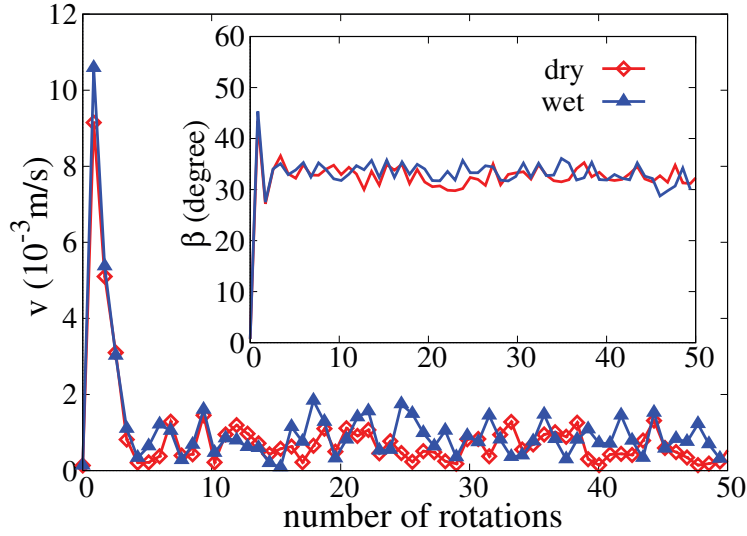


Figure 3.3 – The mean velocity  $v$  of drum flow for dry particles and in the presence of wet particles with  $Fr = 0.5$  as a function of the number of rotations of the drum. The inset shows the evolution of the free surface inclination angle  $\beta$  as a function of the number of rotations.

The flow regime mainly depends on the value of the Froude number. For dry particles, the value  $Fr = 0.5$  leads to a flow regime intermediate between rolling and cascading regimes [15, 25]. Since these regimes have been established for dry particles, we investigated the effect of the wet particles by comparing the velocity profiles for dry particles, on the

one hand, and in the presence of wet particles, on the other hand, for  $Fr = 0.5$ . We observe practically the same velocity profiles in both cases. Fig. 3.3 shows the mean particle velocity  $v$  and free surface inclination  $\beta$  for the two simulations with  $\alpha = 5$ . We see that both  $v$  and  $\beta$  have the same value in both flows. The only difference is that there are more fluctuations in the presence of free wet particles that can be attributed to the higher inhomogeneity of the flow in this case.

### 3.3 Growth, accretion and erosion

In this section, we are interested in the evolution of the granule size, in terms of the total number of particles  $N_g$  embodied in the granule, as well as the relative contributions of the accretion and erosion events. The cumulative accretion is the number  $N_g^+$  of free wet particles captured by the granule whereas the cumulative erosion  $N_g^-$  is the number of wet particles leaving the granule. The rates of these events depend on the relative importance of force chains and cohesive stresses acting on the granule. The values of the process parameters affect the rates so that the granule may grow at different rates. When the rate becomes negative, the granule initially inserted into the granular bed will disappear by excess erosion. Unless explicitly stated, the liquid properties are those of water ( $\eta = 1$  mPa.s and  $\gamma_s = 0.072$  N/m). From the parametric study, we will determine the phase diagram of granule growth for size polydispersity vs. mean particle size.

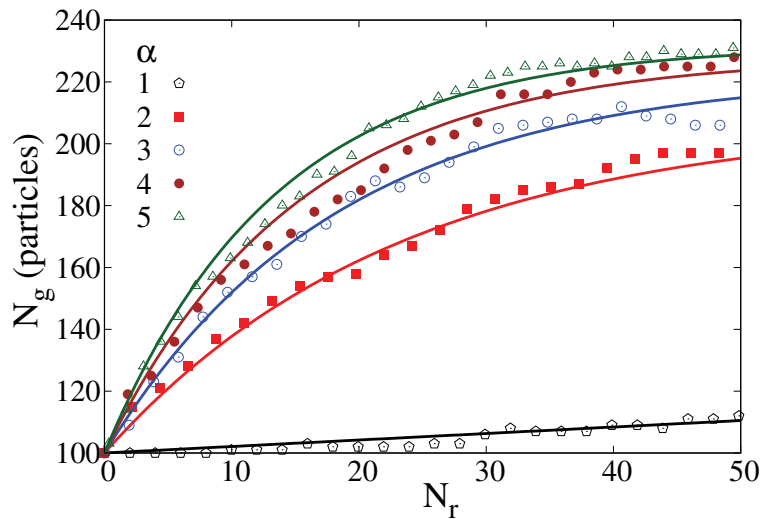


Figure 3.4 – Evolution of the granule size  $N_g$  (in number of particles) for different values of size ratio  $\alpha$  and  $d_{min} = 10 \mu m$ . The solid lines are exponential fits given by equation (3.6).

Figure 3.4 shows the evolution of the granule size as a function of the number of drum rotations  $N_r = \omega t / 2\pi$ , where  $t$  is the agglomeration time, for different values of the size

ratio  $\alpha$ ,  $Fr = 0.5$  and  $\mu = 0.5$ . In these simulations,  $d_{min}$  is kept constant and equal to  $10 \mu\text{m}$ . This means that  $\alpha$  is increased here by increasing  $d_{max} = \alpha d_{min}$ . We see that the granule grows with  $N_r$  at a rate that increases with  $\alpha$  and levels off as the number of wet particles is exhausted. The increase of agglomeration rate with increased size polydispersity is more spectacular when compared to the mono-disperse case ( $\alpha = 1$ ) in which the granule growth is negligibly small after 50 rotations. As we are interested in this chapter in the evolution of captured and eroded particles, the granule size  $N_g$  is expressed in terms of the number of wet particles in the granule. Even for broad size polydispersity, we find that the total volume of wet particles belonging to the granule is a linear function of their number, as shown in Fig. 3.5, up to a factor that depends on the size polydispersity. Hence, the trends of  $N_g$  investigated below are similar to those of the total volume of the granule or the total volume of particles in the granule.

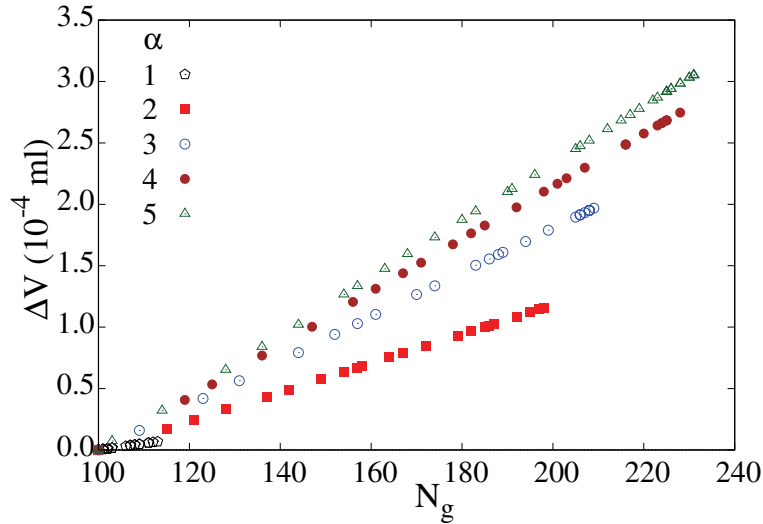


Figure 3.5 – Variation  $\Delta V$  of the volume of particles inside the granule as a function of their number  $N_g$  for different values of size ratio  $\alpha$  and  $d_{min} = 10 \mu\text{m}$ .

The cumulative accreted and eroded particles are plotted in Fig. 3.6 as a function of  $N_r$  only for polydisperse samples in which we have a significant number of particles captured and eroded. The accretion grows at a negative rate whereas erosion is a linear function. We will see below with other values of material parameters that the erosion can grow in a non-linear way and faster than accretion so that the linear evolution observed in Fig. 3.6 may be considered as a first-order effect in the limit of low erosion rates. Fig. 3.6 also shows that both accretion and erosion increase with  $\alpha$  to an extent that is higher for accretion than for erosion.

The increase of the number of accreted particles  $N_g^+$  at a negative rate is a consequence of the decreasing number of available free wet particles in the granular bed while they are captured by the granule. The number of free wet particles is given by  $N_w - N_g$ , where

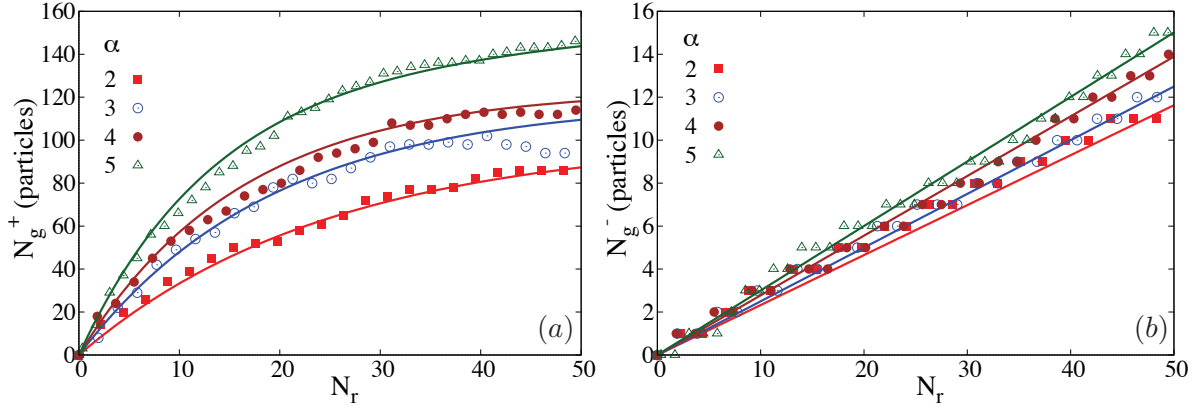


Figure 3.6 – Cumulative accretion (a) and cumulative erosion (b) of particles for different values of the size ratio  $\alpha$ . The lines are fitting forms given by equations (3.7) and (3.8), respectively.

$N_w$  is the total number of wet particles including those belonging to the granule. This is equivalent to the decrease of the available liquid for agglomeration as the granules grow. Hence, in the steady flow, we may assume that the variation  $\Delta N_g^+$  of the captured particles is proportional to the current number  $N_w - N_g$  of wet particles and to the elapsed time  $\Delta t$  or angular rotation  $\Delta N_r = \omega \Delta t$ :

$$\Delta N_g^+ = k^+ \frac{N_w - N_g}{N_w} \Delta N_r, \quad (3.3)$$

where  $k^+$  is the relative accretion rate. As to the number  $N_g^-$  of eroded particles, we assume that its rate  $k^-$  is constant :

$$\Delta N_g^- = k^- \Delta N_r. \quad (3.4)$$

These equations are consistent with our numerical data shown in Fig. 3.6 although we expected the number of eroded particles to be proportional to the number of particles at the surface of the granule. This may reflect the fact that the average curvature of the granule surface diminishes as its size increases so that the particles lying at the surface of the granule are more strongly attached to the granule and less subjected to the eroding action of granular flow. This effect may counter-balance the increase of the granule surface area. However, for much larger granules in number of primary particles this effect may disappear.

With the above assumptions, the rate equation for the granule size is simply  $\Delta N_g = \Delta N_g^+ - \Delta N_g^- = (-k^+ N_g / N_w + k^+ - k^-) \Delta N_r$ , which leads to a simple differential equation:

$$\frac{dN_g}{dN_r} = k^+ (1 - N_g / N_w) - k^- \quad (3.5)$$

with the following solution:

$$N_g(N_r) = N_{g0} + \{N_w(1 - k^- / k^+) - N_{g0}\} (1 - e^{-\frac{k^+}{N_w} N_r}). \quad (3.6)$$

This model predicts an exponential growth and an asymptotic granule size  $N_g(t \rightarrow \infty) = N_w(1 - k^-/k^+)$ , as observed in our simulations. A similar growth and level-off is observed in experiments with a finite amount of available liquid although the experimental conditions and the agglomeration method are not the same as in our simulations [184, 199]. The steady agglomeration state corresponds to the condition  $\Delta N_g^+ = \Delta N_g^-$ . For  $k^- \ll k^+$ , the final granule embodies nearly all wet particles:  $N_g \simeq N_w$ . On the other hand, the granule disappears if  $k^- > k^+$ .

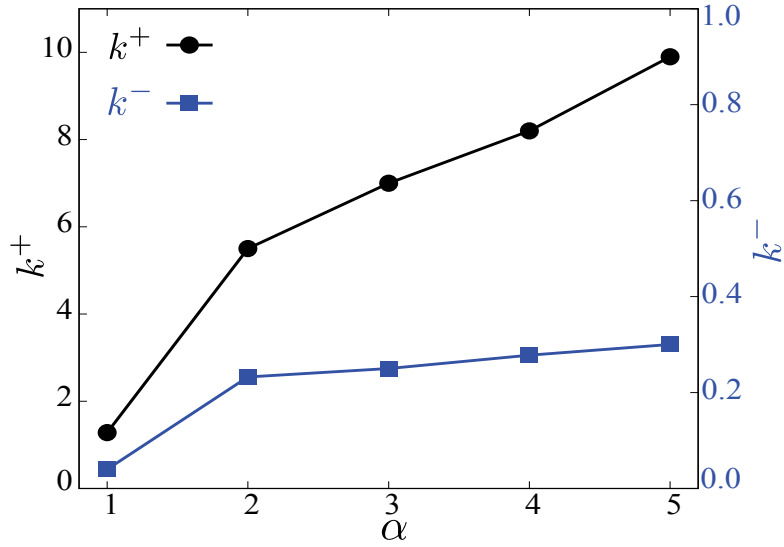


Figure 3.7 – Fitted values of accretion rate  $k^+$  and erosion rate  $k^-$  as a function of polydispersity parameter  $\alpha$ .

The evolution of  $N_g^+$  and  $N_g^-$  as a function of drum rotation can be obtained from equations (3.6), (3.3) and (3.4). We get

$$N_g^- = k^- N_r \quad (3.7)$$

and

$$N_g^+ = \{N_w(1 - k^-/k^+) - N_{g0}\}(1 - e^{\frac{-k^+}{N_w} N_r}) + k^- N_r \quad (3.8)$$

In view of the present model, the influence of particle size ratio  $\alpha$  observed in Figs. 3.4 and 3.6 can be interpreted in terms of the accretion and erosion rates. Fig.3.7 shows the fitted values of  $k^-$  and  $k^+$  as a function of  $\alpha$ . The increase of accretion rate  $k^+$  with  $\alpha$  is rather counter-intuitive since the cohesive strength is inversely proportional to the mean particle size, which increases here with  $\alpha$ . This means that the higher polydispersity, allowing for a better filling of the pore space and thus higher density of the granule, over-compensates the decrease of the cohesive stress. But the latter explains the increase of the erosion rate  $k^-$ , which is quite small compared to  $k^+$ .

### 3.4 Effects of material parameters

We now consider the effect of the mean particle size  $\langle d \rangle$ , which directly controls the cohesive stress of wet particles. Fig. 3.8 displays the cumulative number of particles for both accretion and erosion in the case  $\alpha = 5$ ,  $\mu = 0.5$ . Note that, in these simulations, the higher values of  $\langle d \rangle$  imply higher values of both  $d_{min}$  and  $d_{max}$ . But, according to equation (3.1),  $d_{max}$  increases faster than  $d_{min}$ . Fig. 3.8 shows that accretion  $N_g^+$  increases as an exponential function of the number of drum rotations whereas erosion  $N_g^-$  is quasi-linear. As expected, since the cohesive stress declines, accretion decreases and erosion increases with increasing  $\langle d \rangle$ . For  $\langle d \rangle = 1666 \mu\text{m}$ , erosion is high enough to cancel the effect of accretion, and thus the granule disappears after 8 rotations. Here, the cumulative erosion does not grow linearly with time and for this reason the erosion rate is not constant. For the linear part of erosion, we have  $k^- \simeq 25$  whereas  $k^+ \simeq 6$ . Clearly,  $k^-$  is strongly dependent on the cohesive stress of the granule, which declines in inverse proportion to the wet particle mean size. The cohesive stress of wet particles affects, albeit to a lesser extent, the accretion rate  $k^+$ .

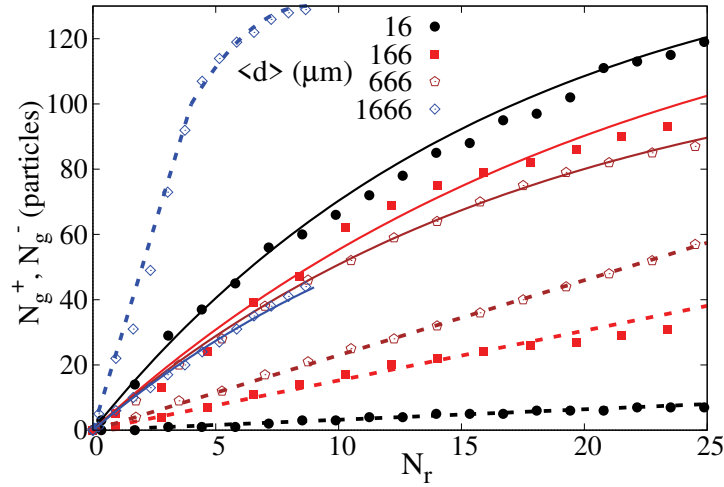


Figure 3.8 – Evolution of the cumulative number of wet particles for accretion (solid lines) and erosion (dashed lines) for four different values of the mean particle diameter  $\langle d \rangle$  and size ratio  $\alpha = 5$ , as a function of the number of drum rotations.

The friction coefficient  $\mu$  between particles is a major parameter for granular flows. Its joint effect with cohesive forces can thus influence the agglomeration process. Fig. 3.9 shows cumulative accretion and erosion for an increasing value of  $\mu$  and exponential fits. Fig. 3.10 displays  $k^-$  and  $k^+$  as a function of  $\mu$ . We observe a slight increase of both rates. The values of  $N_g^+$  and  $N_g^-$  after 50 rotations show that accretion increases slightly with  $\mu$ , which may be understood as a consequence of enhanced capturing of free wet particles when they touch the granule. However,  $N_g^-$  increases to a larger extent with  $\mu$  so that the

granule growth is slower at larger values of  $\mu$ . As erosion is a consequence of interactions between dry particles and boundary wet particles of the granule, the increase of erosion with  $\mu$  may be understood as an increase of shear forces acting on the boundary particles by shear flow of dry particles. This suggests that the agglomeration of rough particles (with higher friction coefficient) is less efficient than smooth particles and it should consume more energy.

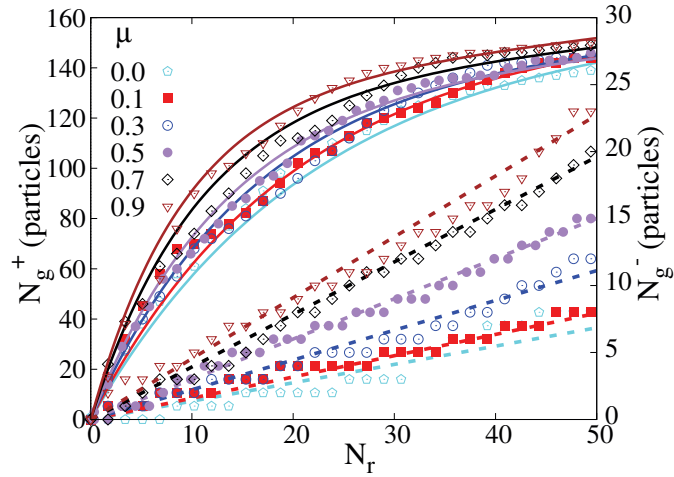


Figure 3.9 – Cumulative accretion (solid lines) and erosion (dashed lines) of wet particles for five different values of the friction coefficient  $\mu$ , size ratio  $\alpha = 5$  and  $d_{min} = 10 \mu\text{m}$ , as a function of the number of drum rotations. The lines are fitting forms given by equations (3.7) and (3.8).

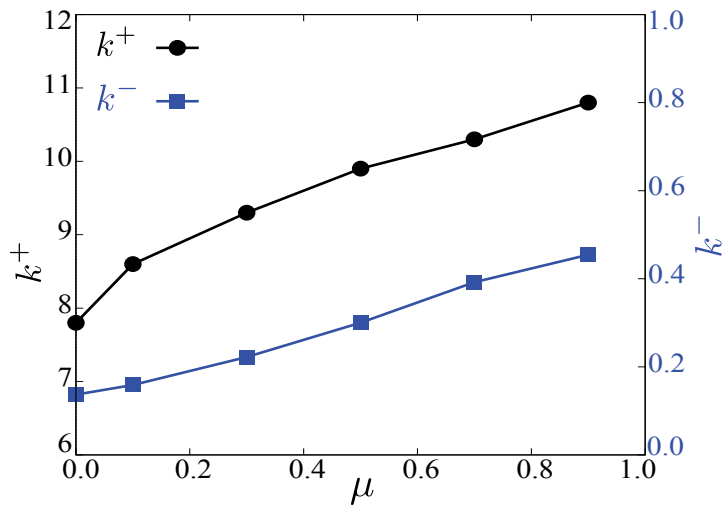


Figure 3.10 – Fitted values of erosion rate  $k^-$  and accretion rate  $k^+$  as a function of friction coefficient  $\mu$  for size ratio  $\alpha = 5$ .

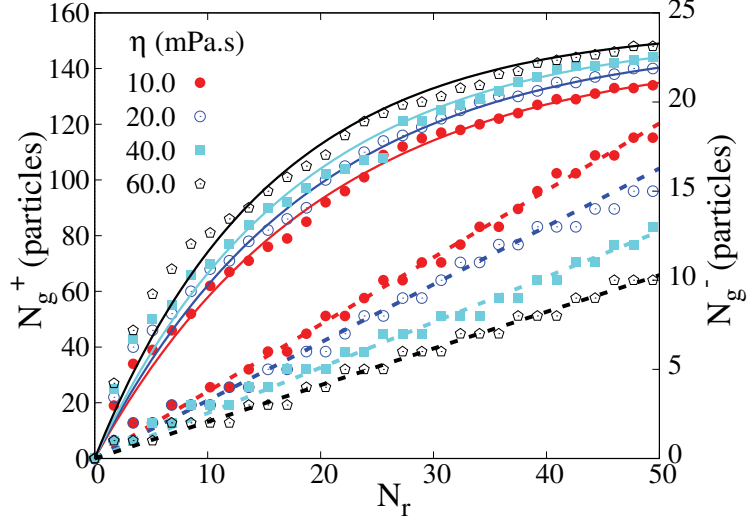


Figure 3.11 – Cumulative accretion (solid lines) and erosion (dashed lines) for four different values of the liquid viscosity  $\eta$  for size ratio  $\alpha = 5$  and  $d_{min} = 10 \mu\text{m}$  as a function of the number of drum rotations. The solid and dashed lines are exponential and linear fits to the data points, respectively.

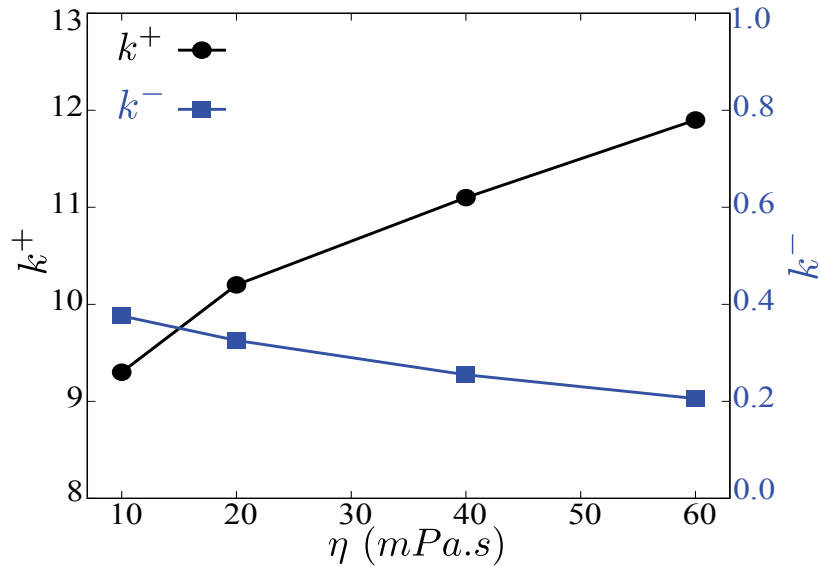


Figure 3.12 – Erosion rate  $k^-$  and accretion rate  $k^+$  as a function of liquid viscosity  $\eta$  for size ratio  $\alpha = 5$  and  $d_{min} = 10 \mu\text{m}$ .

This brings us to the effect of liquid viscosity expressed as a lubrication force between wet particles. We performed several simulations for different values of  $\eta$  in the range  $[10, 60]$

mPa.s and with same value of the liquid-vapor surface tension  $\gamma_s=21$  mN/m. Fig. 3.11 shows the evolution of cumulative accretion and erosion for  $\alpha = 5$ . Again, we observe the exponential increase of  $N_g^+$  vs. the nearly linear increase of  $N_g^-$  with the number of drum rotations. The accretion increases slightly with  $\eta$  whereas the erosion declines. The decrease of  $N_g^-$  is exactly the opposite effect of friction coefficient in Fig. 3.9 which causes an increase of  $N_g^-$ . This means that lubrication forces tend to reduce the shearing effect of the flow on the granule, leading to smaller erosion. On the other hand, the increase of accretion can be attributed to viscous dissipation that can enhance the capture of free wet particles by the granule. Fig. 3.12 shows  $k^-$  and  $k^+$  as a function of  $\eta$ . The variations of the rates with  $\eta$  are small but their opposite effects tend to enhance granule growth. It is also interesting to note that the linear decrease of  $k^-$  was also observed in experiments [25].

### 3.5 Phase diagram

In the simulations reported in this chapter, we have a single granule of size  $N_{g0}$  that can increase or decrease in size depending on the values of various material parameters. In the last section, we analyzed the influence of several parameters on the accretion and erosion rates. The most crucial issue, however, in this single-granule problem is the ranges of the values of those parameters for which the granule will survive and grow, i.e. the phase diagram of agglomeration. We consider here only the phase diagram in the parameter space of the mean particle size  $\langle d \rangle$  vs. size ratio  $\alpha$ . In these simulations, we set  $\eta = 1$ ,  $\gamma_s=72$  mN/m and  $\mu = 0.5$ .

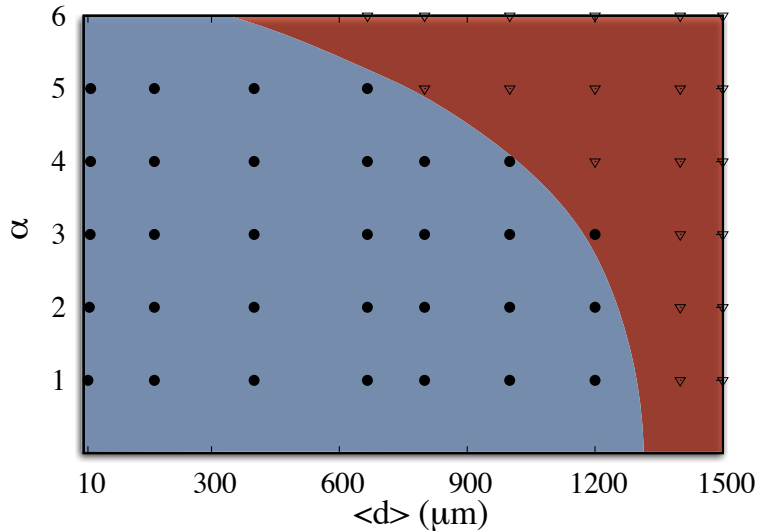


Figure 3.13 – Phase diagram of granule growth in the parametric space of  $\langle d \rangle$  vs.  $\alpha$  for  $\eta = 1$  mPa.s and  $\mu = 0.5$ . The granule grows only in the light blue region and disappears otherwise.

Figure 3.13 displays all the simulated points as a grid in the parameter space  $[\langle d \rangle, \alpha]$  and an approximate frontier between the range of values for which the granule survives, i.e. agglomeration is possible, and the values for which no granule can grow. We see that for  $\langle d \rangle > 1200 \mu\text{m}$  no agglomeration occurs even for large values of  $\alpha$  (larger polydispersity). For smaller values of  $\langle d \rangle$ , the range of the values of  $\alpha$  for agglomeration increases. Note that the limit on the value of  $\alpha$  is related to the fact that for given  $\langle d \rangle$ , the increase of  $\alpha$  requires the increase of  $d_{max}$  and decrease of  $d_{min}$ . The increase of  $d_{max}$  compensates to some extent the effect of decreasing  $d_{min}$  on the cohesive stress.

## 3.6 Conclusions

In this chapter, we used a 3D DEM algorithm with a capillary cohesion law enhanced by the viscous effect of the binding liquid in order to investigate the agglomeration of wet particles in dense granular flows inside a rotating drum. The system was numerically prepared by pouring solid particles into a drum composed of polyhedral elements. We considered in detail the evolution of a single granule acting for a broad range of parameter values. The liquid was assumed to be transported by the particles and its amount was defined by the number of initial wet particles in the granule and the number of free wet particles randomly distributed inside the granular bed.

We showed that the granule grows almost exponentially with time (or the number of drum rotations) as a result of a gradual capture of free wet particles by the granule. The accretion of free wet particles is nearly always an exponential function of time whereas the number of eroded particles grows linearly with time. A simple model based on constant accretion and erosion rates was introduced, predicting the observed exponential increase of granule size that levels off to a constant value at long times. We investigated the effects of size ratio, mean particle size, friction coefficient and liquid viscosity on accretion and erosion of particles. Both accretion and erosion increase when the size ratio or friction coefficient are increased. Accretion declines whereas erosion increases when the mean particle size is increased. Accretion increases whereas erosion declines when liquid viscosity is increased. We determined the phase diagram of agglomeration by varying systematically the size ratio and mean particle size. This will be extended to other parameters in the future.

Our results are based on a simple system with a relatively small number of spherical particles. We considered the evolution of a single granule and this allowed us to perform long-time simulations for a broad range of the values of material parameters. Clearly, these simulations can be extended to obtain the combined effects of parameters in phase-space diagrams. The effects of process parameters such as filling rate, rotation speed and wetting procedure can be studied, too. Further data analysis is also necessary in order to investigate the granule consolidation and nucleation from free wet particles when no granule is initially introduced. Despite its higher computational cost, a larger number of particles may allow for the simulation of multi-granule systems and coalescence phenomena.

*“If A is a success in life, then A equals x plus y plus z. Work is x; y is play; and z is keeping your mouth shut.”*

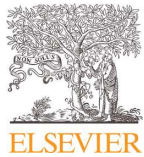
Albert Einstein (1879-1955)

## Chapter 4

# Mechanical strength of wet particle agglomerates

This chapter was published as a regular paper in **Mechanics Research Communications**

Mechanics Research Communications 92 (2018) 1–7



Contents lists available at [ScienceDirect](#)

Mechanics Research Communications

journal homepage: [www.elsevier.com/locate/mechrescom](http://www.elsevier.com/locate/mechrescom)



## Mechanical strength of wet particle agglomerates

Thanh-Trung Vo<sup>a,b</sup>, Patrick Mutabaruka<sup>c</sup>, Saeid Nezamabadi<sup>a</sup>, Jean-Yves Delenne<sup>d</sup>,  
Edouard Izard<sup>e</sup>, Roland Pellenq<sup>c</sup>, Farhang Radjai<sup>a,c,\*</sup>

<sup>a</sup> LMGC, Université de Montpellier, CNRS, Montpellier, France

<sup>b</sup> Bridge and Road Department, Danang Architecture University, Da Nang 553000, Vietnam

<sup>c</sup> (MSE)<sup>2</sup>, UMI 3466 CNRS-MIT, MIT Energy Initiative, 77 Massachusetts Avenue, Cambridge 02139, United States

<sup>d</sup> IATE, UMR1208 INRA - CIRAD - Université de Montpellier SupAgro, 34060 Montpellier, France

<sup>e</sup> ArcelorMittal R&D Maizières, Voie Romaine, F-57283, Maizières-les-Metz, France





Using molecular dynamics simulations, we investigate the strength and microstructure of agglomerates of wet frictional particles subjected to axial compression. The numerical model accounts for the cohesive and viscous effects of the binding liquid up to a debonding distance with the liquid assumed to be distributed homogeneously inside the agglomerate. We show that wet agglomerates undergo plastic deformation due to the rearrangements of primary particles during compression. The compressive strength is thus characterized by the plastic threshold before the onset of failure by the irreversible loss of wet contacts between primary particles. We find that the agglomerate plastic threshold is proportional to the characteristic cohesive stress defined from the liquid-vapor surface tension and the mean diameter of primary particles, with a prefactor that is a nearly linear function of the debonding distance and increases with size span. We analyze the agglomerate microstructure and, considering only the cohesive capillary forces at all bonds between primary particles, we propose an expression of the plastic strength as a function of the texture parameters such as the wet coordination number and packing fraction. This expression is shown to be consistent with our simulations up to a multiplicative factor reflecting the distribution of the capillary bridges.

## Contents

---

<b>4.1</b>	<b>Introduction</b>	<b>71</b>
<b>4.2</b>	<b>Numerical procedures</b>	<b>72</b>
4.2.1	Physical assumptions	72
4.2.2	Ideal granules	73
<b>4.3</b>	<b>Granule strength</b>	<b>76</b>
<b>4.4</b>	<b>Analytical model</b>	<b>78</b>
<b>4.5</b>	<b>Conclusions</b>	<b>82</b>

---



## 4.1 Introduction

The agglomeration or granulation of solid particles is used in many sectors including powder metallurgy, chemical engineering, pharmaceutical industry, and iron-making processes to produce agglomerates or granules from small particles. The agglomerates are used to improve flow properties, enhance permeability for the interstitial gas or reduce segregation in the presence of several types of particles [20, 70, 71, 72]. The binding material is generally a liquid, which is mixed with the primary particles in a granulator [77, 78, 79, 80]. Hence, the mechanical strength of the ‘raw granules’ produced by the agglomeration of primary particles is ensured by the action of capillary and viscous forces due to the presence of liquid clusters in the pore space [73, 84, 81, 83, 85, 82].

The raw granules should be in a densely and homogeneously packed state in order to support the loads to which they are subjected during subsequent operations and give rise to strong solid granules upon sintering [88, 86, 87, 89, 90]. The granule strength is controlled by two types of parameters: 1) process parameters such as the method of mixing particles with the liquid (depending on the granulator) [91, 92] and 2) material parameters such as the nature of the liquid and the size distribution of the particles [78, 92, 99]. The physical processes governing the growth of granules are complex due to the dynamic nature of granulation involving the collisions of particles and transport of the binding liquid inside a partially wet granular material [73, 100, 101, 102, 103, 104]. The agglomeration process in a fluidized bed can be correctly modeled by assuming binary collisions between wet particles [79, 80, 105] whereas in a rotating drum [68], for example, the agglomeration occurs inside a dense cohesive granular flow whose rheology has only recently been studied by careful experiments [25, 67, 108, 110] and simulations [91, 3].

The effect of material parameters on the granule strength reflects both the strength of cohesive bonds between particles and the granular texture, i.e. the organization of the primary particles inside the granule. For example, the strength of pharmaceutical tablets, measured by quasi-static compression between two platens, declines with porosity, which is a function of the consolidation pressure used to manufacture the tablet [200, 201]. In the same way, the compressive strength of cohesive powder mixtures is an increasing function of the relative density [56]. The diametrical compression test is a simple way of measuring the tensile strength of powder compacts as the compressive strength (the stress at incipient failure of a granule) is proportional to the tensile strength of the granule [202]. This method has, however, been mostly used to study the fracture stress of brittle materials composed of particles glued via solid bonds [203, 204, 205]. In contrast, wet granules have been much less investigated. While their cohesive strength is mainly controlled by the Laplace pressure and surface energy of the liquid phase, the effects of granular texture resulting from the granulation process and material parameters are still poorly understood.

In this chapter, we are interested in the influence of material parameters on the strength of wet spherical agglomerates in which the liquid is assumed to be distributed as binary bridges joining eligible particle pairs. We use the Discrete Element Method (DEM) with a capillary cohesion law in which the attraction force is an explicit function of the gap between particles and liquid-vapor surface tension, and the amount of liquid is mainly accounted for by a debonding distance. By simulating the diametrical compression of spherical agglomerates, we find that, due to particle rearrangements, they show a plastic behavior with a threshold that we analyze as a function of friction coefficient and size span of primary particles. We also introduce a model for the compressive granule strength that accounts for particle size distribution and we discuss the role of the class of fine particles for the plastic threshold.

In section 4.2, we introduce the numerical model and procedures used to prepare and simulate spherical agglomerates. In section 4.3, we discuss the evolution of the granule strength as a function of axial strain and the effects of particle size span and liquid volume. In section 4.4, we introduce an analytical model of granule strength in terms of texture parameters. We conclude in section 4.5 with a short summary of salient results and routes to further research.

## 4.2 Numerical procedures

### 4.2.1 Physical assumptions

The Discrete Element Method (DEM) has been extensively used for the simulation of granular materials [130, 131, 132, 133]. It is based on the step-wise integration of the equations of motion for all particles by taking into account the particle interactions. In advanced applications of the DEM, it is now possible to implement also the presence of an interstitial fluid or a solid binding matrix [81, 134]. However, such applications require substantially more computation power and memory in order to discretize the degrees of freedom associated with the interstitial phase. For this reason, in DEM simulations of granular processes, it is necessary to set up a modeling strategy by making appropriate choices that allow for a balance between computational efficiency (large number of particles) and physical realism. In the case of unsaturated wet granular materials, it is found that the fluid phase can be correctly represented by its cohesive and viscous effect in the particle-particle interactions [135]. Hence, we rely on this approach to model the binding liquid in the granulation process.

On the other hand, the granule strength depends on its internal structure, which is controlled to some extent by the granulation device. Here, we are interested in the simpler case of ‘ideal’ granules of spherical shape where the primary particles and binding liquid are homogeneously distributed. This simplification allows us to investigate the effect of basic parameters such as the particle size distribution and friction between particles on the strength in the absence of specific granulation process parameters. Furthermore, in association with texture analysis, the results of this investigation can provide a reference

behavior against which the effects of process parameters can be quantified in the next step. We use the DEM with a capillary force law and a simple algorithm for the construction of spherical granules. It is worth mentioning here that this approach has been used for the simulation of an assembly of wet agglomerates in the pendular state in application to powder processes such as the coalescence of granules upon collision [206] and impact breakage of crystalline agglomerates [207, 208, 209, 210]. In this section, we describe both the numerical method and the procedure that we used to create our ‘ideal’ granules.

### 4.2.2 Ideal granules

In order to create homogeneous agglomerates of particles of spherical shape, we first prepared large samples by means of isotropic compaction inside a box. The primary particles are spheres with their diameters defined in a range  $[d_{min}, d_{max}]$  with a given size ratio  $\alpha = d_{max}/d_{min}$ . The size distribution is assumed to be uniform by particle volume fractions, i.e. with all size classes having the same volume. As the total volume of particles in each size class  $d_i$  is proportional to  $d_i^3$ , the uniform distribution by volume fractions is defined by the condition that the product  $n_i d_i^3$  is a constant and  $\sum_i P_i = 1$ , where  $P_i$  is the numerical fraction of particles in class  $i$ . These conditions lead to the following distribution  $P$  of particles of diameters  $d$ :

$$P(d) = 2 \frac{d_{max}^2 d_{min}^2}{d_{max}^2 - d_{min}^2} d^{-3} \quad (4.1)$$

This distribution has the advantage of allowing the particles belonging to each size class to be correctly represented by their volume, i.e. a large number of small particles and a small number of large particles. This distribution leads to a dense packing as the pore space between large particles is filled by smaller particles [211, 198].

We constructed different samples with five different values of the size ratio  $\alpha = 1, 2, 3, 4$  and  $5$ . Note that the mean particle diameter  $\langle d \rangle$  is a function of  $d_{min}$  and  $d_{max}$ :

$$\langle d \rangle = \int_{d_{min}}^{d_{max}} d P(d) \delta d = d_{min} \frac{2\alpha}{1+\alpha} = d_{max} \frac{2}{1+\alpha} \quad (4.2)$$

The largest particle size was kept to a constant value  $d_{max} = 10 \mu\text{m}$ , and  $d_{min}$  was decreased from  $10 \mu\text{m}$  to  $2 \mu\text{m}$ . Equation (4.2) shows that, since  $d_{max}$  is fixed, the average diameter  $\langle d \rangle$  declines by a factor 3 when  $\alpha$  is increased from 1 to 5.

For isotropic compaction, the particles were introduced in a box and equal compressive stresses  $\sigma_0$  were applied to the box walls without gravity until a packing in static equilibrium was achieved. During this step, the capillary force was set to zero and the friction coefficient to 0.1 at all contacts between particles in order to obtain a dense sample. Once all particles reached a state of static equilibrium, a spherical probe was placed in the center of the box and its radius was increased until exactly 5000 particles were inside the probe. These particles were then extracted and allowed to relax with the capillary force law activated.

The common numerical parameters in these simulations are  $\theta = 0$ ,  $\gamma_n = \gamma_t = 5 \times 10^{-5}$  Ns/m and  $\gamma_s = 0.072$  N/m (water).

We subjected the granules prepared by the above procedure to axial compression between two platens, as illustrated in Fig. 4.1(a). The bottom platen is fixed and a downward motion is applied to the top platen with a constant velocity  $v_0 = 0.1 \text{ ms}^{-1}$ . Hence, with time step  $\delta t = 10^{-9}$ s used in our simulations, the total downward displacement during one time step is  $v_0 \delta t = 10^{-10}$  m, which is  $10^{-5}$  times the size of the primary particles. This means that the diametrical deformation applied to the granules is slow enough to allow for a quasi-static compression test.

To see how quasi-static is the compression, one may also compare the average elastic force increment  $\delta f_e$  between particles with the cohesive force  $f_c = \pi \gamma_s d$ . The incremental force between particles is simply given by the contact normal stiffness  $k_n$  multiplied by the average normal displacement  $\delta_n$  at the contact points between primary particles. The latter is given by the mean diametral deformation  $v_0 \delta t / D_g$  times the primary particle size  $d$ . We thus can define the dimensionless index:

$$I_e = \frac{\delta f_e}{f_c} = \frac{k_n \delta t v_0}{\pi \gamma_s D_g}. \quad (4.3)$$

For monodisperse particles, from our parameter values we get  $I_e \simeq 2.5 \times 10^{-3}$ , which means that the force increments are generally small compared to the cohesion force. Finally, the time associated with the dissipation of kinetic energy is given by the ratio  $\langle m \rangle / \gamma_n \simeq 10^{-6}$  s, which is small compared to the loading rate defined by  $\langle d \rangle / v_0 \simeq 10^{-4}$  s, showing that the dissipation of the kinetic energy occurs much faster than the typical time evolution of the aggregate.

Figures 4.1(b), (c) and (d) show the initial states of the granules with three different values of  $\alpha$  before diametrical compression. In Fig. 4.2, we display a snapshot of a granule for  $\alpha = 1$  at the end of diametrical compression. At the beginning of the test, at most three primary particles of the granule are in contact with either of the two platens. As the compression proceeds, the granule spreads without breaking between the two platens and the number of contacts between the granule and each platen increases.

The mechanical response of the granule under diametrical compression requires a measure of the axial force and vertical deformation. The vertical deformation in compression is given by

$$\varepsilon = \ln \left( 1 + \frac{\Delta h}{D_g} \right) \approx \frac{\Delta h}{D_g} \quad (4.4)$$

where  $\Delta h = v_0 t$  is the total downward displacement of the top platen (the lower platen being fixed). We also measure the vertical force component  $F$  between the granule and the top platen by summing up the normal forces between the primary particles and the platen. Let us note that, as the granule is in static equilibrium, all forces at each horizontal layer of the granule are balanced so that the vertical force acting between all horizontal layers is equal to  $F$ . By dividing this force by the sectional area  $\pi a^2$  of the granule, where  $a$  is the radius of the central section of the granule perpendicular to the compression axis, we

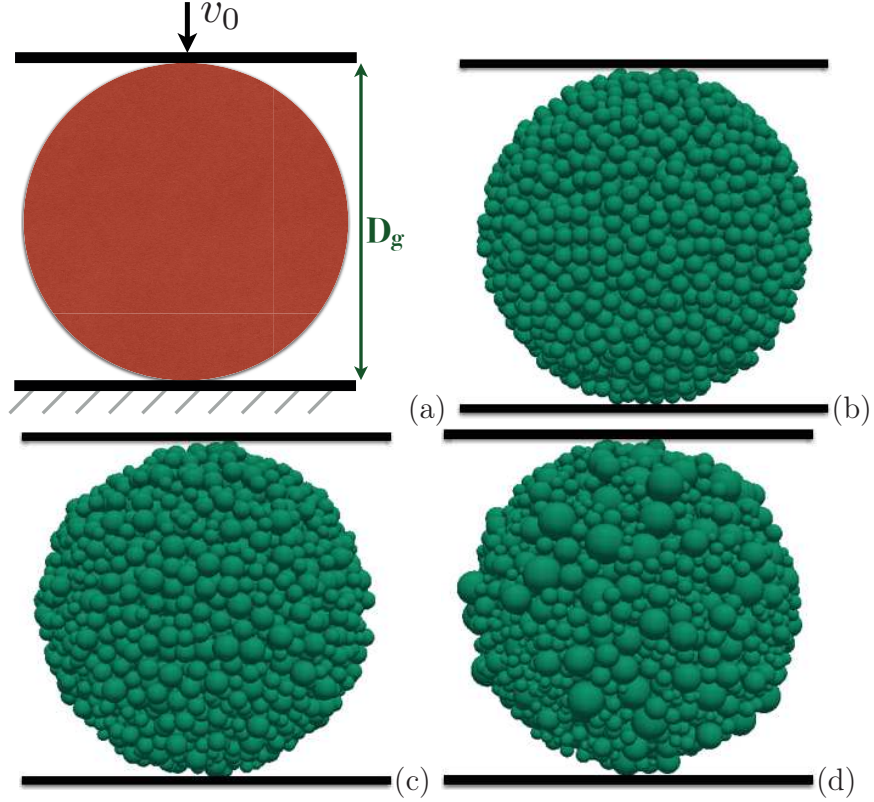


Figure 4.1 – Schematic representation of diametrical compression test (a), and snapshots of granules composed from 5000 primary spherical particles before diametrical compression for (b)  $\alpha = 1$ ; (c)  $\alpha = 2$ , and (d)  $\alpha = 5$ .

get the [average](#) vertical stress  $\sigma'_{zz} = F/(\pi a^2)$  in the center of the granule. The value of  $a$  is estimated from the positions of the particles located at the boundary of the actual central section.

The stress can also be obtained from the values of normal forces and branch vectors (vectors joining particle centers) using [212, 213, 214, 215, 216]

$$\sigma_{zz} = \frac{1}{V_g} \sum_{k=1}^{N_b} f_z^k \ell_z^k = n_b \langle f_z^k \ell_z^k \rangle_k, \quad (4.5)$$

where  $V_g$  is the volume of the granule,  $N_b$  is the number of bonds,  $n_b = N_b/V_g$  is the number density of bonds,  $f_z^k$  and  $\ell_z^k$  are the  $z$ -components of the bond force vector and branch vector, respectively, at the contact  $k$ , including all internal contacts as well as the contacts with the platens. The symbol  $\langle \dots \rangle_k$  denotes averaging over all contacts  $k$  in the volume. We find that  $\sigma_{zz} \simeq \sigma'_{zz}$  during vertical compression. Note that we can define a characteristic cohesive stress  $\sigma_c$  from the capillary force and the mean particle diameter

$\langle d \rangle$ :

$$\sigma_c = \frac{\kappa}{\langle d \rangle} \quad (4.6)$$

This stress depends on  $\langle d \rangle$  and, by virtue of equation (4.2), varies linearly with  $\alpha$  as

$$\sigma_c = \frac{\kappa}{d_{max}} \frac{1 + \alpha}{2} \quad (4.7)$$

Its value increases in our simulations by a factor 3 as  $\alpha$  is increased from 1 to 5 by reducing  $d_{min}$ .

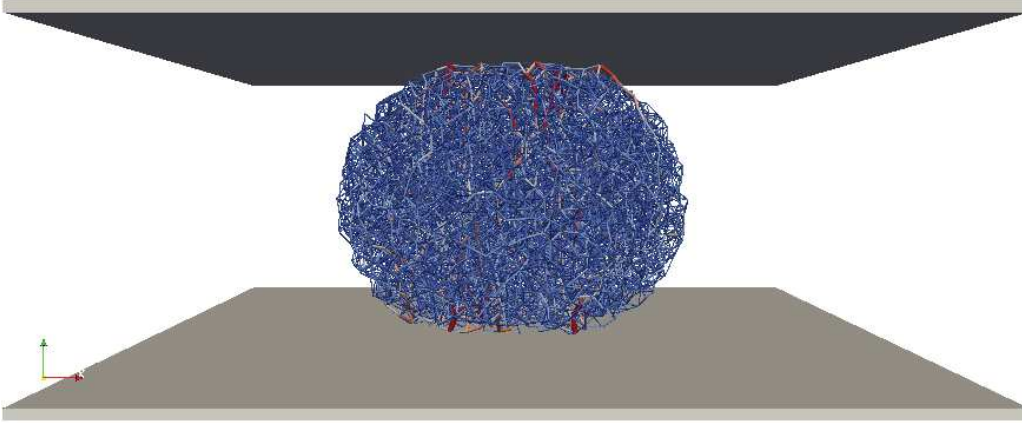


Figure 4.2 – Snapshot of a granule under diametrical compression for  $\alpha = 1$ . The lines are force chains joining the particle centers.

### 4.3 Granule strength

Figure 4.3 shows the evolution of the mean vertical stress  $\sigma_{zz}$  normalized by the reference cohesive stress  $\sigma_c$  as a function of the vertical strain  $\varepsilon$  for different values of granule parameters. In all cases,  $\sigma_{zz}$  first increases with strain and reaches a plateau more or less fast depending on the values of parameters. It then declines smoothly as a result of the gradual loss of cohesive contacts. The stress plateau is a signature of plastic deformation due to particle rearrangements. However, this plateau does not persist as the cohesive contacts break apart and do not heal. This irreversible character of cohesive contacts is assumed to reflect the fact that the liquid contained in a capillary bridge between two particles is not physically available (e.g. due to evaporation or drainage) once the bridge disappears. This may not always be the case as liquid drops may survive at the surface of the particles and migrate through the vapor phase or by diffusion at the surface of the particles to the newly-formed contacts during a continuous deformation of the granule.

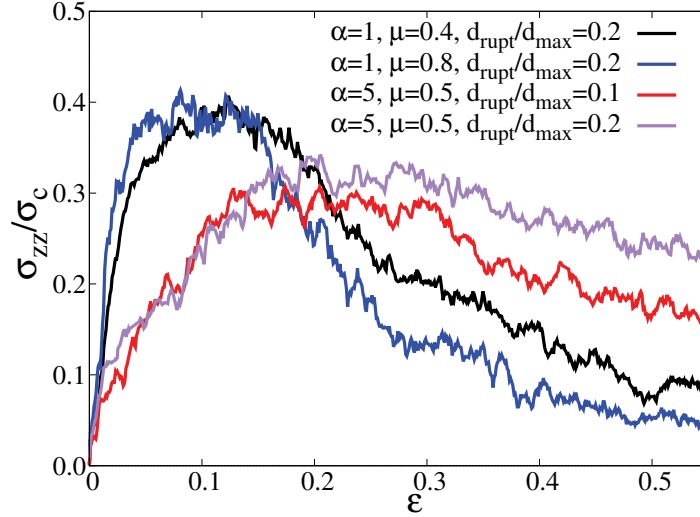


Figure 4.3 – Vertical strength  $\sigma_{zz}$  normalized by the reference stress  $\sigma_c$  for different values of friction coefficient  $\mu$ , size ratio  $\alpha$  and the debonding distance  $d_{rupt}$ , as a function of cumulative vertical strain  $\varepsilon$ .

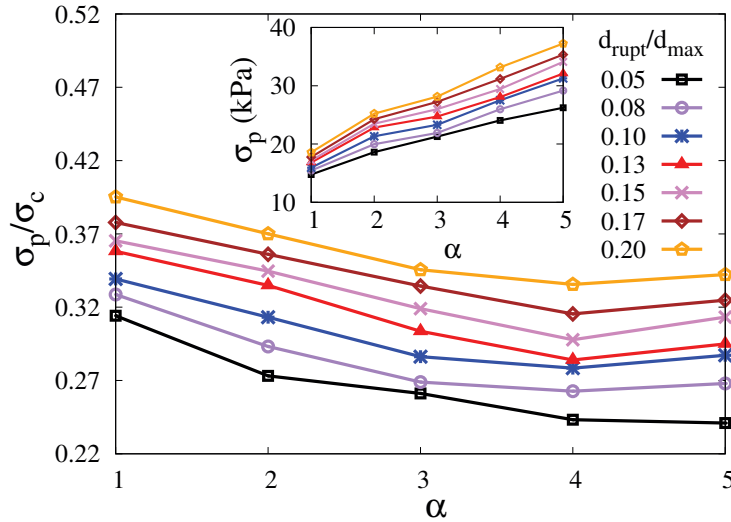


Figure 4.4 – Normalized plastic strength of the granule for several values of the debonding distance as a function of the size ratio  $\alpha$ . The inset shows the non-normalized value of the strength as a function of  $\alpha$ .

In this way, the observed behavior can globally be qualified as ductile with a well-defined plastic plateau before the beginning of a progressive loss of cohesion at strains above 0.2. This means that the debonding events between primary particles do not lead to spontaneous formation of a fracture surface. We also see that the plastic stress threshold

$\sigma_p$  is of the order of  $0.4\sigma_c$  for monodisperse particles and  $0.3\sigma_c$  for  $\alpha = 5$ . On the plateau, the particles are well-connected with one another, and the loss of one or two cohesive bonds of a particle does not lead to macroscopic rupture. The values of parameters affect not only the plastic threshold but also the initial build-up and later fall-off of the stress.

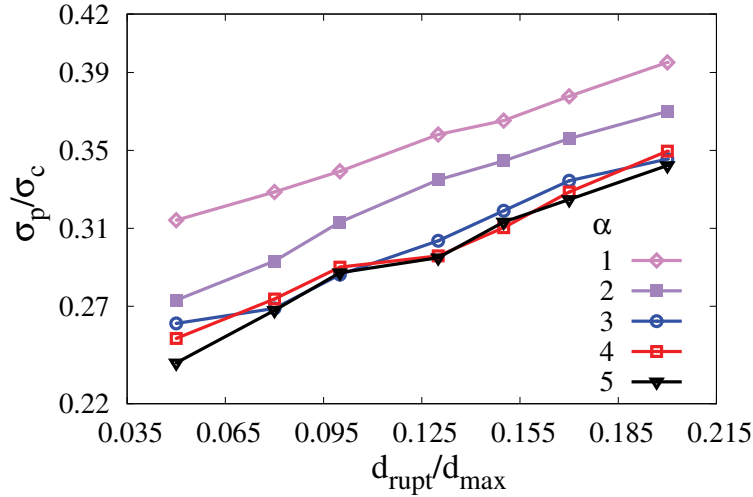


Figure 4.5 – Normalized plastic strength  $\sigma_p/\sigma_c$  of the granules for different values of the size ratio as a function of debonding distance  $d_{rupt}$ .

The effect of size span  $\alpha$  on the plastic strength is displayed in Fig. 4.4 for several values of the debonding distance  $d_{rupt}$ . We see that the ratio  $\sigma_p/\sigma_c$  declines by nearly the same amount in all cases as  $\alpha$  increases from 1 to 5. This is, however, only a small relative loss of strength with respect to  $\sigma_c$  given that, according to equation (4.7),  $\sigma_c$  is multiplied by 3 when  $\alpha$  increases from 1 to 5. Hence, in absolute value, the cohesive strength of the granule increases by nearly a factor 3 as shown in the inset to Fig. 4.4. Fig. 4.5 displays the cohesive (plastic) strength as a function of  $d_{rupt}$  for different values of  $\alpha$ . We see that this dependence is linear and quite weak for all values of  $\alpha$ . As we shall see in the next section, this increase of cohesive strength reflects that of the connectivity of primary particles by liquid bonds as the debonding distance increases.

## 4.4 Analytical model

The granule strength under diametrical compression reflects the microstructure of the granule, which depends in our simulations on the effects of size span and debonding distance (related to the amount of liquid). The granular microstructure can be described in terms of various scalar and tensorial variables such as the coordination number, packing fraction and fabric tensor [160]. Figure 4.6 shows that the initial value of the wet coordination number  $Z_0$  is an increasing function of both  $\alpha$  and the debonding distance  $d_{rupt}$ . The

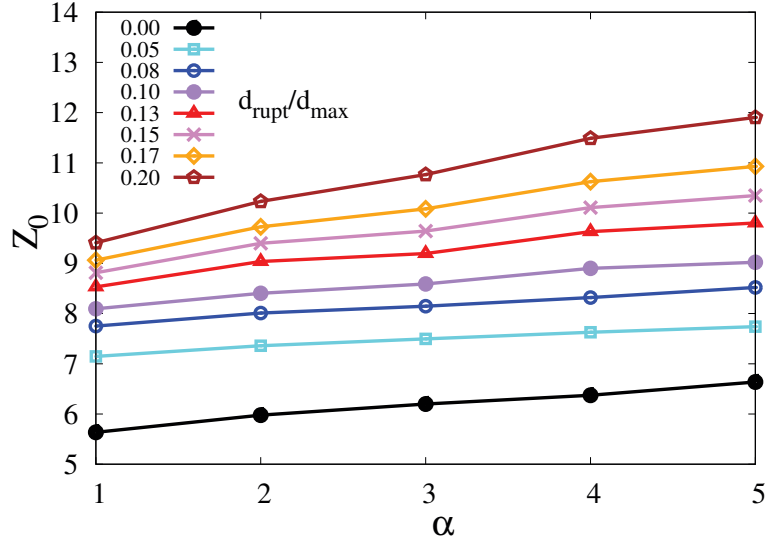


Figure 4.6 – The initial wet coordination number  $Z_0$  of the granules for different values of debonding distance as a function of the size ratio  $\alpha$ .

wet coordination number is defined as the number of capillary bonds per particle. This is slightly above the “dry” coordination number, which accounts for only the geometrically touching particles. We see that the increase of  $Z_0$  is more significant with  $d_{rupt}$  than with  $\alpha$ . Its increase is nonlinear with  $d_{rupt}$  and it levels off around  $Z_0 = 12$ .

In order to get a more clear understanding of the relation between the connectivity of particles and the plastic strength, we may use the expression (4.5) of the stress tensor applied in our case to the whole volume  $V_g$  of the granule. To obtain an analytical expression of the cohesive stress, we consider the cohesive forces  $f_c^{ij} = \pi\gamma_s\sqrt{d_i d_j}$  between particles of diameters  $d_i$  and  $d_j$ . Most of the cohesive strength is carried by this cohesive force acting between particles that are in contact. But many particles are connected by capillary bridges with a nonzero gap, where the cohesive force is below  $f_c^{ij}$  [24]. At plastic threshold, a large number of bonds along the directions perpendicular to the compression axis are tensile whereas many others along the compression axis are compressive.

The ductility of the particle at failure is induced by the effect of tensile bonds that prevent the primary particles from sudden rupture. We will account below for these bonds by a prefactor estimated from simulations. The vertical component at plastic threshold is given by

$$\sigma_p = \sigma_{zz} = n_b \langle f_c^{(ij)} \ell^{(ij)} \rangle_{(ij)} \langle \cos^2 \theta_z^{(ij)} \rangle_{(ij)}, \quad (4.8)$$

where the summation runs over all contacts  $(ij)$  and we have

$$\ell^{ij} = \frac{1}{2}(d_i + d_j) \quad (4.9)$$

The angle  $\theta_z^{(ij)}$  is the angle between the contact normal and the vertical axis. This angle is assumed to be uncorrelated with  $f_c^{(ij)} \ell^{(ij)}$ . For a nearly isotropic distribution of contact

orientations, we have  $\langle \cos^2 \theta_z \rangle = 1/3$ , so that

$$\sigma_p = \frac{\kappa}{12} n_b \langle (d_i + d_j) \sqrt{d_i d_j} \rangle_{(ij)} \quad (4.10)$$

The number density (number per unit volume)  $n_b$  of bonds can be estimated as the number of bonds per particle  $Z/2$  divided by the free volume  $V_f$  occupied by each particle. This volume is simply the particle volume divided by the mean packing fraction  $\Phi$  of the granule such that the sum of all particle free volumes is equal to the granule volume  $V_g$ . Hence,

$$V_f = \frac{\pi}{6\Phi} \langle d^3 \rangle \quad (4.11)$$

so that

$$n_b = \frac{Z}{2V_f} = \frac{3Z\Phi}{\pi \langle d^3 \rangle} \quad (4.12)$$

Introducing this expression in equation (4.10), we get

$$\sigma_p = \frac{Z\Phi\kappa}{4\pi} \frac{\langle (d_i + d_j) \sqrt{d_i d_j} \rangle}{\langle d^3 \rangle} \quad (4.13)$$

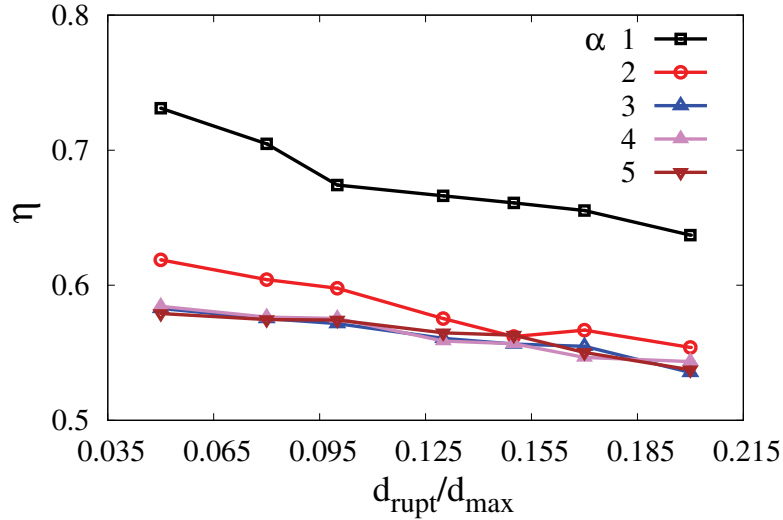


Figure 4.7 – The prefactor  $\eta$  in equation (4.15) as a function of the debonding distance  $d_{rupt}$  for different values of  $\alpha$ .

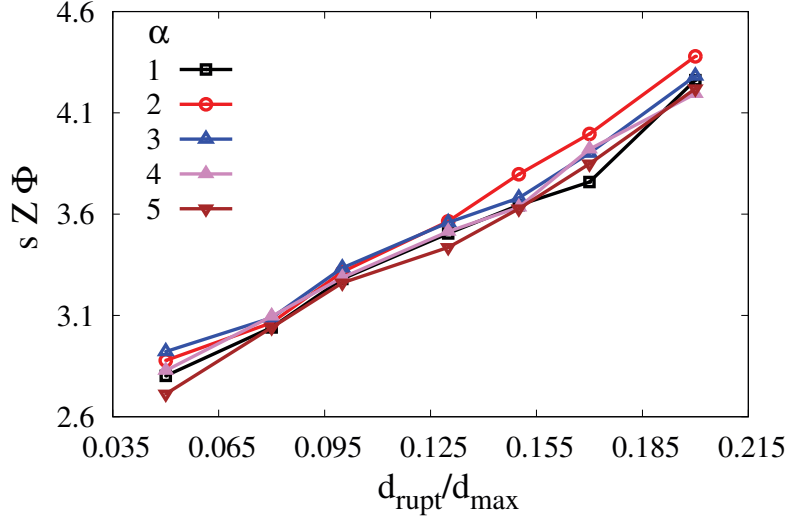


Figure 4.8 – The  $Z\Phi$ s in equation (4.15) as a function of the debonding distance  $d_{rupt}$  for different values of  $\alpha$ .

The geometric factor  $\langle (d_i + d_j) \sqrt{d_i d_j} \rangle$  can be evaluated as [36]

$$\begin{aligned} \langle (d_i + d_j) \sqrt{d_i d_j} \rangle &= \langle d_i^{3/2} d_j^{1/2} \rangle + \langle d_j^{3/2} d_i^{1/2} \rangle \\ &= 2 \langle d^{3/2} \rangle \langle d^{1/2} \rangle \end{aligned} \quad (4.14)$$

with the underlying assumption that there is no size segregation so that  $d_i$  and  $d_j$  are not correlated. Hence, we finally get

$$\sigma_p = \eta \frac{sZ\Phi}{2\pi} \frac{\kappa}{\langle d \rangle} = \eta \frac{sZ\Phi}{2\pi} \sigma_c \quad (4.15)$$

with

$$s = \frac{\langle d^{1/2} \rangle \langle d \rangle \langle d^{3/2} \rangle}{\langle d^3 \rangle} \quad (4.16)$$

The prefactor  $\eta$  is introduced here to account for the bonds with a nonzero gap where the cohesive force is below  $f_c^{ij}$ . Since  $Z$  denotes the coordination number for capillary bonds, equation (4.15) with  $\eta = 1$  can be considered as an upper bound for the plastic strength. In the same way, for  $Z$  equal to the coordination number only for contacts, equation (4.15) provides a lower bound of the plastic strength. As  $Z$  varies between 8 and 12 (see Fig. 4.6), we thus expect that  $\eta$  is generally below but close to 1.

Figure 4.7 displays the values of  $\eta$  computed from our simulations for all values of  $\alpha$  and  $d_{rupt}$ . We see that  $\eta$  declines slightly with  $\alpha$  and  $d_{rupt}$ . For small values of  $d_{rupt}$ , its value is  $\simeq 0.7$  for monodisperse granules and  $\simeq 0.6$  for polydisperse granules. With this prefactor, equation (4.15) predicts that the dependence of the normalized strength

$\sigma_p/\sigma_c$  with respect to  $\alpha$  and  $d_{rupt}$  is mediated by that of  $sZ\Phi$ . Fig. 4.8 displays  $sZ\Phi$  as a function of  $d_{rupt}/d_{max}$  for different values of  $\alpha$ . Interestingly, up to insignificant statistical fluctuations,  $sZ\Phi$  is independent of  $\alpha$  and a nearly linear function of  $d_{rupt}/d_{max}$  as that of  $\sigma_p$  in Fig. 4.5.

We see that the analytical model presented in this section correctly links the microstructure to the overall strength of the agglomerate. The trends are well predicted by the model up to the prefactor  $\eta$ , which appears to be weakly dependent on the material parameters. The physical interpretation of its value may be related to the presence of the large proportion of capillary bonds with nonzero gap, as briefly discussed previously. However, it may also be a consequence of the inhomogeneous stress transmission inside the agglomerate.

## 4.5 Conclusions

In this chapter, we used a 3D particle dynamics algorithm together with a capillary force law to analyze the cohesive strength and microstructure of spherical agglomerates. The agglomerates were constructed by extraction of spherical samples from a granular bed prepared by compaction for different values of particle size span, and subjected to diametrical compression between two platens for different values of debonding distance, which accounts for the amount of liquid in the capillary bonds. Despite the irreversible nature of cohesive bonds (i.e. no new cohesive bond), we observe a plastic plateau before the onset of failure. We showed that the plastic strength is proportional to the characteristic capillary stress  $\gamma_s/\langle d \rangle$  with a multiplicative factor that is a linear function of the debonding distance, increases with the size ratio and is nearly independent of the friction coefficient.

We also introduced an analytical expression of the cohesive strength in terms of the packing fraction, wet coordination number, size polydispersity and debonding distance. This model is in excellent agreement with the observed trends up to a prefactor that we estimated from the numerical data, and which is weakly dependent on the material parameters. As previously discussed in this chapter, our results provide the behavior of an ‘ideal’ granule in the sense that the granules were not created by an agglomeration process. The ideal granule can thus be used as a reference system with which we may compare the behavior of real agglomerates.

Given the broad applications of the agglomeration process, it is desirable to validate the simulations by comparison with experimental observations. Systematic diametrical compression tests were performed in CRM Group in Liège in order to determine the effects of material parameters on the granule strength. In these experiments, particles of the same typical size as in simulations were used. They were mixed with water and agglomerated into granules in a rotating drum. Those experiments are in good agreement with the order of magnitude of the cohesive strength of our agglomerates despite the much more complex structure of the granules observed by tomographic images. Such comparisons should be performed in the future with different values of liquid content and particle size distributions for a more systematic comparisons with simulations.

*“We build too many walls and not enough bridges”*

Isaac Newton (1642-1726)

## Chapter 5

# Evolution of a wet agglomerate in inertial shear flow of dry granular materials

The chapter is a reproduction of a submitted paper.

 We use particle dynamics simulations to investigate the evolution of a wet agglomerate inside homogeneous shear flows of dry particles. The agglomerate is modeled by introducing the theoretical expressions of capillary and viscous forces between particles in addition to frictional contacts. During shear flow, the agglomerate may elongate, break or be eroded by loss of its capillary bonds and primary particles. By systematically varying the shear rate and surface tension of the binding liquid, we characterize the rates of these dispersion modes. All the rates increase with increasing inertial number of the flow and decreasing cohesion index of the agglomerate. We show that the data points for each mode collapse on a master curve for a dimensionless scaling parameter that combines the inertial number and cohesion index. The erosion rate vanishes below a cut-off value of the scaling parameter. This leads to a power-law borderline between the vanishing erosion states and erosion states in the phase space defined by the inertial number and cohesion index.

## Contents

---

<b>5.1</b>	<b>Introduction</b>	<b>85</b>
<b>5.2</b>	<b>Model descriptions and parameters</b>	<b>86</b>
<b>5.3</b>	<b>Time evolution of agglomerates</b>	<b>88</b>
<b>5.4</b>	<b>Scaling behavior</b>	<b>94</b>
<b>5.5</b>	<b>Conclusion</b>	<b>97</b>

---

*5. Evolution of a wet agglomerate in inertial shear flow of dry granular materials*

---

## 5.1 Introduction

Agglomerates of fine particles appear either naturally in wet soils (soil aggregates) and powders (lumps) as a result of the binding action of capillary bridges between particles [217, 123] or through an agglomeration process used for the manufacture of pellets [26, 117, 179, 66] and pharmaceutical or food products [65, 106]. Once nucleated, the agglomerates interact with their surrounding granular material. The evolution of the agglomerates and their effect on the soil or powder behavior depends on the nature of these interactions [26, 186, 88, 180, 89, 218, 184, 219]. There are two limit cases: 1) The agglomerate survives by keeping its shape and primary particles if its internal cohesion  $\sigma_c$  is high due to strong cohesive bonds as compared to the forces exerted by dry granular flow around the agglomerate, and 2) The agglomerate spontaneously disintegrates if the cohesive bonds are weak. The internal cohesion of the agglomerate is proportional to the mechanical strength measured by subjecting the agglomerates to compression test between two platens [220, 24, 221, 44]. The strength is basically controlled by the surface tension of the binding liquid but also by the texture of the agglomerate [194].

We consider the case where all the surrounding particles are dry so that the agglomerate may not grow by capturing wet particles. The contact forces exerted by the dry granular flow have their origins either in the confining pressure  $\sigma_p$  or in the particle inertia [134]. The latter can be expressed as a Bagnold-like kinetic pressure  $\sigma_i \sim \rho_s \langle d \rangle^2 \dot{\gamma}^2$ , where  $\rho_s$  is the particle density,  $\langle d \rangle$  is the mean particle diameter, and  $\dot{\gamma}$  is the shear rate [172, 10]. Hence, the fate of the agglomerate depends on the competing actions of  $\sigma_c$ ,  $\sigma_i$  and  $\sigma_p$  or their dimensionless ratios  $I^2 = \sigma_i/\sigma_p$  and cohesion index  $\xi = \sigma_c/\sigma_p$ . The dimensionless number  $I$  is the inertial number of the dry granular flow, defined as the ratio of two time scales (relaxation time  $\langle d \rangle (\rho_s/\sigma_p)^{1/2}$  under load vs. shear time  $\dot{\gamma}^{-1}$ ) [10, 5]. Its relevance was demonstrated by showing that it controls the effective friction coefficient and packing fraction in different flow geometries [1, 9, 6]. The cohesion index  $\xi$  quantifies the effective cohesion of the agglomerate in the presence of confining pressure, and it has been successfully used to scale cohesive aggregates and flows [3, 22, 8].

The behavior of the agglomerate is not, however, restricted to the two extreme limits of survival and disintegration. The primary particles located at the surface of an agglomerate can be eroded by frictional and inertial forces exerted by the surrounding granular flow. The attrition reflects the inhomogeneous distribution of contact forces inside the granular flow, and can lead to progressive loss of peripheral particles even in a strong agglomerate [25, 44]. The agglomerate can also loose its cohesive bonds and break up into smaller agglomerates or simply elongate with or without loss of primary particles or cohesive bonds as a result of the action of shear stresses exerted by the flow. These failure modes and transitions between them are controlled by  $I$  and  $\xi$ .

n cohesive granular flows, particle dynamics simulations in 2D show that a combination

of  $I$  and  $\xi$  can be used to scale the rheological properties [3]. In the same way, in dense suspensions where both viscous and inertial forces come into play, the effective suspension viscosities are scaled by a combination of  $I$  and the viscous number  $\eta\dot{\gamma}/\sigma_p$ , where  $\eta$  is the liquid viscosity [46, 4]. The case of agglomerates embedded in a dry flow is however a very different case since the cohesive forces are involved only in the interactions between wet primary particles inside the agglomerate whereas inertial effects concern mainly dry particles in the surrounding fluid. For the granulation process, where the flow-agglomerate interactions play a crucial role, most investigations have focused on granulators where the packing fraction is low enough to consider only binary collisions between particles [180]. In dense granular flows the issues of agglomerate nucleation, coalescence and growth have been investigated, but it is generally found that the behavior is controlled by capillary, viscous and frictional forces in a complex manner so that the relative importance of the forces can vary greatly with strain rate and the liquid viscosity [119, 120, 88, 222, 223, 126, 127, 124, 125]. In a recent work, Lefebvre *et al.* investigated the erosion of a fixed wet agglomerate of particles subjected to a flow of dry particles inside a half-filled rotating drum [25]. They found that the erosion of the agglomerate is linear as a function of time and the force fluctuations play an important role for the erosion rate but the erosion characteristic time is controlled by the liquid viscosity.

In this paper, we study the evolution of a single agglomerate introduced in a shear flow of dry particles by means of 3D numerical simulations. The simulations were performed by means of the Discrete Element Method (DEM) in which the theoretical expressions of the capillary bridge force and lubrication viscous force as a function of inter-particle distance are implemented in addition to the elastic and friction forces for their contact. We investigate the cumulative erosion (loss of particles from the agglomerate surface), breakage (loss of cohesive bonds) and elongation of the agglomerate for a broad range of values of the shear rate  $\dot{\gamma}$  and surface tension  $\gamma_s$  but keeping the same value of liquid viscosity. We use these data to analyze in detail the rates of these dispersion modes (erosion, breakage, and elongation). As we shall see, the scaling properties of these modes involve nontrivial combinations of the control parameters.

In Section 5.2, we introduce the numerical procedures and parameters. We illustrate different dispersion modes of the agglomerate in Section 5.3. The rates of erosion, breakage and elongation, as well as their scalings with control parameters are presented in Section 5.4. We conclude in Section 5.5 with a summary of remarkable results and future directions of research.

## 5.2 Model descriptions and parameters

We first prepared a dense sample of  $N_p = 20,000$  spherical particles by means of isotropic compaction inside a rectangular box under the action of a compressive stress  $\sigma_p$ . We introduced a small size polydispersity by distributing the particle diameters randomly in the range  $[d_{min}, d_{max} = 2d_{min}]$ . The top and bottom walls were made rough by gluing an array of spherical particles of diameter  $d_w = 2.23d_{min}$  to them. In the second step, we removed

Table 5.1 – Simulation parameters

Parameter	Symbol	Value	Unit
Smallest particle diameter	$d_{min}$	800	$\mu\text{m}$
Density of particles	$\rho_s$	2600	$\text{kg.m}^{-3}$
Number of particles	$N_p$	20,000	
Friction coefficient	$\mu$	0.3	
Normal stiffness	$k_n$	$10^6$	N/m
Tangential stiffness	$k_t$	$8.10^5$	N/m
Normal damping	$\gamma_n$	0.8	Ns/m
Tangential damping	$\gamma_t$	0.8	Ns/m
Contact angle	$\theta$	0	degree
Liquid viscosity	$\eta$	1.0	mPa.s
Time step	$\delta t$	$7.10^{-7}$	s

the lateral walls along the  $x$  and  $y$  directions and replaced them by periodic boundary conditions. A spherical probe was introduced in the granular bed and its diameter was increased until reaching exactly 300 particles inside the probe, see Fig. 5.2(a). The capillary attraction forces and viscous forces are activated between neighboring particles inside the probe. This defines a wet agglomerate of 300 particles inside a bed of dry particles.

To shear the sample, we applied a constant velocity  $v$  along the  $x$  direction to the top wall while keeping the bottom wall immobile and a constant pressure  $\sigma_p$  on the top wall. We ran a total number of 64 simulations for different values of  $v$  and  $\gamma_s$ . All other parameters are given in Table 5.1. The samples were sheared for about 3 seconds in steady flow. Figures 5.1(a) and (b) show the mean velocity profiles for different values of the cohesion index  $\xi$  and inertial number  $I$ , respectively. We see that, owing to the choice of wall roughness, the shear deformation is nearly uniform despite the presence of the wet agglomerate inside the sample and independently of the values of  $\xi$  and  $I$ . Hence, the steady flows can be characterized by an average shear rate  $\dot{\gamma} = v/h$ , where  $h$  is the sample thickness, and an inertial number

$$I = \dot{\gamma} \langle d \rangle \left( \frac{\rho_s}{\sigma_p} \right)^{1/2}, \quad (5.1)$$

where  $\langle d \rangle$  denotes the mean particle diameter and  $\rho_s$  is the particle density. We varied  $\dot{\gamma}$  in the range  $[0.21, 39.68]s^{-1}$ . For the definition of cohesion index, we used the maximum value of the capillary attraction force  $f_c$  and confining force  $f_p = \sigma_p \langle d \rangle^2$ :

$$\xi = \frac{f_c}{f_p} = \frac{\kappa R}{\sigma_p \langle d \rangle^2} \approx \frac{\pi \gamma_s \cos \theta}{\sigma_p \langle d \rangle}. \quad (5.2)$$

The cohesion index was varied in a range  $[1, 8]$ .

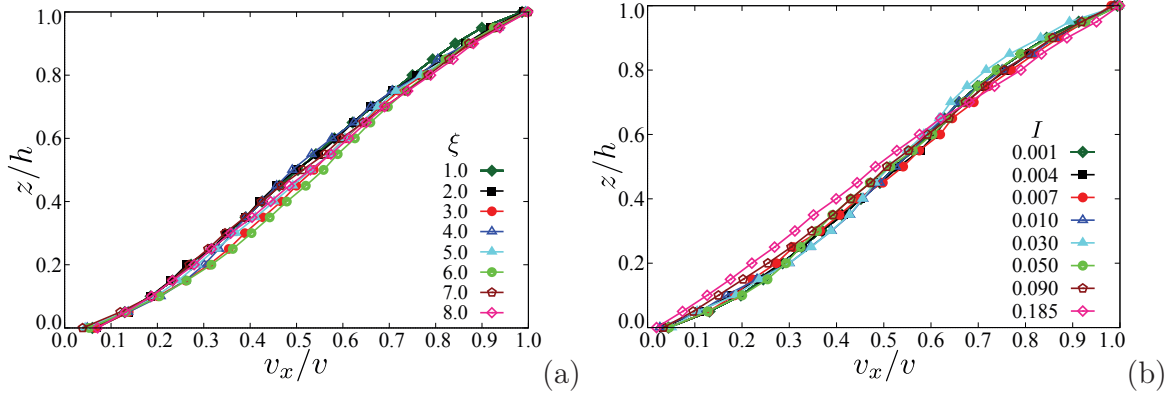


Figure 5.1 – Velocity profiles in steady shear state for different values of the cohesion index  $\xi$  (a) with  $I \simeq 10^{-3}$ , and for different values of the inertial number  $I$  with  $\xi = 5.0$  (b).

### 5.3 Time evolution of agglomerates

Figure 5.2 displays snapshots of the agglomerate in different regimes depending on the values of  $\xi$  and  $I$ . The agglomerate is stable with no loss of wet particles or breakage at high values of  $\xi$  and low values of  $I$ . But it undergoes either sudden dispersion (disintegration) or gradual dispersion by loss of wet particles (erosion), loss of cohesive bonds (breakage) or elongation in other cases. These last three modes of dispersion occur simultaneously. Spontaneous dispersion occurs at low values of  $\xi$ .

We define the cumulate elongation  $M_g$  of the agglomerate as the logarithm of the length of its long axis  $\ell$  divided by its initial diameter  $d_0$ :

$$M_g = \ln \frac{\ell}{d_0}, \quad (5.3)$$

The logarithm function arises as a result of time integration of incremental deformation  $d\ell/\ell$  from the initial size  $d_0$  to the current size  $\ell$ . The cumulative breakage  $M_b$  of the agglomerate is the ratio of the number  $N_{lost_c}$  of broken capillary contacts to the total number of capillary contacts  $N_{ci}$  at the initial state:

$$M_b = \frac{N_{lost_c}}{N_{ci}}. \quad (5.4)$$

In the same way, the cumulative erosion  $M_e$  is the ratio of the number  $N_{lost_p}$  of wet particles leaving the agglomerate to the total initial number  $N_{pi}$  of wet particles:

$$M_e = \frac{N_{lost_p}}{N_{pi}}. \quad (5.5)$$

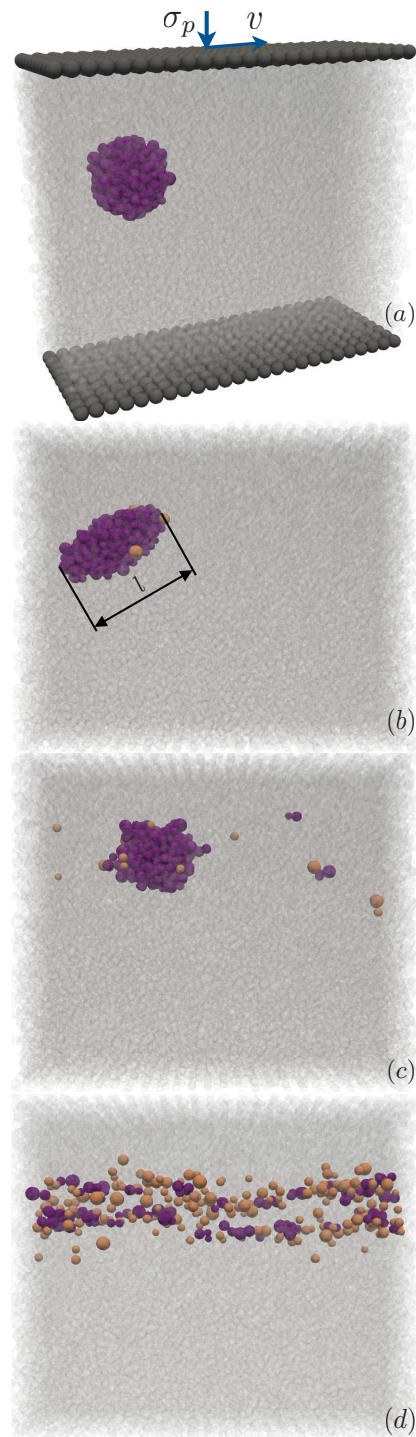


Figure 5.2 – (a) Simulated model of a wet agglomerate in a granular bed of dry particles subjected to a homogeneous shear flow; (b) elongation and erosion of the agglomerate; (c) elongation, erosion, and breakage modes; (d) spontaneous dispersion of wet particles.

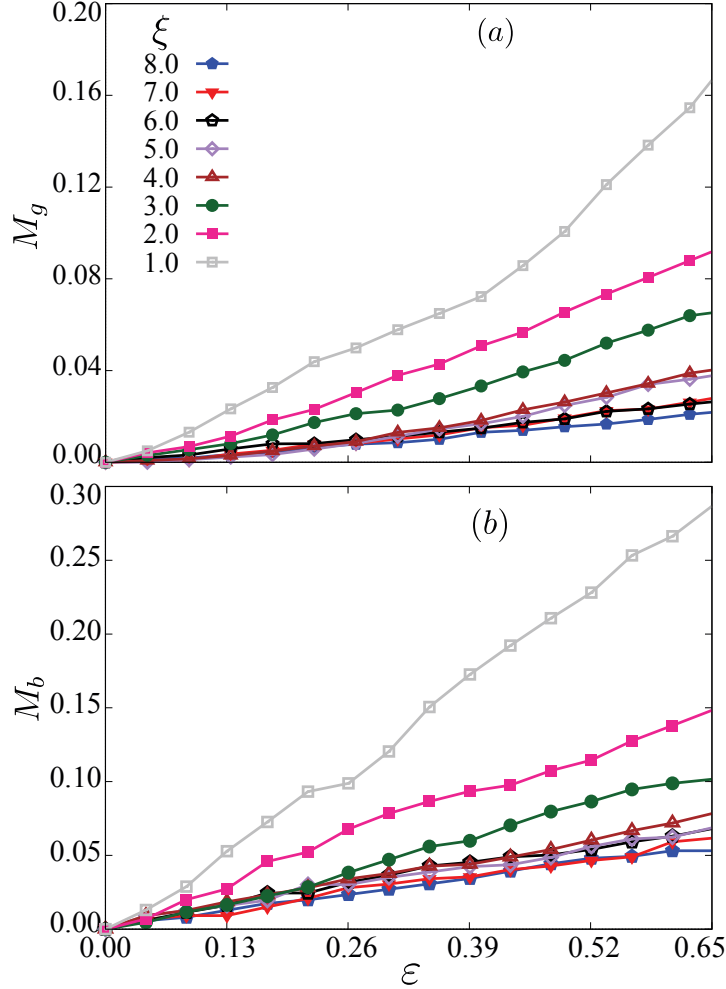


Figure 5.3 – Evolution of cumulative elongation  $M_g$  (a) and breakage  $M_b$  (b) of a wet agglomerate inside a homogeneous shear flow of dry particles as a function of cumulative shear strain  $\varepsilon$  for different values of the cohesion index  $\xi$  and for  $I \simeq 10^{-3}$ .

Figure 5.3 shows  $M_g$  and  $M_b$  as a function of cumulative shear strain  $\varepsilon = \dot{\gamma}t$  for  $I \simeq 10^{-3}$  and all values of the cohesion index  $\xi$ . We see that both elongation and breakage increase as a nearly linear function of  $\varepsilon$  at a rate that declines with increasing  $\xi$ . For the lowest values of the latter, the evolution is fluctuating with sometimes sudden changes of the rate. It is remarkable that both elongation and breakage occur even for the largest values of the cohesion index used in this work. We also observe a similarity between the evolutions of elongation and breakage. This reflects the fact that elongation implies the loss of capillary bonds inside the agglomerate as a result of the rearrangements of primary particles. The examples shown in Fig. 5.3 concern a low value of  $I$ . For larger values of  $I$  the rates increase, as we shall see below.

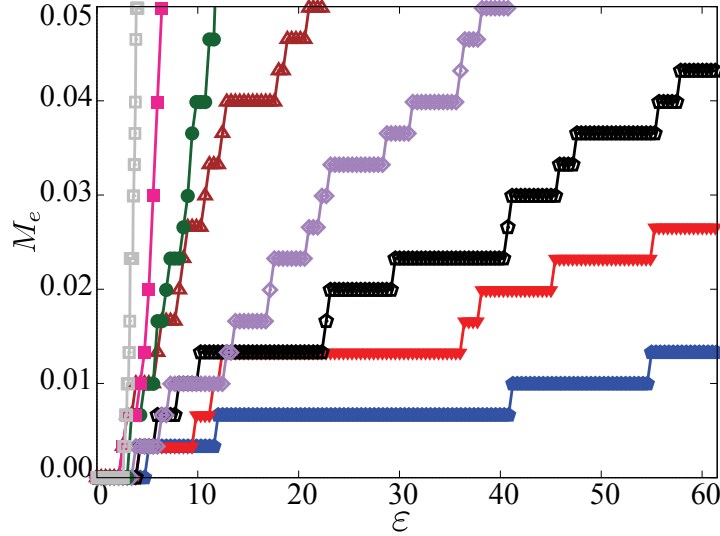


Figure 5.4 – Evolution of cumulative erosion as a function of shear strain  $\varepsilon$  for different values of the cohesion index  $\xi$  and for  $I \simeq 0.1$ .

Figure 5.4 shows the cumulative erosion  $M_e$  as a function of shear strain for different values of  $\xi$  for  $I \simeq 0.1$ . We observe a quick increase of  $M_e$  at low values of  $\xi$ , corresponding to a quick dispersion of the wet particles. The erosion declines for larger values of cohesion index  $\xi$ . The number of eroded wet particles is small as they occur occasionally. In fact, to increase the erosion rate,  $\xi$  should be reduced, resulting in more breakage than erosion. Despite the step-wise evolution of erosion, it may be approximated by an average constant rate.

In order to characterize the three dispersion modes (elongation, breakage and erosion) of the agglomerate, we consider their rates  $K_g$ ,  $K_b$ , and  $K_e$  evaluated from linear fits to the temporal evolutions of  $M_g$ ,  $M_b$ , and  $M_e$ , respectively:

$$K_g = \frac{\Delta M_g}{\Delta t}, \quad (5.6)$$

$$K_b = \frac{\Delta M_b}{\Delta t}. \quad (5.7)$$

$$K_e = \frac{\Delta M_e}{\Delta t}, \quad (5.8)$$

Figures 5.5(a), (b), and (c) display  $K_g$ ,  $K_e$ , and  $K_b$  as a function of the inertial number  $I$  for different values of the cohesion index  $\xi$ . The symbols and their colors represent the same values of the cohesion index  $\xi$  in the three figures. All the rates increase with increasing  $I$  and decreasing  $\xi$ . While  $K_g$  increases almost linearly with  $I$  for all values of  $\xi$ , both  $K_e$  and  $K_b$  increase appreciably and in a nonlinear manner with  $I$ . Note also that, in contrast to breakage and elongation, for each value of  $\xi$  there is a lower threshold of  $I$  below which no erosion occurs. This threshold increases with  $\xi$ .

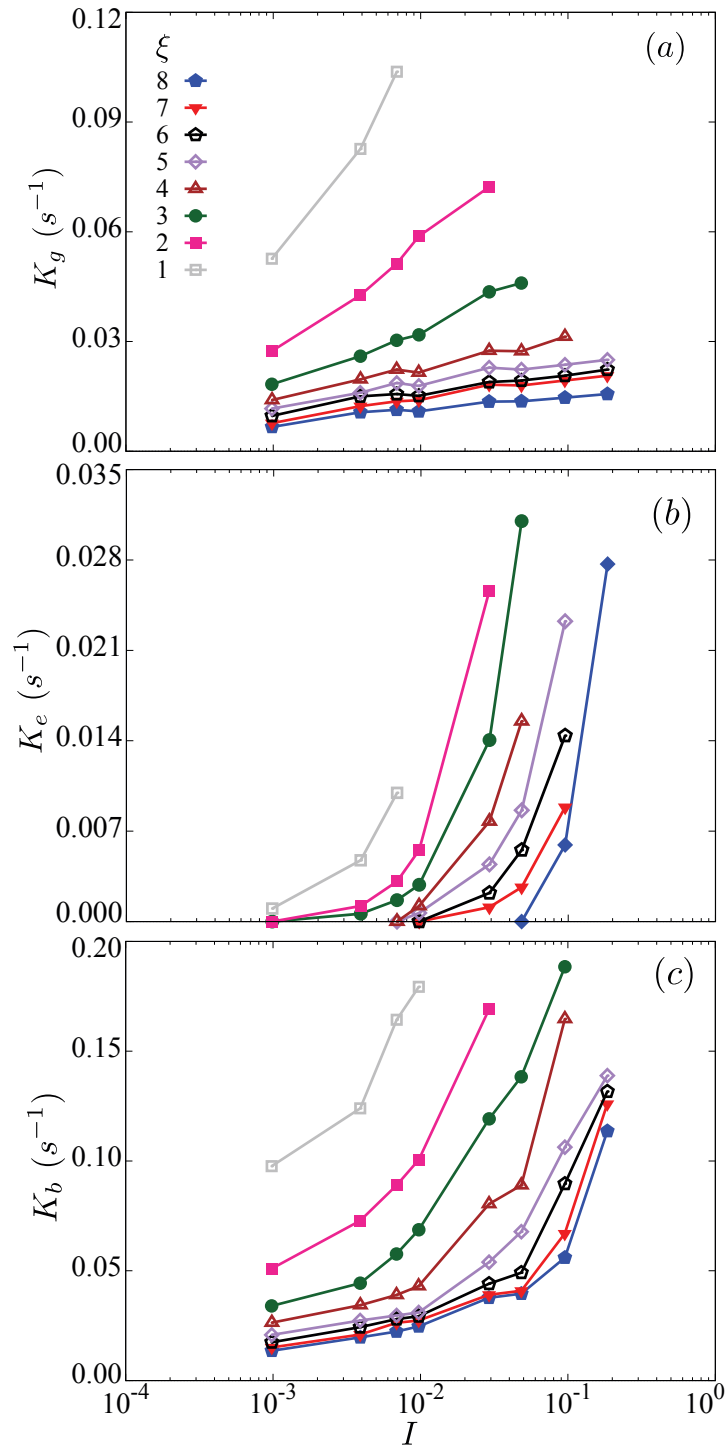


Figure 5.5 – Elongation rate  $K_g$  (a), erosion rate  $K_e$  (b), and breakage rate  $K_b$  (c) of the wet agglomerate as a function of the inertial number  $I$  for different values of the cohesion index  $\xi$ .

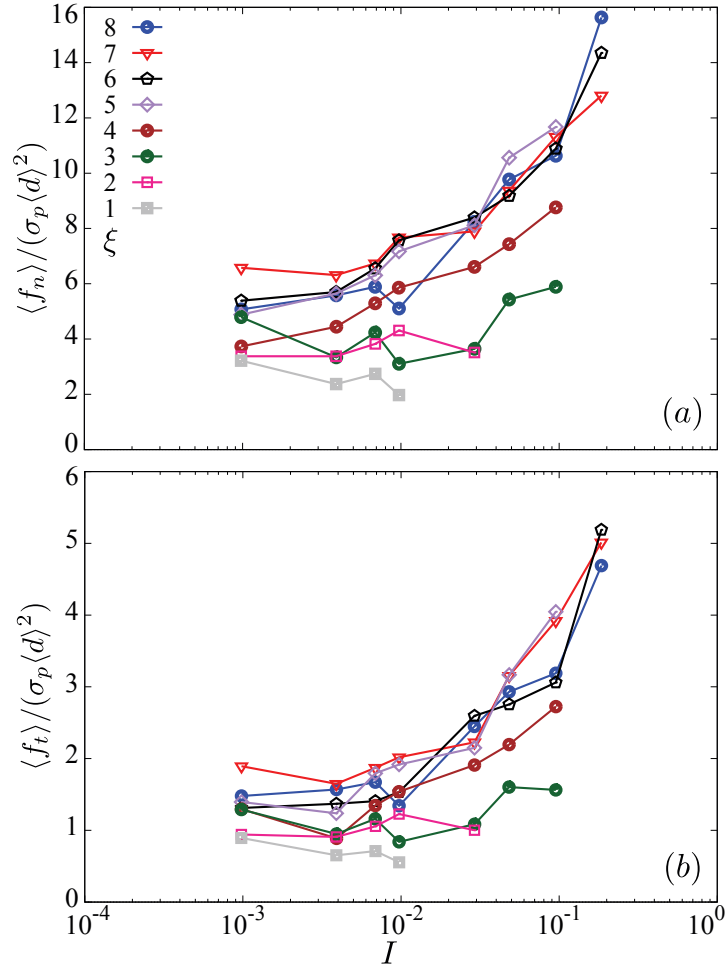


Figure 5.6 – Average normal force (a) and tangential force (b) at the contacts between the dry particles of the flow and the wet particles of the agglomerate as a function of the inertial number for different values the cohesion index. The forces are normalized by the confining force  $\sigma_p \langle d \rangle^2$ .

The strong effect of increasing inertial number on the dispersion rates for all values of cohesion indicates that the inertial stresses prevail as compared to the confining pressure. Figure 5.6 shows the average normal force  $\langle f_n \rangle$  and the average tangential force  $\langle f_t \rangle$  between dry particles of the flow and wet particles located at the surface of the agglomerate as a function of  $I$  for different values of  $\xi$ . These forces are responsible for both erosion of the particles from the agglomerate and its breakage. We see that, even for low values of  $I$ , these forces are larger than the mean force exerted by the confining pressure on the particles. They increase rapidly as  $I$  varies from  $10^{-3}$  to  $10^{-1}$ . It is interesting to see that the average force increases for larger values of the cohesion index  $\xi$ . This can be a consequence of the fact that, at large cohesion, the dry particles ‘see’ the agglomerate as a large rigid particle so that the momenta of the impacting particles are fully transmitted

to the agglomerate. At low cohesion, the impacts may lead to erosion or breakage of the particle, resulting in the partial transmission of the impacting particle momenta to other particles.

## 5.4 Scaling behavior

The behavior of the three dispersion rates in Fig. 5.5 as a function of  $I$  and  $\xi$  suggests that they may be separately collapsed on a master curve as a function of a scaling parameter combining  $I$  and  $\xi$ . Before considering this option, it is necessary to define dimensionless rates by means of a characteristic time. There are three characteristic times in our system: 1) The relaxation time  $\langle d \rangle \sqrt{\rho_s / \sigma_p}$  of the particles under the action of the confining pressure  $\sigma_p$ , 2) The viscous time  $\eta / \sigma_p$  due to viscous force, and 3) The shear (inertial) time  $t_i = \dot{\gamma}^{-1}$ . The relaxation time is constant as the confining stress has a fixed value ( $=140$  Pa) in all simulations. Given the size of the particles, its value is small ( $\sim 10^{-3}$  s). The viscous time has also a constant value in all simulations ( $\sim 10^{-5}$  s). Hence, at the scale of the relaxation and viscous times, the dispersion events are rare and slow. In contrast, the shear time  $t_i$  represents a time during which the agglomerate undergoes a long enough evolution for the erosion, elongation and breakage events to be appreciable although its value depends on the shear rate. Hence, we normalize all the times by the shear time  $t_i$  so that the dimensionless shear rates are given by  $K_g t_i$ ,  $K_b t_i$  and  $K_e t_i$ .

We assume a general scaling parameter  $I^\alpha \xi^\beta$  and search for the values of the exponents  $\alpha$  and  $\beta$  that make all the data points collapse on a single curve for each dispersion mode. Obviously, if the data points collapse for some values of these exponents, they will also collapse for any power of  $I^\alpha \xi^\beta$ , meaning that only the ratio  $\alpha/\beta$  is relevant. Hence, we set the value of  $\beta$  and determine  $\alpha$  for each dispersion mode denoted by a subscript ( $g$  for elongation,  $b$  for breakage, and  $e$  for erosion).

Figures 5.7, 5.8, and 5.9 show the collapsed data on a master curve in linear and log-log scales for an appropriate choice of the exponents. For elongation and breakage, we set  $\beta_g = \beta_b = 1$ . Remarkably, within our statistical precision, we get  $\alpha_g = \alpha_b \simeq 1$  with a good approximation. This means that the scaling parameter for elongation and breakage is

$$I_g = I_b \simeq \xi I, \quad (5.9)$$

with power-law functional fits

$$K_g t_i = A_g I_g^{n_g}, \quad (5.10)$$

where  $A_g \simeq 6.5 \times 10^{-4}$  and  $n_g \simeq -0.88$ , and

$$K_b t_i = A_b I_b^{n_b}, \quad (5.11)$$

with  $A_b \simeq 3.0 \times 10^{-3}$  and  $n_b \simeq -0.65$ .

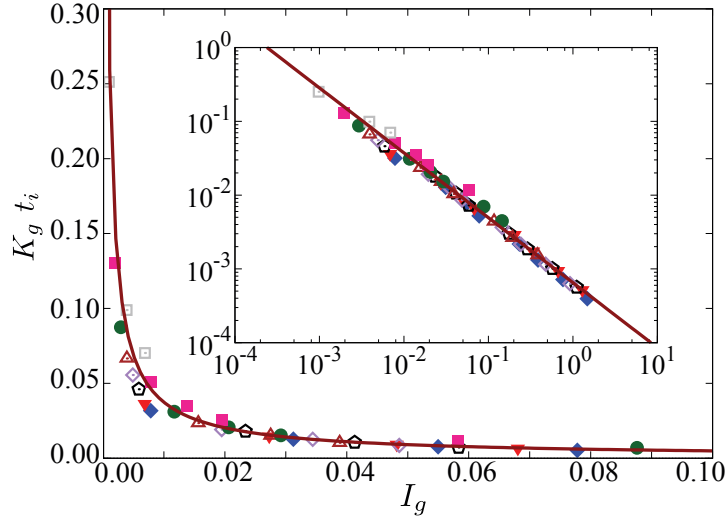


Figure 5.7 – Normalized elongation rate  $K_g t_i$  as a function of the scaling parameter  $I_g = \xi I^{\alpha_g}$  with  $\alpha_g = 1$  for all our simulations. The symbols and their colors represent the same values of cohesion index  $\xi$  as in Fig. 5.3. The solid line is a power-law fitting form (Eq. 5.10).

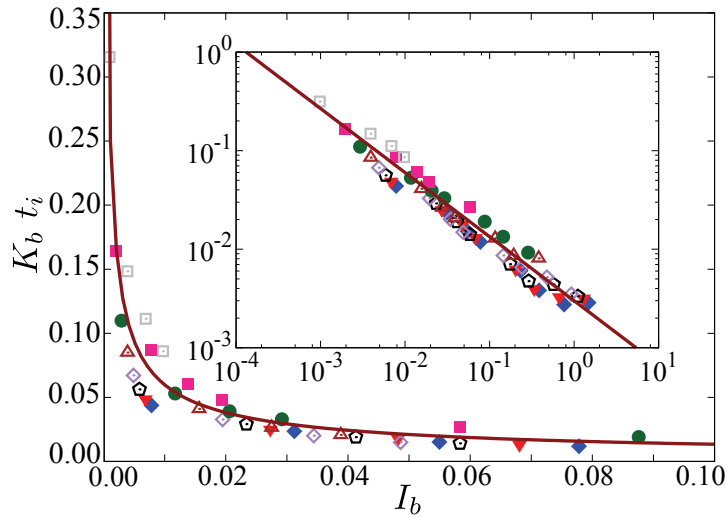


Figure 5.8 – Normalized breakage rate  $K_b t_i$  as a function of the scaling parameter  $I_b = \xi I^{\alpha_b}$  with  $\alpha_b = 1$  for all our simulations. The symbols and their colors represent the same values of cohesion index  $\xi$  as in Fig. 5.3. The solid line is a power-law fitting form (Eq. 5.11).

This power-law scaling implies that the breakage and elongation of agglomerates occur for all values of  $\xi$  and  $I$ , and no transition occurs to a stable agglomerate state (no breakage, no elongation). If such a limit exists, it is out of the range of values of  $I$  and  $\xi$  investigated in this work. The negative values of the exponents  $n_g$  and  $n_b$  mean that the rates decrease

both when  $\xi$  increases (which is an expected behavior) and when  $I$  increases, which is rather counterintuitive as inertial effects should enhance breakage. Actually, this is only a consequence of scaling the time by  $t_i$ . The temporal rates of breakage and elongation do increase with  $I$  as observed in Fig. 5.5.

For erosion, we set  $\beta_e = -1$ , and the data points collapse for  $\alpha_e \simeq 0.25$ . Hence, the scaling parameter is

$$I_e \simeq I^{\alpha_e} \xi^{\beta_e} \quad (5.12)$$

As displayed in Fig. 5.9, when plotted as a function of  $I_e$ , the data points collapse on a truncated power-law function:

$$K_e t_i = A_e (I_e^{n_e} - I_0^{n_e}), \quad (5.13)$$

with  $A_e \simeq 4.5 \times 10^{-2}$ ,  $I_0 \simeq 5.2 \times 10^{-2}$ , and  $n_e \simeq 1.4$ . The threshold  $I_0$  is the value of  $I_e$  below which no erosion occurs. Hence, in the phase space  $(I, \xi)$ , the function  $\xi = I^{\alpha_e}/I_0$  defines the borderline between the states of erosion (below the curve) and vanishing erosion (above the curve), as shown in the phase diagram of Fig. 5.10.

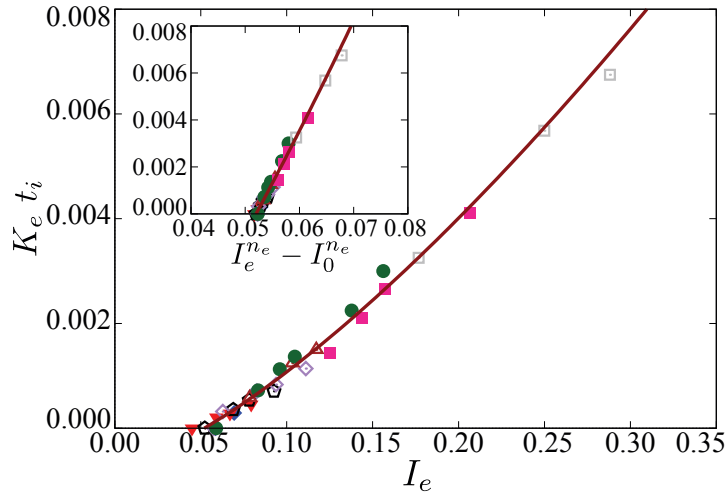


Figure 5.9 – Normalized erosion rate  $K_e t_i$  as a function of the scaling parameter  $I_e \simeq I^{\alpha_e} \xi^{\beta_e}$  with  $\alpha_e = 0.25$  and  $\beta_e = -1$  for all our simulations. The symbols and their colors represent the same values of cohesion index  $\xi$  as in Fig. 5.3. The solid line is a truncated power-law fitting form Eq. (5.13).

The dispersion modes described and scaled here are not independent phenomena. For example, the elongation and erosion of the agglomerate imply gradual loss of contacts, that we count as part of breakage or damage of the agglomerate. As we can see in Fig. 5.5, for each value of the cohesion index, the three rates increase correlatively as a function of the inertial number. However, the dominant mode depends on the values of the cohesion index and inertial number. For example, from equations (5.13) and (5.11), it is easy to see that, for each value of  $\xi$  the dominant mechanism at low  $I$  is erosion compared to breakage, but

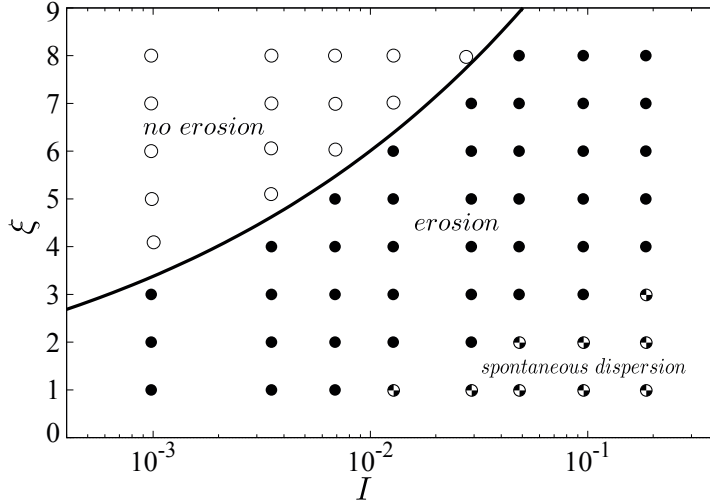


Figure 5.10 – Diagram of erosion states in the phase space  $(I, \xi)$ . The filled and empty symbols represent the states of erosion and vanishing erosion, respectively, for all the simulated values of  $I$  and  $\xi$  with a power-law frontier  $\xi = I^{1/4}/I_0$  between them. The half-filled symbols correspond to the simulations where the agglomerate breaks up spontaneously, i.e. over one time step.

the ratio of erosion rate to breakage rate declines as the inertial number increases. The data presented in this paper do not include those simulations that led to a spontaneous dispersion of the agglomerate. In our analysis, this scenario, which happens only for low values of  $\xi$  and highest values of  $I$ , corresponds to the breakage of the agglomerate over one time step, i.e. a large value of the breakage rate. These simulations are marked by a different symbol in the phase diagram of Fig. 5.10.

## 5.5 Conclusion

In this paper, we used particle dynamics simulations to investigate three dispersion mechanisms of a wet agglomerate in a homogeneous flow of dry particles: 1) breakage (loss of cohesive bonds), 2) erosion (loss of primary particles), and 3) elongation. The inclusion of liquid in the simulations was based on the addition of capillary bridges between neighboring particles up to a debonding distance, as well as the assumption that the eroded particles lose their liquid and can not be re-captured by the agglomerate. We varied two parameters: 1) the agglomerate cohesion index  $\xi$  by varying the surface tension  $\gamma_s$  of the liquid, and 2) the flow inertial number  $I$  by changing the shear rate  $\dot{\gamma}$ . The three mechanisms are simultaneously active but their relative roles change with  $\xi$  and  $I$ . The rates of breakage, erosion and elongation are well defined and they were used for a parametric study of the evolution of the wet agglomerate.

As expected, the three dispersion rates increase with increasing  $I$  and decreasing  $\xi$ . The

effect of  $I$  on the breakage and erosion rates is quite remarkable. A transition is observed for a particular value of  $\xi$  depending on  $I$  from a state of vanishing erosion to a state of erosion. We showed that the rate of evolution for each mechanism can be described by a master function of a scaling parameter combining  $I$  and  $\xi$ . By fitting the collapsed data, we determined this function, which is a power law for the normalized breakage and elongation rates, and a truncated power law for the normalized erosion rate. The truncation is a consequence of transition from a state of vanishing erosion to erosion for particular value of the scaling parameter. In the phase space  $(I, \xi)$  this transition is characterized by a power-law borderline.

To define dimensionless rates, we normalized the time by the inertial time  $t_i = \dot{\gamma}^{-1}$ . The experiments reported in [25] suggested that the liquid viscosity sets the time scale of erosion. However, in our simulations the relevant time scale is the inertial time since the viscous time and relaxation time are both quite small. What is more, the dispersion phenomena are governed by the competing effects of the cohesive stresses and inertial stresses. The scaling proposed in this paper can be further examined by performing more simulations with larger values of liquid viscosity and different values of the confining pressure. A transition to the viscous regime is expected to occur for large values of viscosity [46, 4], where the Stokes number will come into play in addition to the cohesion index and inertial number.

The analysis presented in this paper was made possible by using simple boundary conditions leading to the uniform shear flows. A more detailed analysis is underway in order to characterize also the microscopic mechanisms of erosion, breakage and elongation. This work provides a quantitative ground for a better understanding of the agglomeration process in more complex geometries such as rotating drums, where the growth of granules is controlled by the probabilities of capture and loss of primary particles inside an inertial flow.

# General Conclusions and Outlook



---

## General Conclusions

The main goal of this PhD work was to get a better understanding of the rheological behavior of unsaturated wet granular materials such as wet sand used for the construction of sandcastles on a beach or wetted iron ores in a drum granulator. The origin of the cohesive force in such materials is the presence of capillary liquid bonds between grains. The liquid bonds give also rise to viscous forces when the grains flow. Although the dynamics and distribution liquid inside a granular material are complex, it is believed that in a granular material well mixed with particles or in a humid environment where liquid bridges can condense from the vapor, the material can be modeled as a collection of particles interacting within a debonding distance through cohesive and viscous force laws in addition to elastic and frictional forces. In this approximation, the particle dynamics approaches such as the DEM can be used together with the theoretical expressions of cohesive-viscous force laws to simulate large collections of particles. It has been shown to yield realistic estimates of the macroscopic cohesive strength when compared to experiments. This approach has the advantage of allowing for the simulation of the materials with a sufficiently large number of particle whereas a full simulation of unsaturated granular materials accounting for both particles and liquid would require a coupled approach and almost unfeasible simulations even for a few particles.

It is also important to remark that the focus of most studies during the three last decades has been on dry granular materials. For example, the steady flow behavior has been extensively investigated and models based on the inertial number have been proposed and applied to various flow geometries. In the same way, the quasi-static behavior has been studied in order to analyze the elastic and plastic properties of granular materials in relation to their microstructure. The rheology of cohesive materials has been investigated more recently in physics and mechanics laboratories for its effect on the inertial flow or for its relation with the tensile force at the particle scale. There is, however, a vast panoply of applications in powder technology where the cohesion is of primary importance. The flowability of powders is considered as a major property and measured by various types of rheometers. The mixing and agglomeration of cohesive powders are still important topics of current research. In view of such applications and given the lack of a systematic modeling approach to cohesive materials as compared to cohesionless materials, this PhD work aimed at performing a parametric study of cohesive flows by 3D simulations and particle agglomeration in simple flows and rotating drums in order to address several fundamental issues related to cohesive granular materials but without seeking direct application to powders and unsaturated soils.

The fundamental issues that we addressed concern mainly the influence of particle interactions on the effective properties such as shear strength in shear flows, compressive

---

strength of cohesive agglomerates, the erosion of a granule in a shear flow and the effect of inertial stresses. One of the key aspects is the combined effects of cohesive and viscous stresses. When two different types of interactions come into play in a system, it is expected that their simultaneous effect should be different from a simple superposition of their individual effects. The same question can be asked about the simultaneous effects of particle inertia and cohesion in rapid flows. This issue had been previously investigated by numerical simulations for suspensions and it was shown that the apparent friction coefficient and packing fraction can be quite nicely described in terms of a single dimensionless parameter that incorporates both inertial number and Stokes number. This “additivity” of effects has its origin in the additivity of stresses with a weighting coefficient that depends on the details of interactions. The issue addressed in this PhD work is similar: to what extent the cohesive, viscous and inertial effects are additive? The related questions are whether the rheology of such “complex” granular materials is an extension of that of dry granular materials and whether a single control parameter (as an extension of the inertial number) can capture all those effects?

Such issues can be safely investigated under homogeneous boundary conditions. But wet granular materials occur often under complex loading conditions. The granulation process is a well-known example. The granulation in rotating drums involves complex flow regimes such as cascading flows, inhomogeneous distribution of liquid and nucleation of granules undergoing consolidation or erosion during flow. The effects of control parameters such as the rotation speed or material parameters such as the amount of binding liquid on the process are interesting issues in this field that we tried to address. One relevant question in this respect is whether the modified inertial number can be used to scale the granule behavior. We focused more specially on the behavior of a single granule inside a dry granular flow in order to determine under what conditions the granule grows, disappears or simply is deformed by the flow. The cohesive strength of an agglomerate under diametrical compression was also considered.

Our results, published or submitted as four papers, were discussed in detail at the end of each chapter. For dense flows in the presence of cohesive and viscous forces, we found that the “additive rheology” works. We argued that this property is related to the nature of granular materials in which the particle interactions occur at the contact points, and the local dynamics is controlled by the shear rate. Hence, a single scaling parameter can be defined as the ratio of the weighted sum of stresses that depend on the shear rate to the weighted sum of those that are independent. This *visco-cohesive-inertial* number provides thus an extension of the inertial number to the wet interactions between particles. Its application to cohesive flows requires the distinction of the quasistatic limit by normalizing the packing fraction and apparent friction coefficient by their values in this limit, which depend only on the cohesion index. Then, all the data points for friction coefficient and packing fraction nicely collapse on a master curve. In the same way, a mapping can be made between these flow variables as a function of the modified inertial number and the effective viscosities of the flow as a function of packing fraction. From this analysis, we finally proposed a unique scale parameter for strongly cohesive granular materials in which cohesion is largely above the external stresses such as gravity. This scaling parameter

---

is  $I_m = \{\text{Ca}(\beta + \text{St})/\alpha\}^{1/2}$ , which incorporates the capillary number  $\text{Ca}$  and the Stokes number  $\text{St}$ .

For the growth of agglomerates, the simulations were performed in a rotating drum, in which a small agglomerate was initially introduced. Its evolution was governed by the accretion of wet particles and erosion as a result of inertial flow. The important assumption here is that the liquid is transported by the particles, and the capillary bonds occur only between two wet particles. In fact, although the evolution of the binding liquid is a key aspect of the agglomeration process, we need to distinguish two time scales: 1) The time associated with the wetting and redistribution of the liquid, and 2) The shear time. In our simulations, we assume that all the liquid is already distributed in the granular sample both inside the granule and into individual particles dispersed uniformly in the bulk. In inertial flows, the redistribution time is larger than the flow time. Hence, a wetted particle transports the liquid and it can share it only with another wet particle. Under these conditions, the granule grows exponentially with the number of drum rotations by capturing the free wet particles. Interestingly, the accretion of wet particles is an exponential function of time whereas the number of eroded particles grows linearly with time. As the available liquid (or equivalently, the number of wet particles) is limited, the granule size tends to a constant value. The effect of the material parameters is sometimes counter-intuitive. For example, both accretion and erosion increase when the size ratio or friction coefficient are increased. The effects of particle size ratio and mean particle size were investigated, and we found that both parameters influence the growth rate. Although we were able to analyze separately the accretion and erosion processes, it was not possible to perform a detailed analysis of the particle-scale mechanisms because of the complexity of the flow in the rotating drum.

For the cohesive strength of agglomerates, we performed diametrical compression tests on spherical agglomerates of spherical particles for a wide range of the values of particle size span and debonding distance (which accounts for the amount of liquid). We showed that the stress-strain curve has a plastic plateau before the onset of failure, and the plastic strength is proportional to the characteristic capillary stress with a multiplicative factor that is a linear function of the debonding distance, increases with the size ratio and is nearly independent of the friction coefficient. We introduced an analytical expression of the cohesive strength in terms of the packing fraction, wet coordination number, size polydispersity, and debonding distance. Our ‘ideal granule’ should be considered as a reference system for real granules produced by the agglomeration process in a drum granulator with fine particles. The granules of iron ores, for example, have a complex structure due to the broad size distribution of primary particles. Even then, the calculated strength of our granule is in good agreement with the observed trends up to a prefactor that we estimated from the numerical data.

For the investigation of the erosion and deformation of a single cohesive agglomerate, we used a periodic shear flow, which, in contrast to rotating drum, provides nearly homogeneous conditions where it is easier to characterize the evolution of the granule. The issue here was how the cohesive index and inertial number control the evolution of the granule. The important point here is that the cohesive index concerns only the primary particles

---

inside the agglomerate whereas inertial effects concern only the flow of dry particles outside the agglomerate. There are three different dispersion modes: breakage (loss of cohesive bonds), erosion (loss of primary particles), and elongation (shape change). By systematically varying the shear rate and surface tension of the liquid, we characterize the rates of these dispersion modes. All the rates increase with increasing inertial number of the flow and decreasing cohesion index of the agglomerate. We showed also that the data points for each mode collapse on a master curve for a dimensionless scaling parameter that combines the inertial number and cohesion index. The erosion rate has a cut-off value for the scaling parameter above which no erosion occurs. This leads to a power-law borderline between vanishing erosion and erosion states in the phase space defined by the inertial number and cohesion index.

A general picture that we get from this work is that homogeneous granular flows involving cohesive and viscous interactions (such as wet granular flows) are ‘simple’ in the sense that a single scaling parameter accounts for the effects of all interactions. But, this picture can not easily be applied to the agglomeration of particles, which is an inhomogeneous process that implies interactions between cohesive and noncohesive particles, and stress gradients.

## Outlook

The work presented in this PhD thesis can be extended along different lines and directions some of which were already mentioned in different chapters. In particular, the scaling proposed for the evolution of a single agglomerate inside shear flow of dry particles can be further investigated by performing more simulations with larger values of liquid viscosity and different values of the confining pressure. A transition to the viscous regime is expected to occur for large values of viscosity, where the Stokes number will come into play in addition to the cohesion index and inertial number.

One of the most interesting extensions consists in applying the rheology with the modified inertial number to free surface gravity flows on an inclined plane, which is a model for natural flows, or to rotating drums in the rolling regime, which is governed by inertial effects. The predictions of the model can also be compared with appropriate experiments in the same flow geometry. The usual flow regimes of rotating drums will be modified in the presence of viscous and capillary forces, which in combination with centrifugal forces may give rise to more complex regimes.

Another possible extension consists in using coupled particle-liquid methods to simulate cohesive (or colloidal) suspensions. It is expected that the scaling proposed in this work will apply to such flows. Clearly, the nature of cohesive forces in such flows can not be capillary since the system is fully saturated. But in fine powders, the van der Waals forces can play the same role.

The agglomeration process is much more involved in terms of numerical simulations. But the nucleation stage can be easily investigated from a dispersion of wet particles inside a collection of noncohesive particles. As multiple granules may appear and grow from such

---

a process, such simulations require nevertheless large systems and many more particles than considered in this work. The interactions between granules and their coalescence are interesting phenomena that have not yet been subject of simulations. The detailed balance models for agglomeration can also be evaluated by analyzing the accretion and erosion processes at the particle scale. The parametric studies can be pursued also in order to determine the phase-space diagrams of granule growth as a function of all material and operational parameters.

The impact dynamics and fracture of cohesive aggregates of particles is an interesting test for the cohesive-viscous rheology evidenced in this work. The impact experiments can be used in experiments as a simple means to test the rheology. One of the issues in modeling impact dynamics is the relevance of the capillary law used in our simulations. This law is based on the Laplace-Young equation, which describes the equilibrium capillary force. In dynamic tests, it will be necessary to modify this law in order to account for the out-of-equilibrium capillary forces.



## Summary in French

L'objectif principal de ce travail de doctorat a été de mieux comprendre le comportement rhéologique des matériaux granulaires humides insaturés. Ces matériaux sont fréquents dans la vie de tous les jours et présents dans différents domaines scientifiques et industriels. Parmi de nombreux exemples on peut citer des géomatériaux mouillés ou du sable humide à la base de la construction de châteaux sur la plage, des poudres utilisées en chimie ou en agroalimentaires nécessitant une hydratation, l'agglomération de minerais humidifiés dans des tambours tournant (granulateur), etc. Dans chacun de ces cas, l'origine de la cohésion est assurée par des liaisons attractives capillaires entre particules. La présence de liquide génère également des forces visqueuses lorsque les grains sont en mouvement relatif et s'écoulent. La distribution du liquide à l'intérieur d'un matériau granulaire dépend fortement du degré de saturation. Elle peut être très complexe, notamment dans les régimes intermédiaires où l'eau n'est plus présente sous la forme de liaisons binaires entre paires de grains et où l'on n'a pas encore atteint la teneur en eau où seules des bulles persistent dans le milieu.

Dans cette thèse on a fait le choix de considérer un matériau granulaire dans un environnement humide « bien mélangé » où le volume d'eau est suffisamment faible pour que les ponts liquides soient distribués de façon homogène, comme lors de la condensation d'une vapeur par exemple. On s'est limité à la prise en compte de liaisons entre paires de grains, modélisées par des lois de forces visqueuses et cohésives à seuil (avec une distance de décollement) ; venant compléter celles élastiques et frictionnelles représentant les contacts. Avec ces approximations, les approches numériques simulant la dynamique des particules - telles que les méthodes des éléments discrets (DEM) ou de dynamique des contacts (DC) - peuvent être utilisées efficacement pour simuler de grands systèmes. On peut noter que des systèmes statistiquement représentatifs sont inatteignables, dans des temps de calcul raisonnables, avec des simulations basées sur des approches couplées décrivant simultanément le mouvement de toutes les phases (grains, liquide et gaz). Dans cette thèse, en utilisant l'approche DEM et des approximations sur les lois de forces on montre que la cohésion obtenue à l'échelle macroscopique est comparable aux résultats d'expériences.

La plupart des études sur la rhéologie des matériaux granulaires, menées au cours des trois dernières décennies, ont porté sur les matériaux secs. Par exemple, le comportement en régime permanent a fait l'objet d'études approfondies et des modèles basés sur le nombre inertiel ont été proposés et appliqués à diverses géométries d'écoulement. De même, le com-

---

portement quasi- statique a été étudié en détail afin d'analyser les propriétés élastiques et plastiques des matériaux granulaires en relation avec de leur microstructure. La rhéologie des matériaux cohésifs n'a été abordée que plus récemment dans les laboratoires de physique et de mécanique en considérant les effets des interactions cohésives sur l'écoulement inertiel ou leur lien avec la résistance à la traction mesurée à l'échelle d'assemblages de particules. Il existe une vaste panoplie d'applications dans la technologie des poudres où la cohésion est d'une importance primordiale. La fluidité (ou coulabilité) des poudres est considérée comme une propriété majeure, mesurée par différents types de rhéomètres. Le mélange et l'agglomération de poudres cohésives est un sujets de recherche important pour la formulation de produits en pharmacie, métallurgie, agroalimentaire, etc. L'agglomération est également un des mécanismes principal à l'origine de la difficulté à réaliser des broyages ultrafins, c'est-à-dire sub-micrométriques, par voie sèche (c'est à dire sans faire un broyage en conditions immergées). L'intérêt pour ces applications et la nécessité de développer des approches systématiques de modélisation et d'analyse des matériaux cohésifs, ont largement motivé ce travail de thèse. Un élément central à été de réaliser une étude paramétrique extensive des écoulements cohésifs par simulations DEM 3D en tenant compte de l'agglomération des particules. Cette étude qui a été menée dans le cas d'écoulements simples et de tambours tournants, a permis de traiter, de façon générique, plusieurs questions liées aux matériaux granulaires cohésifs. On pourra noter néanmoins que ce travail a été initié dans le cadre d'un projet collaboratif financé par ArcelorMittal (Laboratoire de Recherche de Maizières, France) dont le titre était « Approche multi-échelle du processus d'agglomération ». Ce projet effectué de 2015 à 2017 a associé l'Unité Mixte Internationale CNRS-MIT aux Etats Unis (Massachusetts) et l'Unité Mixte de Recherche IATE (INRA/SupAgro/Cirad/Université de Montpellier) Ingénierie des Agro-polymères et Technologies Emergentes.

Les questions fondamentales que nous avons abordées concernent principalement l'influence des interactions à l'échelles des particules sur les propriétés effectives telles que la résistance au cisaillement lors d'un écoulement, la résistance à la compression d'agglomérats cohésifs, l'érosion d'un granule dans un écoulement cisailé et le rôle joué par les contraintes inertielles. L'un des aspects clés de ces études a été de considérer l'effet combiné des contraintes cohésives et visqueuses. Lorsque deux types différents d'interactions entrent en jeu dans un système, on s'attendrait à ce que leur effet conjoint soit différent de celui d'une simple superposition de leurs effets individuels. Le même type de question peut se poser au sujet des effets simultanés de l'inertie et de la cohésion des particules dans des écoulements rapides. Cette question, qui avait déjà fait l'objet de simulations numériques pour les suspensions, avait permis de montrer que le coefficient de frottement apparent et la compacité peuvent être très bien décrits en fonction d'un seul paramètre sans dimension incorporant à la fois le nombre inertiel et le nombre de Stokes. Cette "additivité" des effets trouve son origine dans l'additivité des contraintes moyennant une pondération qui doit dépendre des détails des interactions. La question abordée dans ce travail de thèse vient généraliser les précédents travaux : dans quelle mesure les effets cohésifs, visqueux et inertiels sont-ils additifs ? En d'autres terme il s'agit de savoir si la rhéologie de ces matériaux granulaires plus "complexes" est une extension de celle des matériaux granulaires secs et

---

si un seul paramètre de contrôle (comme une extension du nombre inertiel) peut capturer tous ces effets ?

De telles questions peuvent être étudiées rigoureusement dans des conditions aux limites homogènes. Mais les matériaux granulaires humides sont souvent mis en oeuvre dans des conditions de chargement complexes. Le processus de granulation en est un exemple bien connu. L'utilisation de tambours tournant implique l'apparition de régimes d'écoulement spécifiques, tels que des écoulements en cascade, une distribution non homogène du liquide, conduisant sous certaines conditions à la nucléation ou à l'érosion d'agglomérats ou granules. Pour une meilleure maîtrise de ces processus, les effets des paramètres de contrôle tels que la vitesse de rotation et ceux des paramètres matériaux (quantité de liquide, granulométrie des particules, tension de surfaces, etc) sont important à préciser. Nous avons abordé certaines de ces questions importante pour le domaine des technologies des poudres. Par exemple, dans quelle mesure le nombre inertiel modifié peut être utilisé pour mettre à l'échelle le comportement des granules ? Dans ce cas, nous nous sommes plus particulièrement concentrés sur le comportement d'un seul granule à l'intérieur d'un écoulement granulaire sec afin de déterminer dans quelles conditions le granule croît, disparaît ou est simplement déformé par cet écoulement. Enfin, la force cohésive d'un agglomérat sous compression diamétrale a également été considérée pour mieux appréhender le rôle des interactions sur la tenue mécanique des granules. L'ensemble de ces résultats ont donné lieu à quatre articles publiés ou soumis. La thèse comporte quatre chapitres, une revue bibliographique et trois chapitres, composés directement à partir des résultats des articles, traitant de la rhéologie des milieux granulaires humides, de l'agglomération des particules dans les écoulements granulaires denses et de la résistance mécanique des agglomérats.

Concernant les écoulements denses en présence de forces cohésives et visqueuses, nous avons constaté que la "rhéologie additive" fonctionne avec une très bonne précision. Cette propriété émerge de la nature des matériaux granulaires, dans lesquels les interactions des particules se produisent au niveau de points de contact, et de la dynamique locale contrôlée par le taux de cisaillement. Ainsi, un seul paramètre de mise à l'échelle peut être défini. Il s'agit du rapport de la somme pondérée des contraintes dépendant du taux de cisaillement à la somme pondérée de des contraintes qui sont indépendantes de ce taux de cisaillement. Le nombre visco-cohésif-inertiel obtenu généralise le nombre inertiel aujourd'hui classique et étend la validité de ce cadre théorique aux cas des interactions humides entre particules. Son application aux écoulements cohésifs nécessite la normalisation de la compacité et du coefficient de frottement apparent par leurs valeurs dans la limite quasi-statique (valeurs qui dépendent uniquement de l'indice de cohésion). Dans ces conditions, toutes des données obtenues se mettent à l'échelle en fonction du nombre visco-cohésif-inertiel, que ce soit dans le cas du coefficient de frottement que dans celui de la compacité. De la même manière, il est possible de définir et déterminer des viscosités effectives tangentielle et normale associées à l'écoulement. Comme dans les cas précédents, ces viscosités se mettent parfaitement à l'échelle avec avec le nombre inertiel modifié. Cette analyse nous a permis de proposer un paramètre d'échelle unique pour les matériaux granulaires fortement cohésifs dans lesquels la cohésion est largement supérieure aux contraintes externes telles que la gravité. Ce paramètre d'échelle  $I_m = \{Ca(\beta + St)/\alpha\}^{1/2}$  incorpore le nombre capillaire  $Ca$  et le nombre

---

de Stokes  $St$ .

L'étude de la croissance/érosion d'agglomérats a été également abordée en détail. Dans ce cas on introduit au préalable un petit agglomérat (granule) dans un lit de grains lui-même placé dans un tambour tournant. L'évolution de cet agglomérat est ensuite suivie au cours de l'écoulement du lit en s'intéressant au gain et à la perte de particules. On montre que cette évolution est gouvernée par l'accrétion de particules humides et par l'érosion due à l'écoulement inertiel. L'hypothèse importante effectuée ici est que le liquide disponible est transporté par les particules et que celles-ci ne forment des liaisons capillaires qu'entre particules « humides ». Bien que l'évolution de la distribution du liquide composant les liaisons soit un aspect clé du processus d'agglomération, il est important de distinguer deux échelles temporelles : 1) un temps associé au mouillage et à la redistribution du liquide, et 2) un temps associé au cisaillement. Dans nos simulations, nous avons supposé que tout le liquide est au préalable distribué dans l'échantillon granulaire, à la fois à l'intérieur du granule et au niveau de particules individuelles dispersées uniformément dans le matériau. Dans les écoulements inertiels, le temps de redistribution est supérieur au temps d'écoulement. Par conséquent, une particule mouillée transportera le liquide et ne pourra le partager qu'avec une autre particule humide. Avec ces hypothèses, la capture progressive des particules humides libres conduit à une croissance du granule exponentielle avec le nombre de rotations du tambour. Il est intéressant de noter qu'au contraire, le nombre de particules érodées augmente linéairement avec le temps. Comme le liquide disponible (ou le nombre équivalent de particules humides) est limité, la taille des granules tend vers une valeur constante. L'effet des paramètres matériels est parfois contre-intuitif. Par exemple, l'accrétion et l'érosion augmentent avec le rapport de taille ou le coefficient de frottement. Les effets du rapport de taille granulométrique et de la taille moyenne des particules ont également été étudiés. Nous avons constaté que ces deux paramètres influencent le taux de croissance. Enfin, bien que nous ayons pu analyser séparément les processus d'accrétion et d'érosion, il n'a pas été possible d'effectuer une analyse détaillée des mécanismes à l'échelle des particules en raison de la complexité de l'écoulement dans le tambour tournant.

La cohésion des agglomérats a été étudiée en réalisant des essais de compression diamétrale sur des granules sphériques pour une large gamme de valeurs de la taille de particules et de distance de décollement (liée à la quantité de liquide). Nous avons montré que la courbe contrainte-déformation présente un plateau plastique avant apparition de la rupture. La résistance plastique est proportionnelle à une contrainte capillaire caractéristique et a un facteur multiplicatif qui quasi-indépendant du frottement interparticulaire mais qui dépend linéairement de la distance de décollement et augmente avec le rapport taille. Nous avons introduit une expression analytique de la force cohésive tenant compte de la compacité, du nombre de coordination humide, de la polydispersité des particules et de la distance de décollement. Ce "granule modèle" peut être considéré comme un système de référence permettant une comparaison directe sur la base des principaux paramètres physiques influant dans les expériences de granulation. C'est le cas notamment pour les produits issus de granulateurs à tambour à particules fines comme les granules de minerai de fer marquées par une structure complexe (essentiellement imputable à une large distribution granulométrique de leurs particules primaires). Même dans ce cas, la résistance calculée grâce aux

---

granules modèle est en bon accord avec les tendances observées moyennant un pré-facteur que nous avons estimé à partir des données numériques.

L'étude de l'érosion et de la déformation d'un agglomérat cohésif unique a également été abordée en conditions périodique d'écoulement sous l'effet d'un cisaillement. Contrairement au cas du tambour tournant cette configuration fournit des conditions aux limites presque homogènes, rendant plus facile la caractérisation de l'évolution du granule. Une question importante était de préciser comment l'indice de cohésion et le nombre inertiel contrôlent cette évolution. En effet un granule peut survivre sans déformation ni érosion, être allongés sans dommage sous l'effet du cisaillement (perte de contacts cohésifs), être endommagé, érodé ou simplement disparaître. Ces résultats ont permis de proposer un diagramme de phases dans un espace - nombre inertiel - l'indice de cohésion. On a montré notamment que même pour de grandes valeurs de l'indice de cohésion, le granule peut être érodé si le nombre inertiel est suffisamment élevé. Cela montre que le détachement des particules humides du granule est fortement dépendant des fluctuations de forces et accentué par l'inertie des particules. On a également constaté que l'allongement pur du granule ne se produit que dans le régime à faible inertie. Cependant, au cours de cet allongement, le granule est progressivement endommagé par la perte irréversible de contacts cohésifs. Les taux d'allongement, d'endommagement ou d'érosion ne sont pas de simples fonctions d'un paramètre d'échelle combinant le nombre inertiel et l'indice de cohésion. En effet, le nombre inertiel décrit l'écoulement de particules non cohésives, et non l'inertie à l'intérieur du granule. Par conséquent, les effets inertiels sont surtout pertinents pour caractériser le niveau d'érosion plutôt que pour l'allongement et l'endommagement. Finalement, on notera que l'image générale que l'on a pu se faire de la « simplicité » des écoulements granulaire humides - en ce sens qu'un seul paramètre d'échelle tient compte des effets de toutes les interactions - doit être nuancée. En effet, cette image ne s'applique pas facilement à l'agglomération de particules qui est un processus non homogène impliquant à la fois des interactions entre particules cohésives et non cohésives. Dans de telles conditions, la représentation en diagramme de phase se révèle être un outil précieux pour classer les différents comportements en lien avec les paramètres tels que le nombre inertiel et l'indice de cohésion.

Les travaux présentés dans cette thèse de doctorat peuvent être étendus selon différentes lignes et orientations. Une des extensions les plus intéressantes consiste à appliquer la rhéologie, avec nombre inertiel modifié, aux écoulements gravitationnels à surface libre ou aux tambours tournants dans le régime de roulement (qui est régi par les effets inertiels). Les prédictions du modèle peuvent également être comparées à des expériences appropriées dans les mêmes géométries d'écoulement. On notera que les régimes classiquement décrits pour des écoulements de particules sèches dans des tambours tournants seront modifiés en présence de forces visqueuses et capillaires. Une description expérimentale systématique de ces nouveaux régimes, a priori plus complexes, serait une avancée importante dans le domaine.

Une autre extension envisageable consisterait à utiliser des méthodes couplées particule-liquide pour simuler des suspensions colloïdales cohésives. On s'attend à ce que la mise à l'échelle proposée dans ce travail s'applique aussi à ces écoulements. Il est clair qu'ici

---

la nature des forces de cohésion ne peut être d'origine capillaire, puisque le système est totalement saturé, mais pour des poudres fines, les forces de van der Waals peuvent jouer un rôle similaire.

Le processus d'agglomération nécessite un investissement important en terme de simulations numériques. L'étape de nucléation peut être facilement étudiée à partir d'une dispersion de particules humides à l'intérieur d'une collection de particules non cohésives. Comme de multiples granules peuvent apparaître simultanément et se développer au cours du processus, de telles simulations nécessitent de grands systèmes et beaucoup plus de particules que ce qui a été considéré jusque ici. Les interactions entre les granules et l'apparition d'une coalescence sont des phénomènes très intéressants, jouant un rôle dans la formation de pâtes par exemple, et qui n'ont pas encore fait l'objet de simulations. Les modèles de bilan détaillés pour l'agglomération peuvent également être évalués en analysant les processus d'accrétion et d'érosion à l'échelle des particules. Des études paramétriques pourront être poursuivies afin de déterminer les diagrammes d'espace de phase de la croissance des granules en fonction de tous les paramètres matériels et opérationnels.

Enfin, la dynamique d'impact et la fracture des agrégats de particules cohésives peut être l'objet d'un test particulièrement intéressant pour l'étude de la rhéologie cohésive-visqueuse. L'un des enjeux de la modélisation de la dynamique d'impact est la pertinence de la loi capillaire utilisée dans nos simulations. Cette loi est basée sur l'équation de Laplace-Young, qui décrit la force capillaire d'équilibre. Dans les essais dynamiques, il sera nécessaire de modifier cette loi afin de tenir compte des forces capillaires hors d'équilibre.

# Bibliography

- [1] GDR-MiDi, On dense granular flows, *Eur. Phys. J. E* 14 (2004) 341–365. [Cited pages 8, 9, 29, 51 et 85.]
- [2] N. Mitarai, F. Nori, Wet granular materials, *Advances in Physics* 55 (1-2) (2006) 1–45. [Cited pages 10 et 11.]
- [3] N. Berger, E. Azéma, J.-F. Douce, F. Radjai, Scaling behaviour of cohesive granular flows, *EPL-Europhysics Letters* 112. [Cited pages 10, 11, 12, 13, 29, 34, 71, 85 et 86.]
- [4] L. Amarsid, J.-Y. Delenne, P. Mutabaruka, Y. Monerie, F. Perales, F. Radjai, Viscoinertial regime of immersed granular flows, *Phys. Rev. E* 96 (2017) 012901. [Cited pages 11, 13, 14, 15, 20, 29, 34, 51, 53, 86 et 98.]
- [5] P. Jop, Y. Forterre, O. Pouliquen, A constitutive law for dense granular flows, *Nature* 441 (2006) 727–730. [Cited pages 8, 29, 34 et 85.]
- [6] Y. Forterre, O. Pouliquen, Flows of dense granular media, *Annual Review of Fluid Mechanics* 40 (1) (2008) 1–24. [Cited pages 8 et 85.]
- [7] F. Radjai, J.-N. Roux, A. Daouadji, Modeling granular materials: Century-long research across scales, *Journal of Engineering Mechanics* 143 (4) (2017) 04017002. [Cited page 8.]
- [8] M. Badetti, A. Fall, D. Hautemayou, F. Chevoir, P. Aïmediou, S. Rodts, J.-N. Roux, Rheology and microstructure of unsaturated wet granular materials: Experiments and simulations, *Journal of Rheology* 62 (5) (2018) 1175–1186. [Cited pages 8, 10, 11 et 85.]
- [9] O. Pouliquen, C. Cassar, P. Jop, Y. Forterre, M. Nicolas, Flow of dense granular material: towards simple constitutive laws, *Journal of Statistical Mechanics: Theory and Experiment* 2006 (2006) 7020 – 7020. [Cited pages 8, 34 et 85.]
- [10] F. da Cruz, S. Emam, M. Prochnow, J.-N. Roux, F. Chevoir, Rheophysics of dense granular materials: Discrete simulation of plane shear flows, *Physical Review E* 72 (2005) 021309. [Cited pages 9, 29, 32 et 85.]

## BIBLIOGRAPHY

---

- [11] E. Azéma, F. Radjai, Internal structure of inertial granular flows, *Physical Review Letter* 112 (2014) 078001. [Cited pages 9, 34 et 36.]
- [12] O. Pouliquen, Scaling laws in granular flows down rough inclined plane, *Physics of Fluids* 11 (1999) 1956–1958. [Cited page 9.]
- [13] L. E. Silbert, D. Ertz, G. S. Grest, T. C. Halsey, D. Levine, S. J. Plimpton, Granular flow down an inclined plane: Bagnold scaling and rheology., *Phys Rev E Stat Nonlin Soft Matter Phys* 64 (5 Pt 1) (2001) 051302. [Cited page 9.]
- [14] F. Da Cruz, F. Chevoir, J. Roux, I. Iordanoff, Macroscopic friction of dry granular materials, *Tribology series* 43 (2003) 53–61. [Cited page 9.]
- [15] B. J. Ennis, Agglomeration and size enlargement session summary paper, *Powder Technology* 88 (3) (1996) 203 – 225. [Cited pages 10, 15, 51 et 57.]
- [16] H. G. Kristensen, Particle agglomeration in high shear mixers, *Powder Technology* 88 (3) (1996) 197 – 202. [Cited page 10.]
- [17] D. Bika, M. Gentzler, J. Michaels, Mechanical properties of agglomerates, *Powder Technology* 117 (2001) 98–112. [Cited page 10.]
- [18] N. Mitarai, F. Nori, Wet granular materials, *Advances in Physics* 55 (1-2) (2006) 1–45. [Cited page 10.]
- [19] P. S. Raux, A.-L. Bianco, Cohesion and agglomeration of wet powders, *Phys. Rev. Fluids* 3 (2018) 014301. [Cited page 10.]
- [20] S. M. Iveson, J. D. Litster, K. Hapgood, B. J. Ennis, Nucleation, growth and breakage phenomena in agitated wet granulation processes: a review, *Powder Technology* 117 (1) (2001) 3–39. [Cited pages 10, 11, 16, 51, 52, 53, 54 et 71.]
- [21] V. Richefeu, M. S. El Yousoufi, R. Peyroux, F. Radjai, A model of capillary cohesion for numerical simulations of 3d polydisperse granular media, *International Journal for Numerical and Analytical Methods in Geomechanics* 32 (2007) 1365–1383. [Cited pages 10 et 24.]
- [22] S. Khamseh, J.-N. Roux, F. m. c. Chevoir, Flow of wet granular materials: A numerical study, *Phys. Rev. E* 92 (2015) 022201. [Cited pages 10, 11, 24, 29 et 85.]
- [23] M. Badetti, A. Fall, F. Chevoir, J.-N. Roux, Shear strength of wet granular materials: Macroscopic cohesion and effective stress, *The European Physical Journal E* 41 (5) (2018) 68. [Cited pages 10 et 29.]
- [24] F. Radjai, V. Richefeu, Bond anisotropy and cohesion of wet granular materials, *Philosophical Transactions of the Royal Society A* 367 (2009) 5123–5138. [Cited pages 10, 11, 24, 29, 35, 38, 79 et 85.]

## BIBLIOGRAPHY

---

- [25] G. Lefebvre, P. Jop, Erosion dynamics of a wet granular medium, *Physical Review E : Statistical, Nonlinear, and Soft Matter Physics* 8 (2013) 032205. [Cited pages 11, 17, 19, 21, 24, 40, 57, 65, 71, 85, 86 et 98.]
- [26] B. J. Ennis, G. Tardos, R. Pfeffer, A microlevel-based characterization of granulation phenomena, *Powder Technology* 65 (1) (1991) 257 – 272. [Cited pages 11, 19, 51, 52 et 85.]
- [27] G. D’Anna, Mechanical properties of granular media, including snow, investigated by a low-frequency forced torsion pendulum, *Phys. Rev. E* 62 (2000) 982–992. [Cited page 11.]
- [28] B. L., C. E., C. S., C. J., Moisture-induced ageing in granular media and the kinetics of capillary condensation, *Nature* 396. [Cited page 11.]
- [29] C. Feng, A. Yu, Quantification of the relationship between porosity and interparticle forces for the packing of wet uniform spheres, *Journal of Colloid and Interface Science* 231 (1) (2000) 136 – 142. [Cited page 11.]
- [30] D. Geromichalos, M. M. Kohonen, F. Mugele, S. Herminghaus, Mixing and condensation in a wet granular medium, *Phys. Rev. Lett.* 90 (2003) 168702. [Cited page 11.]
- [31] P. Y. Liu, R. Y. Yang, A. B. Yu, The effect of liquids on radial segregation of granular mixtures in rotating drums, *Granular Matter* 15 (4) (2013) 427–436. [Cited pages 11 et 56.]
- [32] P. G. Rognon, J.-N. Roux, D. Wolf, M. Naaim, F. Chevoir, Rheophysics of cohesive granular materials, *EPL (Europhysics Letters)* 74 (4) (2006) 644. [Cited pages 11 et 29.]
- [33] P. Rognon, J.-N. Roux, M. Naaim, F. Chevoir, Dense flows of cohesive granular materials, *Journal of Fluids Mechanics* 596 (2008) 21–47. [Cited pages 11 et 29.]
- [34] N. Huang, G. Ovarlez, F. Bertrand, S. Rodts, P. Coussot, D. Bonn, Flow of wet granular materials., *Phys Rev Lett* 94 (2) (2005) 028301. [Cited page 11.]
- [35] F. Radjai, V. Richefeu, Bond anisotropy and cohesion of wet granular materials, *Phil. Trans. R. Soc. A* 367 (2009) 5123–5138. [Cited page 11.]
- [36] V. Richefeu, M. El Youssoufi, F. Radjai, F., Shear strength properties of wet granular materials, *Physical Review E* 73 (2006) 051304. [Cited pages 11, 22, 23, 24, 29, 40 et 81.]
- [37] V. Richefeu, M. S. d El Youssoufi, F. Radjai, Shear strength properties of wet granular materials., *Phys. Rev. E* 73 (5 Pt 1) (2006) 051304. [Cited page 11.]
- [38] V. Richefeu, F. Radjai, M. S. E. Youssoufi, Stress transmission in wet granular materials., *Eur. Phys. J. E* 21 (2007) 359–369. [Cited pages 11, 22, 24, 38, 40 et 52.]

- 
- [39] G. Saingier, A. Sauret, P. Jop, Accretion dynamics on wet granular materials, *Phys. Rev. Lett.* 118 (2017) 208001. [Cited pages 11 et 20.]
- [40] Y. Gu, S. Chialvo, S. Sundaresan, Rheology of cohesive granular materials across multiple dense-flow regimes, *Phys. Rev. E* 90 (2014) 032206. [Cited page 11.]
- [41] P. Pierrat, H. Caram, Tensile strength of wet granular materials, *Powder Technology* 91 (1997) 83–93. [Cited page 11.]
- [42] Z. Fournier, D. Gerimichalos, S. Herminghaus, M. M. Kohonen, F. Mugele, M. Scheel, M. Schulz, B. Schulz, C. Schier, R. Seemann, A. Shudelny, Mechanical properties of wet granular materials, *Applied Physics: Condensed Matter* 17 (2005) 477–502. [Cited page 11.]
- [43] J.-Y. Delenne, M. S. El Youssoufi, F. Cherblanc, J.-C. B enet, Mechanical behaviour and failure of cohesive granular materials, *International Journal for Numerical and Analytical Methods in Geomechanics* 28 (15) (2004) 1577–1594. [Cited page 11.]
- [44] T-Trung. Vo, P. Mutabaruka, S. Nezamabadi, J.-Y. Delenne, E. Izard, R. Pellenq, F. Radjai, Mechanical strength of wet particle agglomerates, *Mechanics Research Communications* 92 (2018) 1–7. [Cited pages 11, 22, 24 et 85.]
- [45] F. Boyer, E. Guazzelli, O. Pouliquen, Unifying suspension and granular rheology, *Phys. Rev. Lett.* 107 (2011) 18. [Cited pages 11, 13, 14, 29, 35 et 43.]
- [46] M. Trulsson, B. Andreotti, P. Claudin, Transition from the viscous to inertial regime in dense suspensions, *Phys. Rev. Lett.* 109 (2012) 118305. [Cited pages 11, 14, 29, 34, 86 et 98.]
- [47] A. Gnoli, L. de Arcangelis, F. Giacco, E. Lippiello, M. P. Ciamarra, A. Puglisi, A. Sarracino, Controlled viscosity in dense granular materials, *Phys. Rev. Lett.* 120 (2018) 138001. [Cited page 11.]
- [48] Q. Xu, A. V. Orpe, A. Kudrolli, Lubrication effects on the flow of wet granular materials, *Phys. Rev. E* 76 (2007) 031302. [Cited page 11.]
- [49] O. Pitois, P. Moucheron, X. Chateau, Liquid bridge between two moving spheres: An experimental study of viscosity effects, *Journal of Colloid and Interface Science* 231 (1) (2000) 26 – 31. [Cited page 11.]
- [50] R. Brewster, G. Grest, J. Landry, A. Levine, Plug flow and the breakdown of bag-nold scaling in cohesive granular flows, *Physical Review E* 72 (2005) 061301. [Cited page 11.]
- [51] R. Nedderman, *Statics and kinematics of granular materials*, Cambridge University Press, Cambridge, 1992. [Cited page 11.]

## BIBLIOGRAPHY

---

- [52] F. Radjai, S. Roux, Features of granular texture, in: Y. Kishino (Ed.), *Powders and Grains 2001*, A. A. Balkema, Amsterdam, 2001, pp. 21–24. [Cited page 11.]
- [53] F. Gilibert, J.-N. Roux, A. Castellanos, Computer simulation of model cohesive powders: plastic consolidation, structural changes and elasticity under isotropic loads., *Physical Review E* 78 (2008) 031305. [Cited page 11.]
- [54] R. Y. Yang, R. P. Zou, A. B. Yu, Computer simulation of the packing of fine particles, *Phys. Rev. E* 62 (3) (2000) 3900–. [Cited pages 11 et 12.]
- [55] J. Fourcade, P. Sornay, F. Sudreau, P. Papet, Experimental approach of uo2 compaction and analytical modelling of pellet diametric deformations, *Powder Metallurgy* 49 (2) (2006) 125–134. [Cited page 12.]
- [56] C.-Y. Wu, S. M. Best, A. C. Bentham, B. C. Hancock, W. Bonfield, A simple predictive model for the tensile strength of binary tablets, *European Journal of Pharmaceutical Sciences* 25 (2) (2005) 331 – 336. [Cited pages 12 et 71.]
- [57] R. M. Iverson, The physics of debris flows, *Reviews of Geophysics* (1997) 245 – 296. [Cited page 13.]
- [58] O. Hungr, S. G. Evans, M. J. Bovis, J. N. Hutchinson, A review of the classification of landslides of the flow type, *Environmental & Engineering Geoscience* 7 (3) (2001) 221–238. [Cited page 13.]
- [59] F. Legros, The mobility of long-runout landslides, *Engineering Geology* 63 (3) (2002) 301 – 331. [Cited page 13.]
- [60] K. Hewitt, Gifts and perils of landslides (vol 98, pg 410, 2010), *American Scientist* 99 (2010) 5–5. [Cited page 13.]
- [61] M. J. Rhodes, *Introduction to particle technology* / Martin Rhodes, John Wiley Chichester ; New York, 1998. [Cited page 13.]
- [62] J. J. Stickel, R. L. Powell, Fluid mechanics and rheology of dense suspensions, *Annual Review of Fluid Mechanics* 37 (1) (2005) 129–149. [Cited page 13.]
- [63] O. Reynolds, On the dilatancy of media composed of rigid particles in contact, *Philos. Mag. Ser. 5* 50-20 (1885) 469. [Cited page 13.]
- [64] S. Courrech du Pont, P. Gondret, B. Perrin, M. Rabaud, Granular avalanches in fluids, *Phys. Rev. Lett.* 90 (2003) 044301. [Cited page 14.]
- [65] S. H. Chien, G. Carmona, L. I. Prochnow, E. R. Austin, Cadmium availability from granulated and bulk-blended phosphate-potassium fertilizers., *J Environ Qual* 32 (5) (2003) 1911–1914. [Cited pages 15, 51 et 85.]

- [66] A. Nosrati, J. Addai-Mensah, D. J. Robinson, Drum agglomeration behavior of nickel laterite ore: Effect of process variables, *Hydrometallurgy* 125–126 (2012) 90 – 99. [Cited pages 15, 51 et 85.]
- [67] K. V. Sastry, P. Dontula, C. Hosten, Investigation of the layering mechanism of agglomerate growth during drum pelletization, *Powder Technology* 130 (1) (2003) 231 – 237. [Cited pages 15, 17, 51 et 71.]
- [68] R. Aguado, S. Roudier, L. Delgado (Eds.), Best available techniques (BAT) reference document for iron and steel production., Joint Research Centre of the European Commission, Luxembourg: Publications Office of the European Union, 2013. [Cited pages 15, 51, 56 et 71.]
- [69] G. M. Walker, Chapter 4 drum granulation processes, *Handbook of Powder Technology* 11 (2007) 219 – 254, granulation. [Cited pages 15, 16 et 51.]
- [70] S. Herminghaus, Dynamics of wet granular matter, *Advances in Physics* 54 (3) (2005) 221–261. [Cited pages 16, 29, 51 et 71.]
- [71] J. Litster, B. Ennis, *The Science and Engineering of Granulation Processes*, Vol. 15, Springer Netherlands, 2014. [Cited pages 16, 18, 51 et 71.]
- [72] C. Liao, S. Hsiau, S. Wen, Effect of adding a small amount of liquid on density-induced wet granular segregation in a rotating drum, *Advanced Powder Technology* 27 (4) (2016) 1265 – 1271. [Cited pages 16, 18, 19, 51 et 71.]
- [73] S. Iveson, J. Litster, Growth regime map for liquid-bound granules, *AIChE journal* 44 (7) (1998) 1510–1518. [Cited pages 16, 19, 51, 52 et 71.]
- [74] X. Xiao, Y. Tan, H. Zhang, R. Deng, S. Jiang, Experimental and dem studies on the particle mixing performance in rotating drums: Effect of area ratio, *Powder Technology* 314 (2017) 182 – 194. [Cited pages 16 et 51.]
- [75] B. Alchikh-Sulaiman, M. Alian, F. Ein-Mozaffari, A. Lohi, S. R. Upreti, Using the discrete element method to assess the mixing of polydisperse solid particles in a rotary drum, *Particuology* 25 (2016) 133 – 142. [Cited pages 16 et 51.]
- [76] A. Bouwman, M. Henstra, D. Westerman, J. Chung, Z. Zhang, A. Ingram, J. Seville, H. Frijlink, The effect of the amount of binder liquid on the granulation mechanisms and structure of microcrystalline cellulose granules prepared by high shear granulation, *International Journal of Pharmaceutics* 290 (1) (2005) 129 – 136. [Cited pages 16 et 51.]
- [77] J. Degrève, J. Baeyens, M. V. de Velden, S. D. Laet, Spray-agglomeration of npk-fertilizer in a rotating drum granulator, *Powder Technology* 163 (3) (2006) 188 – 195. [Cited pages 16, 51, 52 et 71.]

- [78] J. D. Osborne, R. P. Sochon, J. J. Cartwright, D. G. Doughty, M. J. Hounslow, A. D. Salman, Binder addition methods and binder distribution in high shear and fluidised bed granulation, *Chemical Engineering Research and Design* 89 (5) (2011) 553 – 559. [Cited pages 16, 51 et 71.]
- [79] S. K. Pawar, F. Henrikson, G. Finotello, J. T. Padding, N. G. Deen, A. Jongsma, F. Innings, J. H. Kuipers, An experimental study of droplet-particle collisions, *Powder Technology* 300 (2016) 157 – 163. [Cited pages 16, 17, 51 et 71.]
- [80] R. Pashminehazar, A. Kharaghani, E. Tsotsas, Three dimensional characterization of morphology and internal structure of soft material agglomerates produced in spray fluidized bed by x-ray tomography, *Powder Technology* 300 (2016) 46 – 60. [Cited pages 16, 17, 51 et 71.]
- [81] G. Lian, C. Thornton, M. Adams, A theoretical study of the liquid bridge forces between two rigid spherical bodies, *Journal of Colloid and Interface Science* 161 (1993) 138–147. [Cited pages 16, 20, 23, 24, 39, 40, 52, 71 et 72.]
- [82] M. Scheel, R. Seemann, M. Brinkmann, M. D. Michiel, A. Sheppard, S. Herminghaus, Liquid distribution and cohesion in wet granular assemblies beyond the capillary bridge regime, *Journal of Physics: Condensed Matter* 20 (49) (2008) 494236. [Cited pages 16, 22, 23, 40, 41, 52, 53 et 71.]
- [83] C. Willett, M. Adans, S. Johnson, J. Seville, Capillary bridges between two spherical bodies, *Langmuir* 16 (2000) 9396–9405. [Cited pages 16, 40, 52 et 71.]
- [84] J.-Y. Delenne, V. Richefeu, F. Radjai, Liquid clustering and capillary pressure in granular media, *Journal of Fluid Mechanics* 762. [Cited pages 16, 20, 22, 23, 40, 41 et 71.]
- [85] F. Štěpánek, P. Rajniak, C. Mancinelli, R. Chern, R. Ramachandran, Distribution and accessibility of binder in wet granules, *Powder Technology* 189 (2) (2009) 376 – 384. [Cited pages 16, 51, 52 et 71.]
- [86] C. Thornton, Z. Ning, A theoretical model for the stick/bounce behaviour of adhesive, elastic-plastic spheres, *Powder Technology* 99 (2) (1998) 154 – 162. [Cited pages 16, 51 et 71.]
- [87] L. X. Liu, J. D. Litster, S. M. Iveson, B. J. Ennis, Coalescence of deformable granules in wet granulation processes, *AIChE Journal* 46 (2000) 529 – 539. [Cited pages 16, 17, 51 et 71.]
- [88] S. Iveson, J. Beathe, N. Page, The dynamic strength of partially saturated powder compacts: the effect of liquid properties, *Powder Technology* 127 (2002) 149–161. [Cited pages 16, 19, 29, 51, 71, 85 et 86.]

- 
- [89] M. Ghadiri, A. D. Salman, M. Hounslow, A. Hassanpour, D. W. York, Editorial: Special issue – agglomeration, *Chemical Engineering Research and Design* 89 (5) (2011) 499. [Cited pages 16, 51, 71 et 85.]
- [90] J. Rojek, S. Nosewicz, M. Maździarz, P. Kowalczyk, K. Wawrzyk, D. Lumelskyj, Modeling of a sintering process at various scales, *Procedia Engineering* 177 (2017) 263 – 270. [Cited pages 16, 51 et 71.]
- [91] N. Rahmanian, A. Najji, M. Ghadiri, Effects of process parameters on granules properties produced in a high shear granulator, *Chemical Engineering Research and Design* 89 (5) (2011) 512 – 518. [Cited pages 16, 17, 51 et 71.]
- [92] K. E. Ileleji, Y. Li, R. K. Ambrose, P. H. Doane, Experimental investigations towards understanding important parameters in wet drum granulation of corn stover biomass, *Powder Technology* 300 (2016) 126 – 135. [Cited pages 16, 51 et 71.]
- [93] J.-P. Pan, T.-J. Wang, J.-J. Yao, Y. Jin, Granule transport and mean residence time in horizontal drum with inclined flights, *Powder Technology* 162 (1) (2006) 50 – 58. [Cited pages 16 et 51.]
- [94] R. Spurling, J. Davidson, D. Scott, The transient response of granular flows in an inclined rotating cylinder, *Chemical Engineering Research and Design* 79 (1) (2001) 51 – 61. [Cited pages 16 et 51.]
- [95] F. Wang, I. Cameron, A multi-form modelling approach to the dynamics and control of drum granulation processes, *Powder Technology* 179 (1) (2007) 2 – 11. [Cited pages 16 et 51.]
- [96] J. M. N. T. Gray, Granular flow in partially filled slowly rotating drums, *Journal of Fluid Mechanics* 441 (2001) 1–29. [Cited pages 16 et 51.]
- [97] J. Third, D. Scott, G. Lu, C. Müller, Modelling axial dispersion of granular material in inclined rotating cylinders with bulk flow, *Granular Matter* 17 (1) (2015) 33–41. [Cited page 16.]
- [98] S. Forrest, J. Bridgwater, P. R. Mort, J. Litster, D. J. Parker, Flow patterns in granulating systems, *Powder Technology* 30 (2002) 91–96. [Cited page 16.]
- [99] R. Ramachandran, J. M.-H. Poon, C. F. Sanders, T. Glaser, C. D. Immanuel, F. J. Doyle, J. D. Litster, F. Stepanek, F.-Y. Wang, I. T. Cameron, Experimental studies on distributions of granule size, binder content and porosity in batch drum granulation: Inferences on process modelling requirements and process sensitivities, *Powder Technology* 188 (2) (2008) 89 – 101. [Cited pages 16, 51 et 71.]
- [100] S. Iveson, J. Litster, B. Ennis, Fundamental studies of granule consolidation part 1: Effects of binder content and binder viscosity, *Powder Technology* 88 (1) (1996) 15 – 20. [Cited pages 16 et 71.]

- 
- [101] S. M. Iveson, P. A. Wauters, S. Forrest, J. D. Litster, G. M. Meesters, B. Scarlett, Growth regime map for liquid-bound granules: Further development and experimental validation, *Powder Technology* 117 (1–2) (2001) 83 – 97. [Cited pages 16 et 71.]
- [102] B. Mishra, C. Thornton, D. Bhimji, A preliminary numerical investigation of agglomeration in a rotary drum, *Minerals Engineering* 15 (1) (2002) 27 – 33. [Cited pages 16 et 71.]
- [103] P. A. Wauters, R. B. Jakobsen, J. D. Litster, G. M. Meesters, B. Scarlett, Liquid distribution as a means to describing the granule growth mechanism, *Powder Technology* 123 (2) (2002) 166 – 177. [Cited pages 16 et 71.]
- [104] F. Štěpánek, M. Ansari, Computer simulation of granule microstructure formation, *Chemical Engineering Science* 60 (14) (2005) 4019 – 4029. [Cited pages 16 et 71.]
- [105] T. Mikami, H. Kamiya, M. Horio, Numerical simulation of cohesive powder behavior in a fluidized bed, *Chemical Engineering Science* 53 (10) (1998) 1927 – 1940. [Cited pages 17, 23, 24, 29 et 71.]
- [106] P. Suresh, I. Sreedhar, R. Vaidhiswaran, A. Venugopal, A comprehensive review on process and engineering aspects of pharmaceutical wet granulation, *Chemical Engineering Journal* 328 (2017) 785–815. [Cited pages 17, 18, 51 et 85.]
- [107] B. J. Ennis, J. D. Litster, Particle size enlargement, *Perry’s Chemical Engineers’ Handbook*. [Cited page 17.]
- [108] P. Wauters, R. van de Water, J. Litster, G. Meesters, B. Scarlett, Growth and compaction behaviour of copper concentrate granules in a rotating drum, *Powder Technology* 124 (3) (2002) 230 – 237. [Cited pages 17 et 71.]
- [109] G. Félix, V. Falk, U. D’Ortona, Granular flows in a rotating drum: the scaling law between velocity and thickness of the flow., *Eur Phys J E Soft Matter* 22 (1) (2007) 25–31. [Cited page 17.]
- [110] I. Govender, Granular flows in rotating drums: A rheological perspective, *Minerals Engineering* 92 (2016) 168 – 175. [Cited pages 17, 52 et 71.]
- [111] T. Elperin, A. Vikhansky, Granular flow in a rotating cylindrical drum, *EPL (Europhysics Letters)* 42 (6) (1998) 619. [Cited page 17.]
- [112] H. Norouzi, R. Zarghami, N. Mostoufi, Insights into the granular flow in rotating drums, *Chemical Engineering Research and Design* 102 (2015) 12 – 25. [Cited page 17.]
- [113] N. Taberlet, P. Richard, E. J. Hinch, The S shape of a granular pile in a rotating drum, *Physical Review E : Statistical, Nonlinear, and Soft Matter Physics* 73 (2006) 050301(R). [Cited page 17.]

## BIBLIOGRAPHY

---

- [114] R. Yang, A. Yu, L. McElroy, J. Bao, Numerical simulation of particle dynamics in different flow regimes in a rotating drum, *Powder Technology* 188 (2) (2008) 170 – 177. [Cited pages 17, 52 et 56.]
- [115] J. Mellmann, The transverse motion of solids in rotating cylinders—forms of motion and transition behavior, *Powder technology* 118 (3) (2001) 251–270. [Cited pages 17, 52 et 56.]
- [116] S. Yang, A. Cahyadi, J. Wang, J. W. Chew, Dem study of granular flow characteristics in the active and passive regions of a three-dimensional rotating drum, *AIChE Journal* 62 (11) (2016) 3874–3888. [Cited page 18.]
- [117] E. Rondet, M. Delalonde, T. Ruiz, J. P. Desfoursb, Fractal formation description of agglomeration in low shear mixer, *Chemical Engineering Journal* 164 (2010) 376–382. [Cited pages 18, 29, 51 et 85.]
- [118] G. Lefebvre, A. Merceron, P. Jop, Interfacial instability during granular erosion, *Phys. Rev. Lett.* 116 (2016) 068002. [Cited page 19.]
- [119] S. P. Rwei, I. Manas-Zloczower, D. L. Feke, Characterization of agglomerate dispersion by erosion in simple shear flows, *Polymer Engineering & Science* 31 (8) (1991) 558–562. [Cited pages 20 et 86.]
- [120] M. I. Khan, G. I. Tardos, Stability of wet agglomerates in granular shear flows, *Journal of Fluid Mechanics* 347 (1997) 347–368. [Cited pages 20 et 86.]
- [121] G. Reynolds, J. Fu, Y. Cheong, M. Hounslow, A. Salman, Breakage in granulation: A review, *Chemical Engineering Science* 60 (14) (2005) 3969 – 3992. [Cited page 20.]
- [122] M. Ghadiri, R. Moreno-Atanasio, A. Hassanpour, S. J. Antony, Chapter 19 analysis of agglomerate breakage, in: A. D. Salman, M. Ghadiri, M. J. Hounslow (Eds.), *Particle Breakage*, Vol. 12 of *Handbook of Powder Technology*, Elsevier Science B.V., 2007, pp. 837 – 872. [Cited page 20.]
- [123] J. Sarkar, D. Dubey, Failure regimes of single wet granular aggregate under shear, *Journal of Non-Newtonian Fluid Mechanics* 234 (2016) 236 – 248. [Cited pages 20 et 85.]
- [124] N. D. Vassileva, D. van den Ende, F. Mugele, J. Mellema, Fragmentation and erosion of two-dimensional aggregates in shear flow, *Langmuir* 23 (5) (2007) 2352–2361. [Cited pages 20 et 86.]
- [125] D. Liu, Z. Wang, X. Chen, M. Liu, Simulation of agglomerate breakage and restructuring in shear flows: Coupled effects of shear gradient, surface energy and initial structure, *Powder Technology* 336 (2018) 102 – 111. [Cited pages 20 et 86.]

- 
- [126] A. Hassanpour, S. Antony, M. Ghadiri, Effect of size ratio on the behaviour of agglomerates embedded in a bed of particles subjected to shearing: dem analysis, *Chemical engineering science* 62 (2006) 935–942. [Cited pages 20 et 86.]
- [127] A. Hassanpour, S. J. Antony, M. Ghadiri, Modeling of agglomerate behavior under shear deformation: effect of velocity field of a high shear mixer granulator on the structure of agglomerates, *Advanced Powder Technology* 18 (6) (2007) 803 – 811. [Cited pages 20 et 86.]
- [128] A. Hassanpour, S. J. Antony, M. Ghadiri, Influence of interface energy of primary particles on the deformation and breakage behaviour of agglomerates sheared in a powder bed, *Chemical Engineering Science* 63 (23) (2008) 5593 – 5599. [Cited page 20.]
- [129] A. Hassanpour, C. Kwan, B. Ng, N. Rahmanian, Y. Ding, S. Antony, X. Jia, M. Ghadiri, Effect of granulation scale-up on the strength of granules, *Powder Technology* 189 (2) (2009) 304 – 312, special Issue: 3rd International Workshop on Granulation: Granulation across the Length Scales. [Cited page 20.]
- [130] P. A. Cundall, O. D. L. Strack, A discrete numerical model for granular assemblies, *Géotechnique* 29 (1) (1979) 47–65. [Cited pages 20 et 72.]
- [131] C. Thornton, Quasi-static shear deformation of a soft particle system, *Powder Technology* 109 (1999) 179–191. [Cited pages 20 et 72.]
- [132] H. J. Herrmann, S. Luding, Modeling granular media with the computer, *Continuum Mechanics and Thermodynamics* 10 (1998) 189–231. [Cited pages 20, 53 et 72.]
- [133] F. Radjai, F. Dubois, *Discrete-element modeling of granular materials*, Wiley-Iste, 2011. [Cited pages 20, 21, 52, 53 et 72.]
- [134] F. Radjai, V. Topin, V. Richefeu, C. Voivret, J.-Y. Delenne, E. Azéma, M. S. El Yousoufi, Force Transmission in Cohesive Granular Media, in: J. D. Goddard, J. T. Jenkins, P. Giovine (Eds.), *Mathematical Modeling and Physical Instances of granular Flows*, AIP, 2010, pp. 240–260. [Cited pages 20, 72 et 85.]
- [135] V. Richefeu, M. S. El Youssoufi, F. Radjaï, Shear strength of unsaturated soils: Experiments, dem simulations, and micromechanical analysis, in: *Theoretical and Numerical Unsaturated Soil Mechanics*, Springer, 2007, pp. 83–91. [Cited pages 20, 23 et 72.]
- [136] P. Mutabaruka, J.-Y. Delenne, K. Soga, F. Radjai, Initiation of immersed granular avalanches, *Phys. Rev. E* 89 (2014) 052203. [Cited page 20.]
- [137] V. Topin, Y. Monerie, F. Perales, F. Radjaï, Collapse dynamics and runout of dense granular materials in a fluid, *Phys. Rev. Lett.* 109 (2012) 188001. [Cited page 20.]

## BIBLIOGRAPHY

---

- [138] T. Zhao, S. Utili, G. B. Crosta, Rockslide and impulse wave modelling in the vajont reservoir by dem-cfd analyses, *Rock Mechanics and Rock Engineering* 49 (6) (2016) 2437–2456. [Cited page 20.]
- [139] T. Zhao, F. Dai, N.-w. Xu, Coupled dem-cfd investigation on the formation of landslide dams in narrow rivers, *Landslides* 14 (1) (2017) 189–201. [Cited page 20.]
- [140] J. Duran, A. Reisinger, P. de Gennes, *Sands, Powders, and Grains: An Introduction to the Physics of Granular Materials, Partially Ordered Systems*, Springer New York, 1999. [Cited page 21.]
- [141] T-Trung. Vo, P. Mutabaruka, J-Y. Delenne, S. Nezamabadi, F. Radjai, Strength of wet agglomerates of spherical particles: effects of friction and size distribution, *EPJ Web Conf.* 140 (2017) 08021. [Cited pages 22 et 40.]
- [142] J. Schäfer, S. Dippel, D. E. Wolf, Force schemes in simulations of granular materials, *J. Phys. I France* 6 (1996) 5–20. [Cited pages 22 et 41.]
- [143] S. Dippel, G. G. Batrouni, D. E. Wolf, How transversal fluctuations affect the friction of a particle on a rough incline, *Phys. Rev. E* 56 (1997) 3645–3656. [Cited pages 22 et 41.]
- [144] S. Luding, Collisions and contacts between two particles, in: H. J. Herrmann, J.-P. Hovi, S. Luding (Eds.), *Physics of dry granular media - NATO ASI Series E350*, Kluwer Academic Publishers, Dordrecht, 1998, p. 285. [Cited pages 22, 39 et 41.]
- [145] D. Shi, J. McCarthy, Numerical simulation of liquid transfer between particles, *Powder Technology* 184 (1) (2008) 64 – 75. [Cited pages 23 et 53.]
- [146] B. Mohan, C. Kloss, J. Khinast, S. Radl, Regimes of liquid transport through sheared beds of inertial smooth particles, *Powder Technology* 264 (2014) 377 – 395. [Cited pages 23 et 53.]
- [147] F. Soulié, F. Cherblanc, M. E. Youssoufi, C. Saix, Influence of liquid bridges on the mechanical behaviour of polydisperse granular materials, *International Journal for Numerical and Analytical Methods in Geomechanics* 30 (3) (2006) 213–228. [Cited page 23.]
- [148] G. Gagneux, O. Millet, Analytic calculation of capillary bridge properties deduced as an inverse problem from experimental data, *Transport in porous media* 105 (2014) 117–139. [Cited page 24.]
- [149] G. Lian, J. Seville, The capillary bridge between two spheres: New closed-form equations in a two century old problem, *Advances in colloid and interface science* 227 (2016) 53–62. [Cited page 24.]

## BIBLIOGRAPHY

---

- [150] J. Happel, H. Brenner, *Low Reynolds Number Hydrodynamics*, Martinus Nijhoff Publishers, 1983. [Cited pages 24 et 40.]
- [151] S. B. Savage, K. Hutter, The dynamics of avalanches of granular materials from initiation to runout. Part I: Analysis, *Acta Mechanica* 86 (1991) 201. [Cited page 29.]
- [152] C. S. Campbell, P. W. Cleary, M. Hopkins, Large-scale landslide simulations: Global deformation, velocities and basal friction, *Journal of Geophysical Research: Solid Earth* 100 (B5) (1995) 8267–8283. [Cited page 29.]
- [153] D. Cruden, D. Varnes, Spec. Rep., Vol. 247, Transp. Res. Board, Natl. Res. Council., Washington, D. C., 1996, Ch. Landslide types and processes, in *Landslides: Investigation and Mitigation*, pp. 36–75. [Cited page 29.]
- [154] P. Tegzes, T. Vicsek, P. Schiffer, Avalanche dynamics in wet granular materials, *Phys. Rev. Lett.* 89 (2002) 094301. [Cited page 29.]
- [155] A. Remaître, J.-P. Malet, O. Maquaire, C. Ancey, J. Locat, Flow behaviour and runout modelling of a complex debris flow in a clay-shale basin, *Earth Surface Processes and Landforms*, BSG 30 (4) (2005) 479–488. [Cited page 29.]
- [156] L. Staron, E. Hinch, The spreading of a granular mass: role of grain properties and initial conditions, *Granular Matter* 9 (3-4) (2007) 205–217. [Cited page 29.]
- [157] P. Mutabaruka, J.-Y. Delenne, K. Soga, F. Radjai, Initiation of immersed granular avalanches, *Phys. Rev. E* 89 (2014) 052203. [Cited page 29.]
- [158] R. Delannay, A. Valance, A. Mangeney, O. Roche, P. Richard, Granular and particle-laden flows: from laboratory experiments to field observations, *J. Phys. D* 50 (2017) 053001. [Cited page 29.]
- [159] H. Jaeger, S. Nagel, Granular solids, liquids and gases, *Reviews of Modern Physics* 68 (1996) 1259–1273. [Cited page 29.]
- [160] F. Radjai, J.-N. Roux, A. Daouadji, Modeling granular materials: Century-long research across scales, *Journal of Engineering Mechanics* 143 (4) (2017) 04017002. [Cited pages 29, 35 et 78.]
- [161] F. Radjai, D. E. Wolf, M. Jean, J. Moreau, Bimodal character of stress transmission in granular packings, *Physical Review Letter* 80 (1998) 61–64. [Cited page 29.]
- [162] D. M. Mueth, G. Debrégeas, G. S. Karczmar, P. Eng, S. R. Nagel, H. M. Jaeger, Signatures of granular microstructure in dense shear flows, *Nature* 406 (2000) 385–389. [Cited page 29.]
- [163] F. Radjai, S. Roux, Turbulentlike fluctuations in quasistatic flow of granular media., *Phys Rev Lett* 89 (6) (2002) 064302. [Cited page 29.]

## BIBLIOGRAPHY

---

- [164] E. I. Corwin, H. M. Jaeger, S. R. Nagel, Structural signature of jamming in granular media., *Nature* 435 (7045) (2005) 1075–1078. [Cited page 29.]
- [165] P. Richard, M. Nicodemi, R. Delannay, P. Ribière, D. Bideau, Slow relaxation and compaction of granular systems., *Nat Mater* 4 (2) (2005) 121–128. [Cited page 29.]
- [166] L. Staron, P.-Y. Lagrée, C. Josserand, D. Lhuillier, Flow and jamming of a two-dimensional granular bed: Toward a nonlocal rheology?, *Physics of Fluids* 22 (11) (2010) 113303. [Cited page 29.]
- [167] T. Miller, P. Rognon, B. Metzger, I. Einav, Eddy viscosity in dense granular flows, *Phys. Rev. Lett.* 111 (2013) 058002. [Cited page 29.]
- [168] S. Luding, So much for the jamming point, *Nature Physics* 12. [Cited page 29.]
- [169] B. Kou, Y. Cao, J. Li, C. Xia, Z. Li, H. Dong, A. Zhang, J. Zhang, W. Kob, Y. Wang, Granular materials flow like complex fluids, *Nature* 551 (2017) 360. [Cited page 29.]
- [170] K. Kamrin, G. Koval, Nonlocal constitutive relation for steady granular flow, *Phys. Rev. Lett.* 108 (2012) 178301. [Cited page 29.]
- [171] S. Roy, S. Luding, T. Weinhart, A general(ized) local rheology for wet granular materials, *New Journal of Physics* 19 (4) (2017) 043014. [Cited pages 29, 34 et 38.]
- [172] R. A. Bagnold, Experiments on a gravity-free dispersion of large solid spheres in a newtonian fluid under shear, *Proc. Royal Soc. London* 225 (1954) 49–63. [Cited pages 29 et 85.]
- [173] L. Bocquet, A. Colin, A. Ajdari, Kinetic theory of plastic flow in soft glassy materials, *Phys. Rev. Lett.* 103 (2009) 036001. [Cited page 35.]
- [174] L. Rothenburg, R. J. Bathurst, Analytical study of induced anisotropy in idealized granular materials, *Geotechnique* 39 (1989) 601–614. [Cited page 35.]
- [175] F. Radjai, J.-Y. Delenne, E. Azéma, S. Roux, Fabric evolution and accessible geometrical states in granular materials, *Granular Matter*. [Cited page 36.]
- [176] H. Brenner, The slow motion of a sphere through a viscous fluid towards a plane surface, *Chemical Engineering Science* 16 (1961) 242–251. [Cited page 38.]
- [177] V. D. Than, S. Khamseh, A. M. A. Tang, J.-M. Pereira, F. Chevoir, J.-N. Roux, Basic Mechanical Properties of Wet Granular Materials: A DEM Study, *Journal of Engineering Mechanics* 143 (1). [Cited page 40.]
- [178] F. Radjai, F. Dubois (Eds.), *Discrete Numerical Modeling of Granular Materials*, Wiley-ISTE, New-York, March 2011, ISBN: 978-1-84821-260-2. [Cited page 41.]

- [179] A. Barkouti, E. Rondet, M. Delalonde, T. Ruiz, Influence of physicochemical binder properties on agglomeration of wheat powder in couscous grain, *Journal of Food Engineering* 111 (2012) 234–240. [Cited pages 51 et 85.]
- [180] K. Saleh, P. Guigon, *Handbook of Powder Technology, Granulation*, Vol. 11, Elsevier, Amsterdam, 2007, Ch. Coating and encapsulation processes in powder technology, pp. 323–375. [Cited pages 51, 52, 85 et 86.]
- [181] A. Hassanpour, M. Pasha, L. Susana, N. Rahmanian, A. C. Santomaso, M. Ghadiri, Analysis of seeded granulation in high shear granulators by discrete element method, *Powder Technology* 238 (2013) 50 – 55, special Issue: 5th International Granulation Workshop Granulation across the length scale 2011. [Cited page 51.]
- [182] M. Butensky, D. Hyman, Rotary drum granulation. an experimental study of the factors affecting granule size, *Ind. Eng. Chem. Fundam.* 10 (1971) 212–219. [Cited page 51.]
- [183] K. Kamrin, D. L. Henann, Nonlocal modeling of granular flows down inclines, *Soft Matter* 11 (2015) 179–185. [Cited page 51.]
- [184] M. A. Behjani, N. Rahmanian, N. F. bt Abdul Ghani, A. Hassanpour, An investigation on process of seeded granulation in a continuous drum granulator using dem, *Advanced Powder Technology* 28 (10) (2017) 2456 – 2464. [Cited pages 52, 54, 61 et 85.]
- [185] J.-Y. Delenne, V. Richefeu, F. Radjai, Liquid clustering and capillary pressure in granular media, *Journal of Fluid Mechanics* 762. [Cited pages 52, 53 et 54.]
- [186] I. Talu, G. I. Tardos, M. I. Khan, Computer simulation of wet granulation, *Powder Technology* 110 (2000) 59–75. [Cited pages 52, 54 et 85.]
- [187] E. L. Chan, K. Washino, G. K. Reynolds, B. Gururajan, M. J. Hounslow, A. D. Salman, Blade-granule bed stress in a cylindrical high shear granulator: Further characterisation using dem, *Powder Technology* 300 (2016) 92–106. [Cited page 52.]
- [188] P. Lau, M. Kind, Cfd-pbe simulation to predict particle growth in a fluidized bed melt granulation batch process, *Powder Technology* 300 (2016) 28–36. [Cited page 52.]
- [189] S. Sarkar, B. Chaudhuri, Dem modeling of high shear wet granulation of a simple system, *Asian Journal of Pharmaceutical Sciences* 13 (2018) 220–228. [Cited page 52.]
- [190] D. Barrasso, A. Tamrakar, R. Ramachandran, A reduced order pbm–ann model of a multi-scale pbm–dem description of a wet granulation process, *Chemical Engineering Science* 119 (2014) 319–329. [Cited page 52.]
- [191] V. Richefeu, M. S. El Youssoufi, E. Azéma, F. Radjai, Force transmission in dry and wet granular media, *Powder Technology* 190 (2009) 258–263. [Cited page 53.]

- 
- [192] H. Matuttis, S. Luding, H. Herrmann, Discrete element simulations of dense packings and heaps made of spherical and non-spherical particles, *Powder Technology* 109 (1) (2000) 278 – 292. [Cited page 53.]
- [193] C. Thornton, Numerical simulations of deviatoric shear deformation of granular media, *Géotechnique* 50 (1) (2000) 43–53. [Cited page 53.]
- [194] F. Radjai, I. Preechawuttipong, R. Peyroux, Cohesive granular texture, in: P. Vermeer, S. Diebels, W. Ehlers, H. Herrmann, S. Luding, E. Ramm (Eds.), *Continuous and discontinuous modelling of cohesive frictional materials*, Springer Verlag, Berlin, 2001, pp. 148–159. [Cited pages 53 et 85.]
- [195] A. Leonardi, M. Cabrera, F. K. Wittel, R. Kaitna, M. Mendoza, W. Wu, H. J. Herrmann, Granular-front formation in free-surface flow of concentrated suspensions, *Phys. Rev. E* 92 (2015) 052204. [Cited page 54.]
- [196] K. Melnikov, R. Mani, F. K. Wittel, M. Thielmann, H. J. Herrmann, Grain-scale modeling of arbitrary fluid saturation in random packings, *Phys. Rev. E* 92 (2015) 022206. [Cited page 54.]
- [197] C. Voivret, F. Radjaï, J.-Y. Delenne, M. S. E. Youssofi, Space-filling properties of polydisperse granular media, *Physical Review E* 76 (2007) 021301. [Cited page 55.]
- [198] C. Voivret, F. Radjai, J.-Y. Delenne, M. S. E. Youssofi, Multiscale force networks in highly polydisperse granular media, *Physical Review Letter* 102 (2009) 178001. [Cited pages 55 et 73.]
- [199] S. A. de Koster, K. Pitt, J. D. Litster, R. M. Smith, High-shear granulation: An investigation into the granule consolidation and layering mechanism, *Powder Technology* 355 (2019) 514 – 525. [Cited page 61.]
- [200] B. Song, S. Rough, D. Wilson, Effects of drying technique on extrusion–spheronisation granules and tablet properties, *International Journal of Pharmaceutics* 332 (1) (2007) 38 – 44. [Cited page 71.]
- [201] F. Fichtner, Å. Rasmuson, G. Alderborn, Particle size distribution and evolution in tablet structure during and after compaction, *International Journal of Pharmaceutics* 292 (1) (2005) 211 – 225. [Cited page 71.]
- [202] O. Tsoungui, D. Vallet, J.-C. Charmet, Numerical model of crushing of grains inside two-dimensional granular materials, *Powder Technology* 105 (1) (1999) 190 – 198. [Cited page 71.]
- [203] J. Fu, G. K. Reynolds, M. J. Adams, M. J. Hounslow, A. D. Salman, An experimental study of the impact breakage of wet granules, *Chemical Engineering Science* 60 (14) (2005) 4005 – 4018. [Cited page 71.]

## BIBLIOGRAPHY

---

- [204] D.-H. Nguyen, E. Azéma, P. Sornay, F. Radjai, Bonded-cell model for particle fracture, *Phys. Rev. E* 91 (2015) 022203. [Cited page 71.]
- [205] D. Cantor, E. Azéma, P. Sornay, F. Radjai, Three-dimensional bonded-cell model for grain fragmentation, *Computational Particle Mechanics* (2016) 1–10. [Cited page 71.]
- [206] G. Lian, C. Thornton, M. J. Adams, Discrete particle simulation of agglomerate impact coalescence, *Chemical Engineering Science* 53 (19) (1998) 3381–3391. [Cited page 73.]
- [207] K. Kafui, C. Thornton, Numerical simulations of impact breakage of a spherical crystalline agglomerate, *Powder Technology* 109 (1) (2000) 113 – 132. [Cited page 73.]
- [208] B. Mishra, C. Thornton, Impact breakage of particle agglomerates, *International Journal of Mineral Processing* 61 (4) (2001) 225 – 239. [Cited page 73.]
- [209] C. Thornton, M. T. Ciomocos, M. J. Adams, Numerical simulations of diametrical compression tests on agglomerates, *Powder Technology* 140 (2004) 258–267. [Cited page 73.]
- [210] L. Liu, K. Kafui, C. Thornton, Impact breakage of spherical, cuboidal and cylindrical agglomerates, *Powder Technology* 199 (2) (2010) 189 – 196. [Cited page 73.]
- [211] C. Voivret, F. Radjaï, J.-Y. Delenne, M. S. E. Youssofi, Space-filling properties of polydisperse granular media., *Phys Rev E Stat Nonlin Soft Matter Phys* 76 (2 Pt 1) (2007) 021301. [Cited page 73.]
- [212] L. Rothenburg, A. P. S. Selvadurai, A micromechanical definition of the cauchy stress tensor for particulate media, in: A. P. S. Selvadurai (Ed.), *Mechanics of Structured Media*, Elsevier, 1981, pp. 469–486. [Cited page 75.]
- [213] J. Christoffersen, M. M. Mehrabadi, S. Nemat-Nasser, A micromechanical description of granular material behavior, *J. Appl. Mech.* 48 (1981) 339–344. [Cited page 75.]
- [214] M. M. Mehrabadi, S. Nemat-Nasser, M. Oda, On statistical description of stress and fabric in granular materials, *Int. J. Num. Anal. Meth. Geomech.* 6 (1982) 95–108. [Cited page 75.]
- [215] J. J. Moreau, New computation methods in granular dynamics, in: *Powders & Grains* 93, A. A. Balkema, Rotterdam, 1993, p. 227. [Cited page 75.]
- [216] L. Staron, F. Radjai, J. Vilotte, Multi-scale analysis of the stress state in a granular slope in transition to failure, *Eur. Phys. J. E* 18 (2005) 311–320. [Cited page 75.]
- [217] J. Nimmo, Aggregation | physical aspects, in: D. Hillel (Ed.), *Encyclopedia of Soils in the Environment*, Elsevier, Oxford, 2005, pp. 28 – 35. [Cited page 85.]

## BIBLIOGRAPHY

---

- [218] N. Rahmanian, M. Ghadiri, X. Jia, Seeded granulation, *Powder Technology* 206 (1) (2011) 53 – 62, 9th International Symposium on Agglomeration and 4th International Granulation Workshop, 2009. [Cited page 85.]
- [219] T. Trung Vo, S. Nezamabadi, P. Mutabaruka, J.-Y. Delenne, E. Izard, R. Pellenq, F. Radjai, Agglomeration of wet particles in dense granular flows, *The European Physical Journal E* 42 (9) (2019) 127. [Cited page 85.]
- [220] A. Taboada, N. Estrada, F. Radjai, Additive decomposition of shear strength in cohesive granular media from grain-scale interactions., *Phys. Rev. Lett.* 97 (9) (2006) 098302. [Cited page 85.]
- [221] B. Saint-Cyr, F. Radjai, J.-Y. Delenne, P. Sornay, Cohesive granular materials composed of nonconvex particles, *Physical Review E* 87 (2013) 052207. [Cited page 85.]
- [222] G. I. Tardos, K. P. Hapgood, O. O. Ipadeola, J. N. Michaels, Stress measurements in high-shear granulators using calibrated “test” particles: application to scale-up, *Powder Technology* 140 (3) (2004) 217 – 227, 1st International Workshop on Granulation (Granulation across the length scales: linking microscopic experiments and models to real process operation). [Cited page 86.]
- [223] A. Scurati, D. Feke, I. Manas-Zloczower, Analysis of the kinetics of agglomerate erosion in simple shear flows, *Chemical Engineering Science* 60 (23) (2005) 6564 – 6573. [Cited page 86.]



## MODELING THE RHEOLOGY OF WET GRANULAR MATERIALS

**Abstract :** By means of extensive particle dynamics simulations in three dimensions, we investigate the rheology and agglomeration process of granular materials such as wet powders, which involve cohesive and viscous interactions in addition to frictional contact forces. In shear flow simulations, we show that the flow variables such as effective friction coefficient and packing fraction and texture variables such as coordination number and anisotropy can be described as a function of a single dimensionless number that incorporates the inertial, cohesive and viscous forces. We also study the evolution of an agglomerate inside a granular shear flow of dry particles and in a rotating drum containing wet particles. The evolution of the agglomerate depends on the accretion and erosion dynamics, which are governed by cohesive interactions. We determine the phase-space diagrams in terms of the agglomerate growth, deformation, damage and erosion as a function of the cohesion index and inertial number. The compressive strength of the agglomerates is also investigated under diametral compression and shown to be proportional to the adhesion force between the particles with a pre-factor that depends on the connectivity of the primary particles.

**Key words :** granular matter, rheology, DEM, capillary bridge, agglomeration.

## MODÉLISATION DE LA RHÉOLOGIE DES MATÉRIAUX GRANULAIRES HUMIDES

**Résumé :** Dans cette thèse, nous avons étudié par simulations numériques la rhéologie et le processus d'agglomération de matériaux granulaires humides impliquant des interactions cohésives et visqueuses venant s'ajouter à celles de contact-frottant. Des écoulements en cisaillement, simulés par une approche de type éléments discrets 3D, nous ont permis de montrer que les variables caractérisant le comportement (coefficient de frottement effectif et compacité) ainsi que celles décrivant la texture (nombre de coordination et anisotropie) peuvent être décrites comme fonction d'un unique nombre sans dimension ; incorporant les forces inertielles, cohésives et visqueuses. Nous nous sommes également intéressés à l'évolution d'un agglomérat à l'intérieur d'un écoulement de particules sèches cisillées ainsi que dans un tambour rotatif contenant des particules humides. Il a été montré que l'évolution de l'agglomérat dépend de la dynamique d'accrétion et d'érosion et que celle-ci est régie par les interactions cohésives. Des diagrammes de phase en termes de croissance, de déformation, d'endommagement et d'érosion sont présentés en fonction de l'indice de cohésion et du nombre inertiel. Enfin, la résistance à la compression des agglomérats a été également étudiée sous compression diamétrale. On montre qu'elle est proportionnelle à la force d'adhésion entre particules avec un pré-facteur qui dépend de la connectivité des particules primaires.

**Mots-clés :** matière granulaire, rhéologie, DEM, pont capillaire, agglomération.